Ph.D. DISSERTATION

Development of Miniaturized, Subcutaneously Head-mountable Deep Brain Stimulation System

소형화된, 두피 아래 이식 가능한 심뇌자극 시스템의 개발

BY

Seung-Hee Ahn

FEBRUARY 2020

DEPARTMENT OF ELECTRICAL
AND COMPUTER ENGINEERING
COLLEGE OF ENGINEERING
SEOUL NATIONAL UNIVERSITY

Development of Miniaturized, Subcutaneously Head-mountable Deep Brain Stimulation System

지도교수 김 성 준

이 논문을 공학박사 학위 논문으로 제출함

2020년 1월

서울대학교 대학원

전기·정보공학부

안 승 희

안 승 희의 공학 박사 학위 논문을 인준함

2019년 12월

위 원 장 박 병 국 (인)

부위원장 김 성 준 (인)

위 원 장 진 우 (인)

위 원 서 종 모 (인)

위 원 정 준 수 (인)

ABSTRACT

Deep brain stimulation (DBS) is a neurosurgical technique that alleviates symptoms of neurological disorders such as Parkinson's disease, essential tremor, dystonia, and neuropathic pain. Since the US Food and Drug Administration (FDA) has approved DBS in 1997 for Parkinson's disease, more than 150,000 patients have been treated with it worldwide. However, due to its size and structure, conventional DBS has some problems with the possibility of infection and difficulty of surgery. The main factor of this size is the implantable pulse generator (IPG). Since the IPG made of titanium alloy-based package has relatively big, the package is in the chest of the patient. An extension wire is used to connect the IPG with the electrode in the brain under the skin from the chest to the parietal region. Since the tunneling surgery is highly invasive, there is a risk of infection along the surgical area or fracture of the connection. Therefore, several studies on miniaturizing the DBS system are being conducted.

Neuropathic pain is a pain caused by a lesion or disease of the somatosensory nervous system. The worldwide prevalence rate of neuropathic pain in the adult population is estimated at around 7-8 % in 2014. Patients of the neuropathic pain seem to have an as low rated health-related quality of life as for those with clinical depression, coronary artery disease, recent myocardial infarction, or poorly controlled diabetes. For severe neuropathic patients with drug-resistance, neuromodulation is a very considerable treatment.

In this dissertation, we developed a subcutaneously head-mountable miniaturized DBS system. The system consists of an implantable device and an external device. The implantable device has 13 mm diameter, 5 mm height package and 20 mm electrode, therefore it can be implanted between the scalp and skull of the patient. This allows us to minimize the incision and lower the difficulty of device implantation surgery. The implantable device is monolithically fabricated based on liquid crystal polymer, which is a biocompatible material and has been demonstrated very good long-term reliability in previous studies. The device consists of a multichannel depth electrode, current stimulation ASIC and receiving coil. The external device is miniaturized; therefore, it can be attached to the patient's scalp above the implantable device. It has a width of 20 mm, length of 35 mm, and thickness of 12mm body, which contains Li-Po battery, ZigBee receiver, and Class-E amplifier. And a transmitter coil is connected to the body to deliver power and data to the implantable device via an inductive link. Since the battery is located outside of the body, the system has a few advantages than the conventional DBS systems such as better compatibility with MRI, no possibility of battery leakage and easier battery replacement. A benchtop operation test is conducted to demonstrate the electronic system, and an in vitro evaluation of the electrode is conducted by electrochemical impedance spectroscopy and cyclic voltammetry. And an *in vivo* animal behavioral experiment is conducted to validate the system. The validation is performed using von Frey filament on neuropathic pain modeled rats. Spared Nerve Injury model is adopted to induce the pain on a hind limb of

the rats. The implantable device of the suggested LCP-DBS is implanted targeting the ventral posterolateral nucleus of the rats. The mechanical withdrawal threshold of the rats is measured with and without delivering DBS pulses. As expected, the results show a significant increase in the mechanical withdrawal threshold as the stimulation current increases. Finally, several discussions on the developed device are described

Keywords: deep brain stimulation, implantable electronics, liquid crystal polymer, neuropathic pain, monolithic package, inductive link

Student Number: 2014-21699

CONTENTS

List of Figures

List of Tables

List of Abbreviations

Abbreviation	Term
ASIC	Application-Specific Integrated Circuit
CAD	Computer Aided Design
CSC_C	Cathodic Charge Storage Capacity
CV	Cyclic Voltammetry
DBS	Deep Brain Stimulation
DLP	Direct Laser Patterning
EIS	Electrochemical Impedance Spectroscopy
FEM	Finite Element Method
GPe	external Globus Pallidus
GPi	internal Globus Pallidus
IPG	Implantable Pulse Generator
LCP	Liquid Crystal Polymer
MCS	Motor Cortex Stimulation
MCU	Micro-Controller Unit
MEMS	MicroElectroMechanical System
PCB	Printed Circuit Board
PD	Parkinson's Disease
PR	PhotoResist
PVD	Physical Vapor Deposition
PWM	Pulse-Width Modulation
SAR	Specific Absorption Rate

SCS	Spinal Cord Stimulation
SNc	Substantia Nigra pars compacta
SNr	Substantia Nigra pars reticulata
STN	SubThalamic Nucleus
VL	Ventral Lateral thalamic nucleus
VPL	Ventral Posterolateral Nucleus

Note

Some parts of this dissertation are extracted and adapted from the following publications which were published during the course of this study:

Ahn, S.-H., Jeong, J., & Kim, S. J. (2019), Emerging Encapsulation Technologies for Long-Term Reliability of Microfabricated Implantable Devices, *Micromachines*, 10(8), 508.

Chapter 1

Introduction

1.1. Biological Background

1.1.1. Overview of Brain Stimulation (DBS)

1.1.1.1. Neuromodulation

Neuromodulation is a technique for normalizing the activity of the nervous system by transmitting electric or chemical signals to the central nervous system. These techniques are intended to alleviate the symptoms caused by abnormalities of the nervous system. Considering that all the functions of our body are involved in the central nervous system, especially the brain, not only the neuropathic diseases but also abnormalities of the sensory organ have the potential to be resolved through neuromodulation.

Neuromodulation varies depending on the medium of the signal and the type of the target tissue. It can be broadly classified into invasive and non-invasive methods. In the case of non-invasive methods, such as transcranial direct current stimulation (tDCS) or repetitive transcranial magnetic stimulation (rTMS), applies electric or magnetic signals from outside the body by non-invasive methods. On the other hand, invasive methods, such as DBS, spinal cord stimulation (SCS), motor cortex stimulation (MCS), etc. delivers signals to the target by invasive methods using electrode implantation.

1.1.1.2. Deep Brain Stimulation

Deep brain stimulation is a method of alleviating the symptoms of neuropathy disorders by applying electrical stimulation on a specific region of the deep brain that is considered to be related diseases [1]. The distinctive feature of DBS that distinguishes it from other neuromodulation is that the target organization of the stimulation is the deep brain. The deep brain is including the thalamus and basal ganglia, which are involved in most of the motor and sensory functions of humans. Some studies have also shown that DBS may also contribute to the enhancement of cognitive function.

DBS was first approved by the US FDA in 1997 to relieve symptoms of motor symptoms and was used to treat uncontrollable shaking caused by tremor or Parkinson's disease (PD) or twisting caused by dystonia. Before DBS, nerve resection, which deliberately destroys parts of the brain tissue called thalamotomy or pallidotomy, was used in patients who could not benefit from medication. It is a treatment that has advantages in that it can be seen.

Among the brains, subthalamic nucleus (STN) and internal globus pallidus (GPi) are already widely used as target tissues for DBS treatment. Attempts have

been made to use the therapies for various neurological diseases such as Alzheimer's disease.

1.1.1.3. Mechanisms of DBS

Although DBS has already been applied and successfully used in many patients, the mechanisms by which DBS affects PD and many other diseases is unclear [2]. However, DBS has clearly shown a consistent effect and based on this, models of circuits related to the deep brain are presented. Figure 1-1 shows DeLong's box model of basal ganglia-related circuit published in 1986. In this model, the cerebral cortex and several thalamic tissues involve the neural circuit for motor control. Each thalamic tissues, such as the external Globus Pallidus (GPe), the GPi, the STN, the Striatum, the Substantia Nigra pars compacta (SNc), and the Ventral Lateral thalamic nucleus (VL), and the cerebral cortex antagonize each other and act as the neural circuit for motor control.

As shown in Figure 1-1 b), for Parkinson's disease patient in this model, dysfunction in the SNc confuses the entire neural circuit for motor control leads to a chain of malfunction of each tissue that makes up the circuit. When the SNc malfunctions, the Striatum over-fires. Since the Striatum to the GPe connection is

inhibitory, the firing rate of GPe decreases. Then, the STN the GPi and the SNr overfires, leads to underfiring of VL and the cortical tissue.

For the case of a patient with the DBS applied, in this model, the DBS suppresses the overactive STN, and it normalizes the GPi, SNr, VL and the cortex in chain. Through this, the motor control circuit becomes normal.

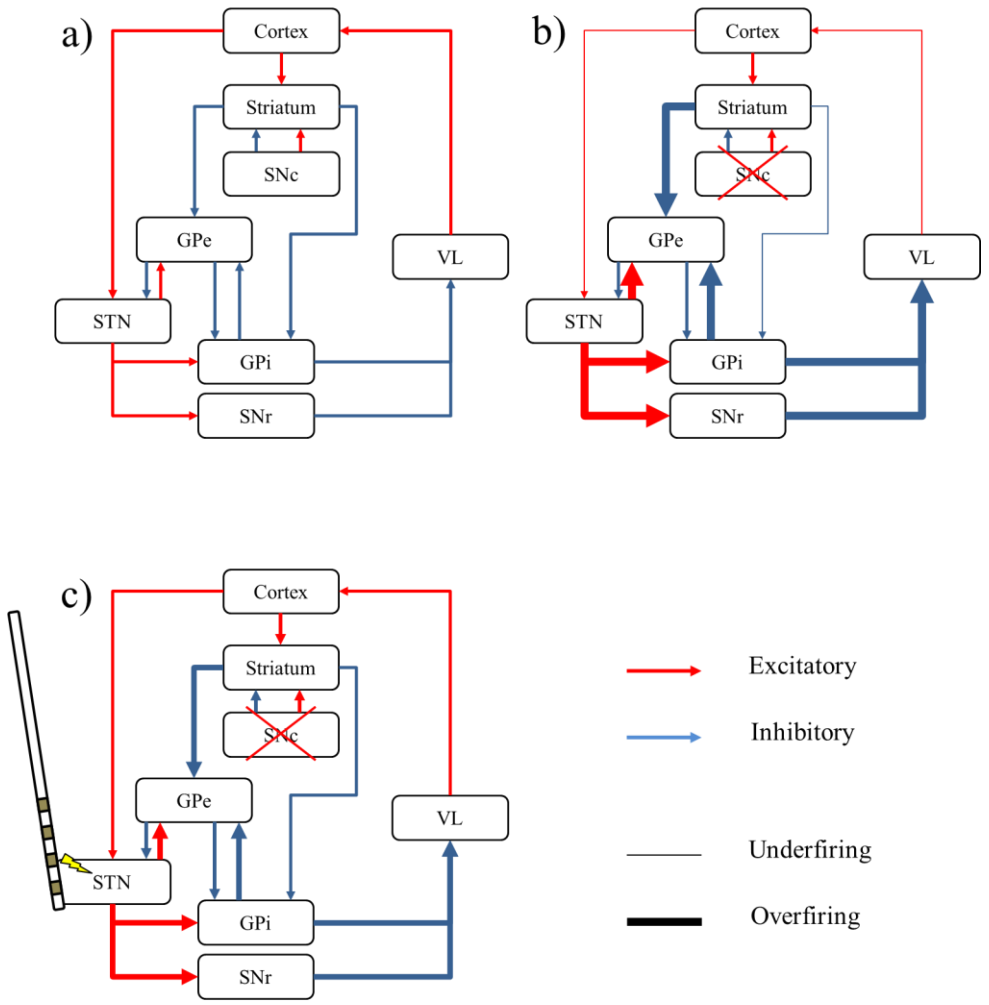

Figure 1-1. The DeLong Box model of cortex and basal ganglia motor circuit of a normal person, a Parkinson's disease patient, and a patient with DBS. a) For a normal person, the cerebral cortex and several thalamic tissues such as SNc, SNr, GPe, GPi, STN, VL antagonistically construct the motor circuit; b) The DeLong Box model of the neural circuit for motor control of a Parkinson's disease patient. The SNc dysfunction induces overfiring of the Striatum, underfiring of the GPe, VL, cortex, overfiring of the STN, GPi, and the SNr. Therefore, the motor circuit of the patient is out of control; c) The DeLong Box model of the neural circuit for motor control of a Parkinson's disease patient after the DBS applied. By inhibiting, or paralyzing STN, the DBS modulates the neural circuit for the motor control;
(GPe = external Globus Pallidus; GPi = internal Globus Pallidus; STN = SubThalamic Nucleus; SNc = Substantia Nigra pars compacta; SNr = Substantia Nigra pars reticulata; VL = Ventral Lateral thalamic nucleus) [2]

1.1.1.4. Conventional DBS

The commercial DBS, which has already been used successfully in over 150,000 patients [3], consists of an electrode that delivers the stimulus waveform to the deep brain, an implantable pulse generator (IPG) that generates the stimulus waveform, and a lead wire connecting the two [4].

The IPG is a part of the DBS system that is implanted into the patient's body and generates stimulation pulses. Although the IPGs in the early days of DBS had to be replaced about every 10 years because they used the primary battery, but recently a device with rechargeable batteries has been introduced and is on the market. As shown in Table 1, commercial DBSs on the market now weigh about 30-50 g and are about 50 mm in size. Due to its size, the IPG is unable to be implanted around skull. Therefore, it is typically placed in the chest region below the collarbone.

Table 1. Conventional DBS systems of Medtronic, Boston Scientific and Abbott. [5]–[7]

	Medtronic Activa™ RC	**Boston Scientific Vercise™**	**Abbott St. Jude Medical Infinity™**
			
Power Supply	**Rechargeable Battery**	**Rechargeable Battery**	**Non-rechargeable Battery**
Weight	**40 g**	**33 g**	**48.9 g**
Size	**54 mm × 54 mm (9 mm thick)**	**55 mm × 45 mm (11 mm thick)**	**55.5 mm × 49.5 mm (13.4 mm thick)**
# of Channel	**16 ch. (8 ch. Bilateral)**	**16 ch. (8 ch. Bilateral)**	**16 ch. (8 ch. Bilateral)**
Channel Spacing	**2 mm**	**2 mm**	**2 mm**

A typical commercial DBS electrode, Medtronic 3389, (Medtronic™, Dublin, Ireland), is made of platinum in the form of a band around a 1.27 mm thick cylindrical electrode shank [8]. This electrode has four 1.5 mm width contacts placed at 0.5 mm intervals with a resolution of 2 mm per channel.

Finally, the extension wire is a line connecting the electrode implanted in the head with the IPG implanted in the chest and due to its size and is the last implanted part in the surgical procedure. However, this wire transplantation requires most of the surgery time because the section from the chest to the crown must be connected under the skin.

To solve this problem, some researches have been conducted on head-mountable DBS, but it is mainly designed to make the metal package thinner and place it in the position of the skull [2], [9]. Still, there is no paper on the head-mountable DBS or the results of experiments using it, and only a few papers are presenting a conceptual view of it.

1.1.1.5. Miniaturized DBS for Small Animal

Meanwhile, efforts to develop miniaturized DBS are underway for other reasons. Researchers in neuroscience are in demand for experiments with DBS on

smaller animals that are much smaller than humans. This is necessary for new DBS stimulation techniques and new target area development, but it is also because there is no DBS system applicable to small laboratory animals that are frequently used in laboratories. Usually, the study of applying DBS to such small animals proceeds with the percutaneous system through wired stimulator [10], [11], but also develops miniaturized DBS systems to conduct experiments on freely moving animals.

1.2. Neuropathic Pain

Neuropathic pain is a neurological disease that has a prevalence of 7~8 % worldwide [12]. Patients of neuropathic pain experience several unpleasant symptoms such as stinging or burning pain, paralysis, etc [13]. Although the mechanism of the disease is not clear, it is known to be mainly caused by accidental sequelae and nervous system abnormalities, and it is regarded as a disease that greatly affects the quality of life of patients.

Currently, patients with neuropathic pain mainly focus on treatment with drugs. In spite of the standard treatment of drug therapy guidelines, patients who experience chronic neuropathic pain for more than 6 months are tested and used SCS as a treatment [14]. SCS was approved by the FDA to relieve chronic pain from nerve

damage in 1989, and SCS can be considered an effective and safe treatment option for patients resistant to pharmacological treatments suffering from neuropathic pain [15].

1.3. Encapsulation Materials for Long-Term Reliability

A variety of organic and inorganic materials and related technologies have been proposed as alternative encapsulation methods for miniaturized biomedical implants as they exhibit mechanical flexibility, compatibility with the MEMS process or batch process, good electrical insulation, and conformal encapsulation of complex topography on top of the basic requirements of biocompatibility and long-term stability in vivo. Additionally, these thin-film coatings add minimized volume and weight to the devices. These emerging materials include inorganic thin-film coatings of Al_2O_3, HfO_2, SiO_2, silicon carbide (SiC), and diamond, as well as organic polymers such as polyimide, Parylene, liquid crystal polymer (LCP), silicone elastomer, SU-8, and cyclic olefin copolymer (COC). Methods of deposition of these materials are diverse, ranging from spin coating, chemical vapor deposition, casting, thermal lamination, and thermal growth to atomic layer deposition (ALD).

Although none of these materials have yet been proven to be as hermetic as metal packaging nor widely utilized in regulatory approved devices for chronic implantation, several studies have endeavored to investigate the feasibility of their use and have demonstrated promising outcomes in terms of their long-term reliability through a multitude of testing methodologies with great potential for further improved longevity. While many review articles have introduced and compared a series of biocompatible materials that are commonly used for implantable devices, their scope is relatively broad; for the most part, the general properties of the materials are discussed [16]–[22]. To select the most appropriate encapsulation material, we have classified the results of various papers by a specific focus on their encapsulation performance. For this purpose, we primarily selected and compared publications that have not only demonstrated device encapsulation but also investigated long-term reliability in aqueous environments to provide a quantitative estimation of the expected lifetime of the encapsulation through accelerated aging or other scientific procedures.

1.3.1. Long-Term Reliability Test

The long-term reliability of encapsulation materials is generally evaluated in accelerated aging experiments by soaking test samples in saline solution of elevated temperatures. The lifespan of the encapsulation, or the mean time to failure (MTTF), during accelerated aging can be translated into the equivalent lifetime at body temperature using the Arrhenius reaction rate function, which describes the temperature dependence of the chemical reaction rate, k, as follows:

$$k = \mathrm{A}e^{-E_a/RT},$$

where A is a constant, Ea is the activation energy, R is the gas constant, and T is the temperature in Kelvin. Therefore, the accelerating factor, k_1/k_2, of the raised test temperature, T_1, to body temperature, T_2, can be obtained as follows:

$$\frac{k_1}{k_2} = exp\left[\frac{E_a}{R}\left(\frac{1}{T_2} - \frac{1}{T_1}\right)\right].$$

The activation energy can be determined if the reaction rates (or MTTF values) at two different test temperatures are provided. As an approximation of the Arrhenius relationship for polymer reactions, the ”10-degree rule” is commonly adopted to extrapolate the lifetime of polymeric materials at 37 °C. This rule states that the chemical reaction rate will double for every 10-degree increase in

temperature, assuming the aging process is first-order or pseudo–first-order [23], [24]:

$$\frac{k_1}{k_2} = 2^{(T_1 - T_2)/10}.$$

It is recommended that the accelerating temperature is kept below 60 °C because the accuracy of the 10-degree rule decreases with greater deviation from the ambient temperature. Besides, higher temperatures can introduce new failure mechanisms that would not occur at the normal operation temperature of 37 °C [23], [24]. However, the 10-degree rule is still useful to predict the worst case lifetime, given that it is known to give a conservative estimation over a wide range of temperatures specifically for most polymeric materials [23], [25].

Common metrics for quantifying encapsulation include leakage current, EIS, and the functionality of working devices. Leakage current measured between a pair of encapsulated interdigitated electrodes (IDEs) under DC bias is the most sensitive It is recommended that the accelerating temperature is kept below 60 °C because the accuracy of the 10-degree rule decreases with greater deviation from the ambient temperature. Also, higher temperatures can introduce new failure mechanisms that would not occur at the normal operation temperature of 37 °C

[23], [24]. However, the 10-degree rule is still useful to predict the worst measure of moisture penetration. An initial current in the typical range of a few to tens of pA abruptly soars into the nA or μA range as a result of failed encapsulation. Additionally, EIS data, which is also usually measured between IDEs under encapsulation, can provide more comprehensive information about the degradation of the encapsulation when the EIS values are fitted into an equivalent circuit model of the encapsulation. Changes in each circuit component can be used to investigate the failure mechanisms of, for example, dissolution, blistering, ion transport, or pore formation [26], [27]. Functional devices such as recording or stimulating electrode arrays [28], [29], neural recording systems with a wired or wireless connection, or wirelessly interrogatable tiny chiplets [30]–[32] can also be used as test vehicles in encapsulation assessment. While these functional devices can provide more practical and exact predictions of the lifetime of certain applications than specially designed test samples, this method is not suitable for investigation of encapsulation performance itself because the loss of the functionality of the full system is associated with various factors other than failed encapsulation.

Lastly, presence of electrical bias generated by wired or wireless powering can introduce another mode of stress accelerating the failure process of the encapsulation. Electrical stress caused by voltage gradient or current flow can

facilitate the electrochemical process including corrosion, material degradation, ion movement, and water electrolysis [33], [34]. While the effect of electrical bias on the encapsulation performance has not been extensively investigated yet, this is an essential part in the field as most of the active implantable devices need electrical powering.

1.3.2. Biocompatible Polymers

Biocompatible polymers are used in several studies, which have the advantage of being light and relatively low-temperature of fabrication processes compared to other sealing materials such as metals or ceramics. However, there are several emerging materials such as Al_2O_3, HfO_2, SiO_2, and SiC. These inorganic materials have shown to have more than 10 years of MTTF at room temperature in some studies, but form very thin film of less than 1 μm thickness because of the deposition method. Considering its physical durability, it is premature to use these materials alone as encapsulation materials for implantable devices. Common methods of encapsulation using biocompatible polymers are spin coating and thermal bond. These methods have relatively low processing temperature than CVD or thermal growing of organic materials. Typical

biocompatible polymers used in the implantable device include polyimide, parylene, silicon elastomer, LCP, SU-8 and COC, among which biocompatible polymers except for COC and SU-8 are already known for their estimates of average life expectancy from accelerated aging tests and are also used in various animal experiments. However, since SU-8 and COC also have their strength over other biocompatible polymers in terms of biocompatibility, chemical inertness, and water absorption rate, these materials seem to have enough potential to be applied in a wider range of studies if further validations are performed.

1.3.2.1. Polyimide

Polyimide is a branch of commercially available polymers and is literally a polymer of imide monomers that is available in the form of film, tape, or spinnable liquid. Polyimide features excellent thermal and chemical stability, high glass transition temperature, and flexibility. Among the several types of polyimide, depending on the type which vary according to their building blocks (dianhydride, diamine, etc.), the BPDA/PPD type is the most commonly used for medical applications. Although it is not certified according to the ISO 10993, various groups have proven its biocompatibility and low cytotoxicity [18], [35]–[37],

placing the polyimide among the most widely used substrate and encapsulating polymer for neural interfaces [38]–[43].

Encapsulation using polyimide is based on spin coating on the substrate followed by curing at ~400 °C. Due to its excellent thermal and chemical stability, polyimide is compatible with most of the MEMS batch process. Photolithography using photosensitive polyimide [44]–[46], liftoff using sacrificial layer [43], and bonding using polyimide as an adhesion [47]–[49] are available techniques for polyimide.

Some of those studies have quantitatively evaluated the long-term reliability of polyimide encapsulation under accelerated aging conditions. Test samples with IDE patterns sandwiched between 10 μm thick polyimide layers were soaked in 75 °C phosphate buffered solution (PBS) saline for accelerated aging, while the leakage currents between IDE channels were measured to detect any encapsulation failure. The leakage current exceeded the threshold of 1 μA after 66 days of soaking [50], which is roughly equivalent to a lifetime of 2.5 years at 37 °C based on the 10-degree rule. The failure modes were dissolution, delamination, blistering, and corrosion. In another study, test samples made of three different commercial polyimide products were soaked in PBS at 37 °C, 60 °C, and 85 °C,

and in deionized water at 85 °C [51]. The mechanical properties of the samples, including Young's modulus, fracture energy, stress at break, strain at break, and stress at 10% strain, were measured for more than 20 months. Over the study period, all the samples were stable in PBS at 37 °C and 60 °C without showing any changes in their properties relative to the control dry samples. On the other hand, degradation was observed in the samples in PBS at 85 °C, including mass loss and decreased mechanical properties [51]. In other studies, 64-channel micro-electrocorticographic (μECoG) electrode arrays fabricated by 5–12.5 μm thick polyimide layers were soaked in 60 °C saline for an accelerated aging test [52], [53]. With the failure criteria being the time point at which the number of working channels dropped below 50% of the initial working channels, two of three samples survived for over 300 days, resulting in a predicted lifetime of four to seven years [53].

1.3.2.2. Parylene

Parylene refers to a class of semi-crystalline polymers discovered in the 1940s and commercialized by the Gorham process about 20 years later which enabled room temperature deposition. Parylene can be deposited as a thin,

conformal, pinhole-free film exhibiting flexibility, optical transparency, chemical inertness, and low water absorption (< 0.1%). Among the commonly available types of parylene, parylene-N, parylene-C, and parylene-HT have acquired the ISO 10993, USP Class VI rating. Parylene-C is the most popular type owing to its lower moisture and gas permeability compared to Parylene-N [18], [54], [55], and is used in a wide range of biomedical applications such as bladder volume sensors [56], microelectrode arrays [57]–[59], orthopedic implants [60], [61], and dental implants [62], [63].

Encapsulation using parylene is based on the CVD process. Due to the molecular level deposition process, a uniform and conformal film can be formed over complex sample surface topography, including sharp edges and crevices [64]–[66]. Parylene film is typically no thicker than 100 μm, which adds minimal volume and weight to the devices, but at the same time it cannot provide mechanical strength or robustness [18]. Therefore, parylene is sometimes used in combination with other encapsulation materials such as silicone elastomer [67], Al_2O_3 [29], [33], and glass [68] to complement its mechanical properties.

Some studies have evaluated the long-term reliability of the parylene encapsulation under accelerated aging conditions. IDE test samples encapsulated

by 10 μm thick parylene-C layers soaked in 75 °C PBS failed after 117 days when the leakage current soared beyond the 1 μA threshold as a result of blistering and delamination [50]. According to the 10-degree rule, the expected lifetime of this sample device at 37 °C is about 4.5 years. In another study, test samples coated by parylene-C over a glass substrate were soaked in 85 °C and 97 °C saline for accelerated aging while the line resistance between multiple channels was measured. The samples failed after 31 days and 15 days, respectively, with the threshold being a 50% change in the resistance value, which is equivalent to approximately 2.5 years at body temperature based on the 10-degree rule. The failure mode of the samples was moisture diffusion through the parylene barrier layers and undercut of the glass [68]. In another study, IDE test samples coated with 6 μm thick parylene-C were soaked in 60 °C PBS with periodic electrochemical characterizations such as EIS, leakage current, and cyclic voltammetry every 6 hours. The MTTF of the six samples was 1117 hours, or 49.1 days, when the leakage current exceeded 1 nA [26]. Similar studies using IDE samples coated with 6 μm thick parylene-C layers have reported an MTTF of 150 days in 57 °C, which is equivalent to 1.64 years at 37 °C [33], 49.1 days at 60 °C, or 0.66 years at 37 °C [26], and 110 days at 67 °C, or 2.41 years at 37 °C [29].

1.3.2.3. Silicone Elastomer

Silicone elastomer is a biostable synthetic polymer which has a backbone made of repeating silicon-oxygen bonds and methyl groups. Among a variety of silicone elastomeric materials, polydimethylsiloxane (PDMS) is the most commonly used silicone in micro- and nanoscale soft lithography including molding, contact printing, and imprinting in biomedical applications because of its advantageous properties such as high elasticity, optical transparency, adjustable surface composition, and biocompatibility. Dipping, casting, and molding are the most common techniques for silicone encapsulation which are followed by curing at typically from room temperature to ~150 °C.

High permeability to gases and vapors, although useful for some applications, may limit the application of silicone elastomer for encapsulation purposes. Nevertheless, the packaging performance of silicone elastomer can be further enhanced when it is used in conjunction with other materials such as glass, parylene and metal [31], [68], [69], or it can be used to make transparent, flexible, and stretchable bioelectrodes [67], [70]–[72].

An additional 5 mm thick coating silicone elastomer on top of a 40 μm t hick parylene-C layer could extend the expected lifetime of the test sampl

es from 2.5 years to 6.7 years at body temperature based on accelerated a ging at 85 °C and 97 °C PBS, during which failure was defined as the resistance value falling below half of the initial value [68]. Recently, PDMS with its surface pores filled by parylene, so called “parylene-caulked PDMS,” has been shown to effectively suppress water permeation through PDMS [67]. When identical electrodes samples were soaked in 36.5 °C PBS for 209 days, impedance of the electrodes samples coated with parylene-caulked PDMS remained within 20% of the initial values, while the impedance values of all samples coated in PDMS decreased almost to zero [67]. Despite the inadequate barrier properties of silicone elastomer, it could be useful as a secondary coating material given its good biochemical stability and mechanical properties.

1.3.2.4. LCP

LCP has increasingly gained attention as an emerging biocompatible material for substrate and packaging of implantable neural devices, primarily owing to its lower moisture absorption rate (<0.04%) than conventional biocompatible polymers such as polyimide (～2.8%), parylene-C (0.06–0.6%), and silicone elastomers [73]. This advantageous property is expected to contribute

to improving the long-term reliability of polymer-based biomedical implants when properly processed. The thermoplasticity of LCP can be utilized to create a non-planar structure for conformation to target tissues by a simple thermoforming process, and to rapidly form a multilayered structure by stacking independently prepared LCP layers and thermally pressing them to bond together. The potential of LCP has been demonstrated in wide range of applications in neural engineering such as a miniaturized all-LCP retinal implant with an eye-conformable structure [74] as well as various shapes of neural electrode arrays for cortical [75], [76], cochlear [77], [78], intraocular [79]–[81], and peripheral applications [82]–[84].

LCP encapsulation begins from LCP films, which are commercially supplied in rolled sheets of varying thicknesses but can be applied to both planar and non-planar packaging. For encapsulation of planar structures such as neural electrode arrays of LCP/metal/LCP configuration, a substrate LCP film of higher melting temperature (~335 °C) with metallized pattern is thermally bonded to a cover LCP layer of a lower melting temperature (282 °C) by heating and pressing them together at a temperature between their melting points. Multiple layers can be fabricated using lower-melting-temperature LCP film as adhesive layers. For non-planar shape such as for packaging of electronics assembled on the substrate LCP layer, the first LCP layer is thermally deformed into, typically, a domed shape,

which is thermally bonded to the substrate LCP film by selectively applying heat pressure onto the perimeter of the package to create a conformal encapsulation [50], [74]. Another approach has also been proposed: filling the cavity between the substrate and the lid with milled LCP powder followed by pressing of the entire area, which could avoid the complex tooling of selective pressing [50].

Some studies have evaluated the long-term reliability of the LCP encapsulation in accelerated aging condition. Test samples with IDE patterns of the basic LCP/metal/LCP sandwiched structure were soaked in 75 °C saline for accelerated aging while the leakage current was measured to detect any moisture penetration. The samples were failed after 379 days in 75 °C saline when the leakage drastically soared up above the 1 μA threshold, presumably due to water infiltration through the LCP-LCP bonding which resulted in complete delamination of two LCP layers as observed in the failed samples [28], [50]. Test samples having opening windows like neural electrodes were also subjected to the aging condition in 87 °C saline by observing the voltage transient while stimulation pulses are continuously applied, which failed after 114 days in on average as confirmed by the loss of the voltage waveform as a result of water penetration and electrically shorting of two channels. Non-planar package samples with IDE pattern, mimicking the circular dome-shaped package part of the all-LCP

retinal implant, failed after 87 days in 87 °C saline. These results imply that the weakest interface against water penetration for this type of polymer encapsulation is polymer-metal adhesion around the channel openings rather than water ingression via the polymer-polymer adhesion and permeation through the bulk polymer surface. Microscale interlocking structure on the gold sites around the openings was reported to improve the MTTF of the device from 185 to 224 days at 75 °C saline, by providing mechanical interlocking between LCP and metal to enhance the bonding strength between them and thus be more resistant to water infiltration [85].

As we can derive see from the results of the accelerated aging test for long-term reliability validation of the biocompatible polymers described above, the longest MTTF of biocompatible polymers that has been verified so far is the LCP. Although the validation has not yet been done through accelerated aging test, it is expected that emerging biocompatible polymers such as COC, which has been studied in several researches, are expected to perform better than the LCP.

LCP encapsulation begins from LCP films, which are commercially supplied in rolled sheets of varying thicknesses but can be applied to both planar and non-planar packaging. For encapsulation of planar structures such as neural electrode

arrays of LCP/metal/LCP configuration, a substrate LCP film of higher melting temperature (~335 °C) with metalized pattern is thermally bonded to a cover LCP layer of a lower melting temperature (282 °C) by heating and pressing them together at a temperature between their melting points. Multiple layers can be fabricated using lower melting-temperature LCP film as adhesive layers. For non-planar shape such as for packaging of electronics assembled on the substrate LCP layer, the first LCP layer is thermally deformed into, typically, a domed shape, which is thermally bonded to the substrate LCP film by selectively applying heat pressure onto the perimeter of the package to create a conformal encapsulation [50], [74].

Chapter 2

Methods

2.1. System Overview

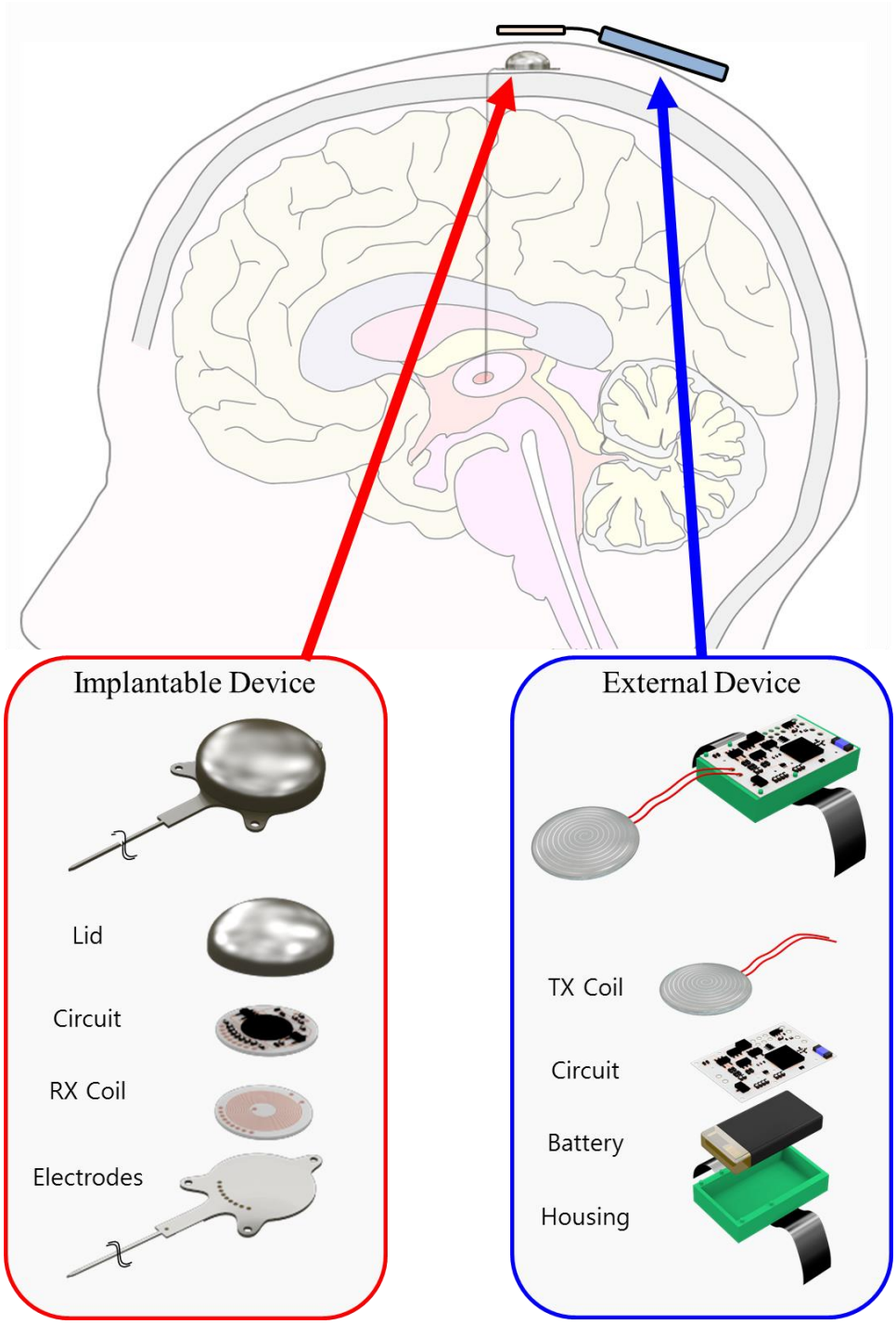

Figure 2-1. Suggested miniaturized DBS system overview.

Miniaturized DBS system suggested in this study has three parts, an implantable device, an external device, and a remote controller. When the user determines parameters of stimulation pulses (in clinical cases, by a physician, in animal experimental cases, by an experimenter) and gives operating instructions to the remote controller by pressing buttons, it delivers the instructions to the external device via the ZigBee protocol remote telecommunication. After the signal is received by the antenna, it is decoded by the microcontroller unit (MCU) embedded in the ZigBee receiver and generates the PWM waveform containing the parameter information. Then the Class-E amplifier modulates the 2.54 MHz carrier frequency with the PWM signal and transfers the RF signal to the implantable device via an inductive link. The implantable device decodes the parameter information and harvest power from the RF signal. An ASIC chip generates current stimulation pulses by the power transferred and the parameters reconstructed from the RF signal. Parameters of the current pulse, such as pulse rate, amplitude, duration are programmable by handheld remote controller. The pulses are delivered to the target tissue through the stimulation electrodes. Figure 2-2 shows the block diagram of the whole system.

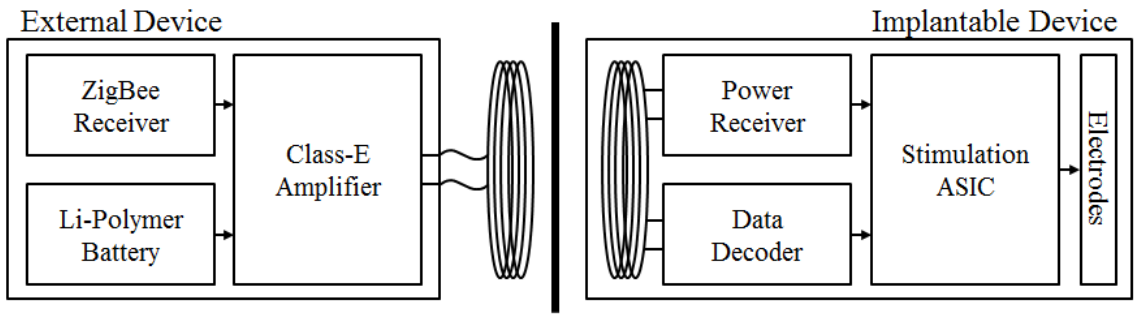

Figure 2-2. Block diagram of the miniaturized deep brain stimulation system. The system has an external device and an implantable device. The external device consists of a class-E amplifier, a ZigBee receiver, and a Li-Po battery. The implantable device consists of a stimulation ASIC, a power receiver, a data decoder, and electrodes.

2.2. Implantable Device

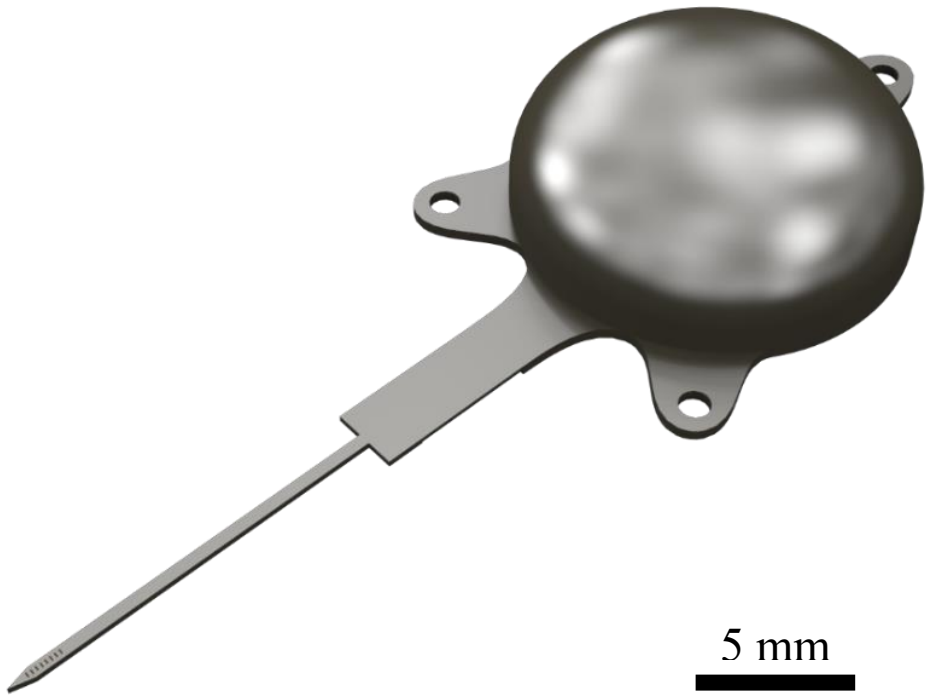

Figure 2-3. 3D model of the implantable device. The device has round, half ellipsoidal package and probe type 8-channel electrodes. The package has a diameter of 13 mm, a height of 4 mm and three holes for device fixing on skull. The electrode has a total length of 18 mm and a thickness of 260 μm.

The implantable device is an essential part of the miniaturized DBS system. It delivers current stimulation pulses using power and data derived from the PWM encoded RF signal. The main components of the implantable device are an electrode, which delivers current stimulation pulses to the target tissue, a circuit, which generates stimulation pulses from RF signal transmitted by the external device, and

a package, which isolates the circuit from *in vivo* environment. The implantable device of the suggested system is designed to have a microscale multichannel neural electrode, a current stimulation pulse generator circuit which is powered and instructed by RF signal transmitted from the external device via an inductive link, and an LCP-based minimum-sized, streamlined package.

2.2.1. Design

2.2.1.1. Circuit Description

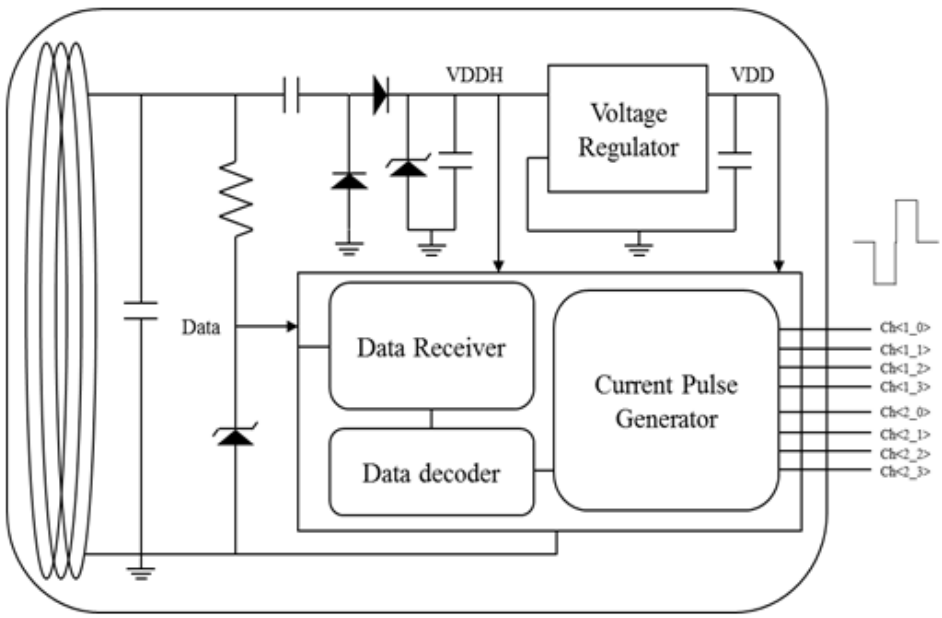

Figure 2-4. Block diagram of the internal circuit for the suggested DBS system. The circuit contains a power circuit, a data circuit, and a pulse generator ASIC. The power circuit rectifies and regulates the AC signal received by the RX coil via an inductive link into two kinds of DC voltages. The data circuit rectifies the PWM signal into a half-wave data signal for the pulse generator ASIC. And the ASIC consists of a data receiver, a data decoder, and a current pulse generator. Current stimulation pulses are generated by the ASIC chip from the PWM signal processed by the data circuit and the DC voltage regulated by the data circuit.

The circuit consists of a power circuit, a data circuit and a pulse generator ASIC. The power circuit rectifies and regulates the AC signal transferred from the external coil via an inductive link into two kinds of DC voltages. One is a compliance

voltage for the analog part of the pulse generator ASIC and the other is 3.3 V operating voltage for the logic circuit. The data circuit rectifies the PWM signal into a half-wave data signal for the pulse generator ASIC. The 16 channel current stimulator ASIC chip previously published in [76] is a silicon chip which generates current stimulation pulse from compliance voltage VDDH (typically over 9 V), operating voltage VDD of 3.3 V, and the data signal. The chip contains data receiver, data decoder, and current pulse generator. The data receiver reconstructs the 128 kHz clock from the data signal by counting peaks of the carrier frequency and converts the half-wave data signal into serial binary data by extracting the envelope. The data decoder classifies the serial data into '0', '1', or 'F', where '0', '1' are ordinary high and low, and 'F' is an end-of-frame indicator. In this system, a frame is a unit of a dataset that contains 18 bits of data including 16 bits of binary data and two frame bits on the most and the least significant bit of the frame. And also, the data decoder fetches the dataset and delivers the parameter information to the current pulse generator. The current pulse generator has four independent H-bridge structure current sources, and each current source has four channels. The parameters of the stimulation pulses are programmable for the duration, pulse rate, and amplitude. The duration of stimulation pulse on a phase has the range of 0 to 630 μs with 10 μs of

unit steps, the pulse rate has the range of 20 to 230 Hz with 5 Hz of unit steps, and the amplitude has the range of 0 to 10.23 mA with 10 μA of unit steps.

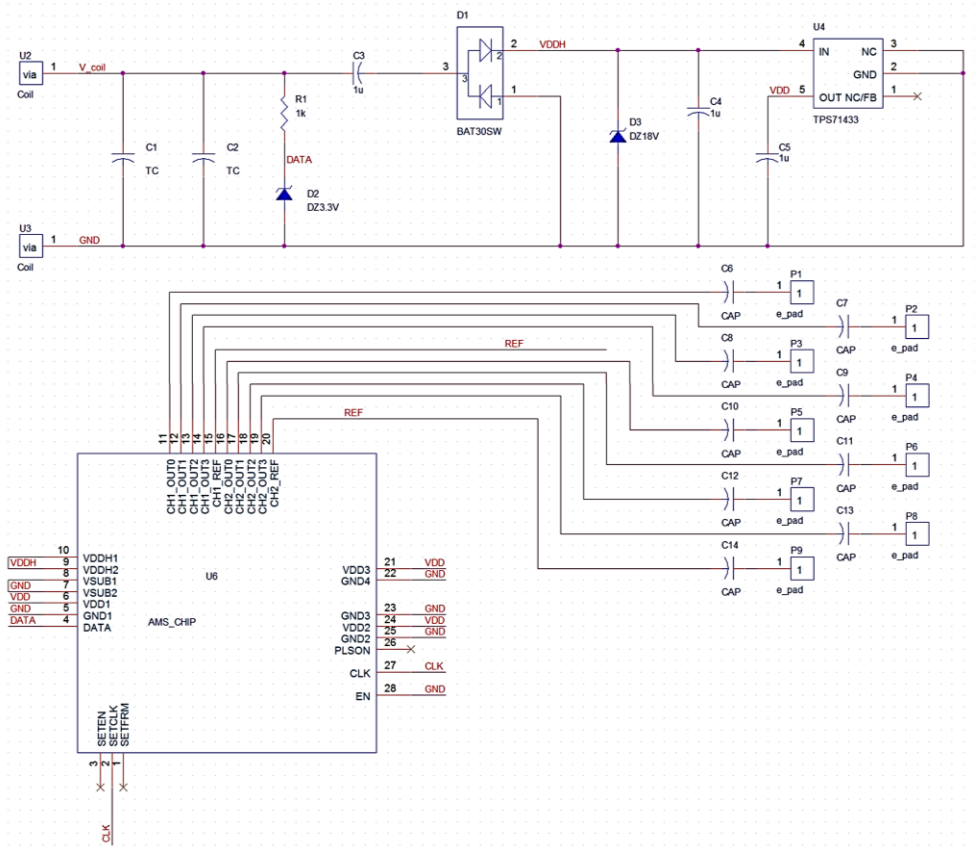

Figure 2-5. Designed schematic of the circuit. The data circuit consists of a resistor and a Zennor diode. The power circuit consists of three capacitors, two Schottky diodes, a Zennor diode, and a regulator. Each channel of the pulse generator ASIC requires a capacitor for DC voltage blocking. Finally, the circuit contains two vias for connection to the coil and nine vias for connection to the electrode channels.

2.2.1.2. Electrode Design

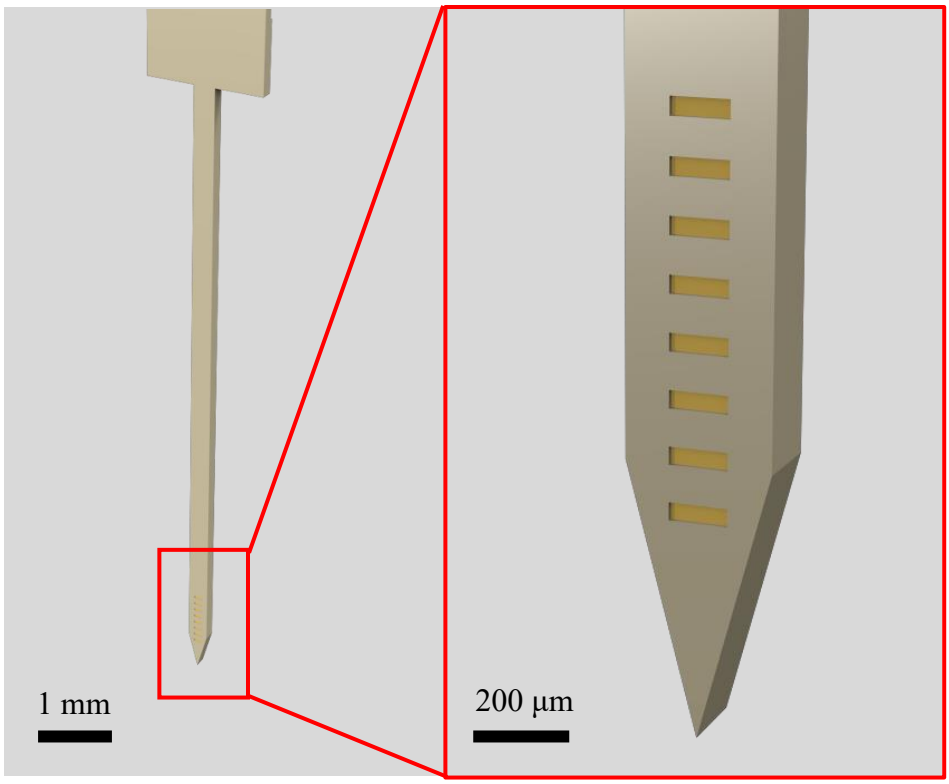

Figure 2-6. 3D model of designed multichannel microelectrode for LCP-DBS with 8-channel. The shank has a width of 300 µm and a thickness of 260 µm. Each stimulation channel is a rectangular gold electroplated site with a width of 160 µm and a height of 50 µm. The channel to channel pitch is 250 µm, therefore the stimulation channels cover 1.8 mm.

In neural prosthetic systems, electrodes serve to deliver the stimulation pulses from the pulse generator circuit to the target tissue. However, there is a possibility of side effects from electrodes. One is damage to surrounding tissue

during the electrode implantation, and another is stimulation on the wrong tissue during neural stimulation. To avoid those side effects, the electrode for neural prosthesis should be able to minimize the damage to the brain tissue during the implantation, and selectively stimulate the designated tissue.

Therefore, to minimize tissue damage during the implantation, the electrode of the neural prostheses should be designed depending on the size, location, and structure of the target tissue. In the case of DBS, the electrodes take the form of thin, long linear electrodes to minimize damage during the implantation since the electrodes must go through the cerebrum to access the thalamus or basal ganglia that is target tissue for stimulation. For selective stimulation, the electrode of the prostheses should have many stimulation contacts in small size, in other words, high resolution.

The DBS electrode in this study has 8 stimulation channels on four layers. Each layer has two channels, and each channel has a size of 50 μm × 160 μm. The electrode shank has a length of 8 mm, a width of 300 μm, and a thickness of 250 μm.

The width is determined concerning the fabrication process. Each layer has two channels on it, and each channel has 30 μm linewidth and 50 μm of spacing. And also, the margin for UV laser cutting is needed because the laser has 50 μm of spot size and error in alignment. The length needs concerning of *in vivo* experiment. Since the *in vivo* validation of this study is conducted in SD-rat and ventral posterolateral nucleus (VPL), the electrode needs to be longer than 6.6 mm, therefore 1.4 mm margin is given. About the thickness, it is needed to have more than 200 μm to have enough rigidity to penetrate the brain tissue. The size of the stimulation site is also determined concerning the *in vivo* experiment. Since the VPL of SD-rat is located from 4.8 mm to 6.6 mm in depth, the stimulation electrode should cover more than half of the VPL. Therefore, every channel of the electrode sites needs to be located within 1 mm length. Each channel has a height of 50 μm and a distance of 100 μm between channels. To minimize the electrochemical impedance, the width of the electrode sites are selected to be the largest value that can be given in consideration of the margin of the UV laser process.

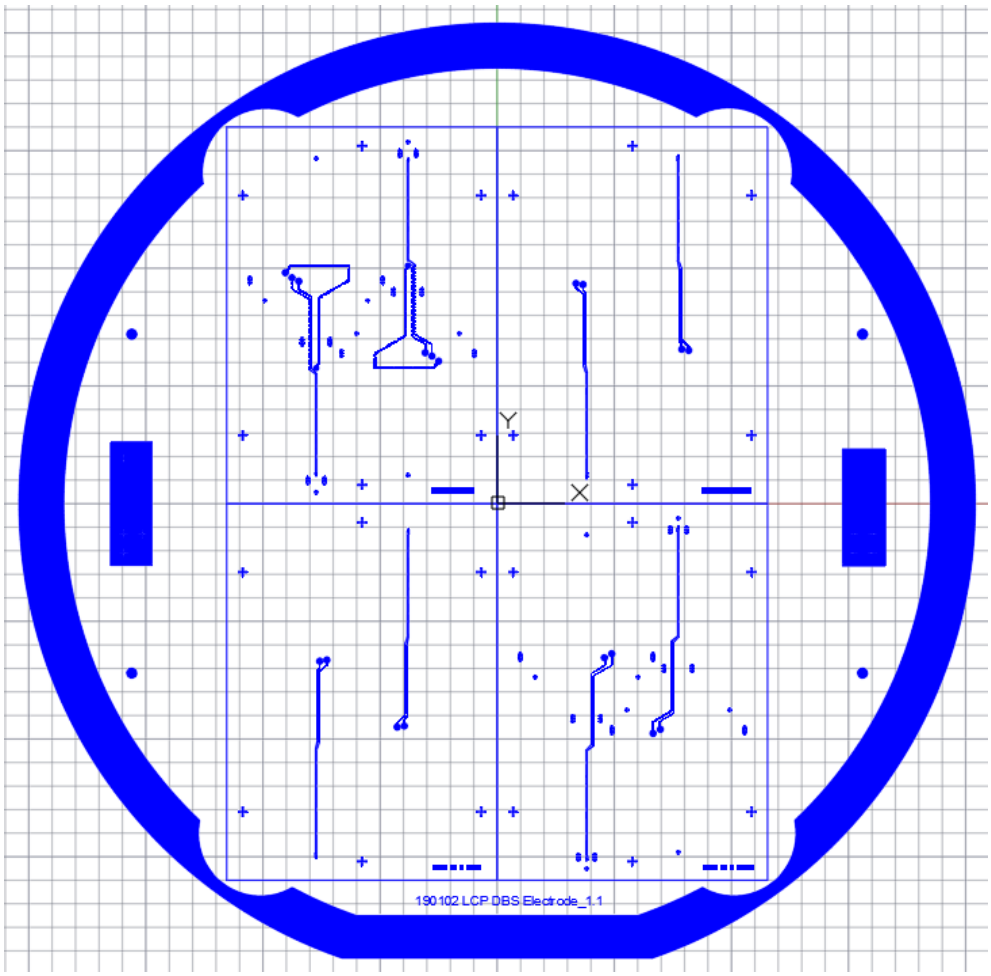

Figure 2-7. Mask for suggested DBS electrode. The mask implies a set of electrodes which are two 8-channel depth-type electrodes. The set has four layers where each layer contains two channels of each electrode. Conduction lines of each channel has a linewidth of 30 μm. In the bending area, the conduction lines have a wavy form to enhance stability during the high-temperature and high-pressure environment of thermal lamination.

To fabricate the electrodes with the design factors mentioned before, the design of the mask described in Figure 2-7. The mask is designed to define four electrode layers on a 4-inch wafer substrate. Each layer has electrode patterns of two devices, and each device has two-channel patterns in it. To ensure durability in the process with high stress such as the high-pressure process during lamination, the packaging with the spot welding, or the bending situation of the electrode, wavy line design is used to each channel in the feedthrough section. The designed layer structure of the electrode is shown in Figure 2-8. Each electrode layer is 25 μm thick, and a 15 μm thick interlayer is located between electrode layers. Above the 1st electrode layer, a 25 μm thickness cover layer is located to insulate the pattern. However, below the 4th electrode, there are support layers for providing extra thickness on the substrate. Since the package method is brazing with the lid, it is needed to secure the extra thickness to melt around.

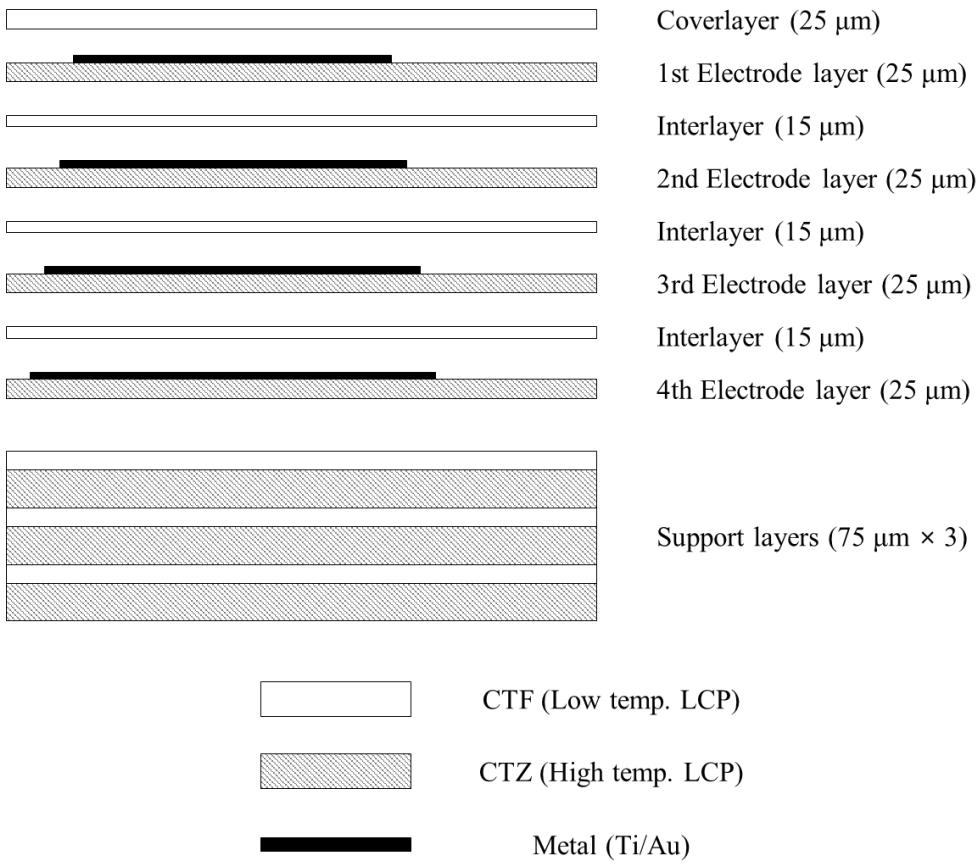

Figure 2-8. The layer structure of the designed DBS electrode. The stack has four electrode layers. Each electrode layer is made of 25 um thick high-temperature LCP film and has two conductor channels. To insulate the electrode layers, three interlayers made of 15 um thick low-temperature LCP film is located between the electrode layers and a cover layer made of 25 um thick low-temperature LCP film is located on the top of the electrode layer. To secure enough rigidity and thickness of the substrate, three 50 um thick high-temperature LCP films are added, and as adhesion layers, three 25 um thick low-temperature LCP films are located above the support layers.

2.2.1.3. Package

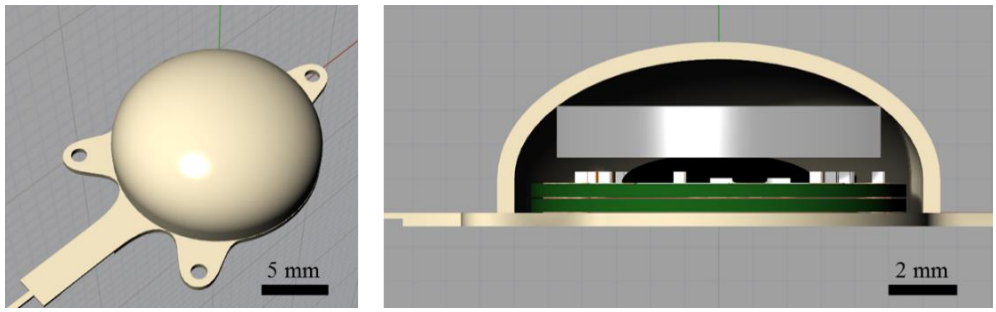

Figure 2-9. Designed package of the implantable device. The model in the left picture represents the perspective view of the implantable package. The package has a hemispherical shape with a diameter of 13 mm. The other picture shows the cross-sectional view of the package. The package encapsulates the stack of coil PCB, circuit PCB, assembled elements, and alignment magnet. The overall height of the package is 5 mm.

The package of the implantable device in the suggested system is the most important factor in miniaturization, which is one of the goals of this study. The design of the package affects not only the size of the package but also the method and size of the surgery. The most important factors of the package are the invasiveness and hermeticity.

Invasiveness refers to the damage that living tissue receives from the implantable device. Of course, as the size of the package decreases, the invasiveness is also likely to decrease, and even though the package sizes may be similar, there may be differences in surgical methods and physical stress applied to surround

tissues after implantation, depending on the shape and structure. It is also thought that the physical stimulus applied to surround tissues after implantation is also associated with inflammation. Therefore, a good package design is one that minimizes invasiveness.

Hermeticity is associated with damage in which the internal circuitry of the implant is affected by an *in vivo* environment. Since the *in vivo* environment is filled with the body fluid of the electrolyte, it is very harsh for the devices that make up the circuit, and organisms can also be affected by the toxic eluents from the circuit. Therefore, packages need the ability to isolate them from each other.

The package of the implantable device suggested in this study has decreased the height to minimum and a curved shape is adopted to minimize tissue injury from physical interaction with the package. shows the designed package, with the circuit PCB, coil PCB, circuit elements, and alignment magnet located inside 5 mm height package lid. The package lid is made by thermal deformation with five LCP films of 100 μm thickness in a custom-made aluminum jig to shape this half-ellipsoidal structure.

2.2.2. Fabrication

2.2.2.1. Electrode

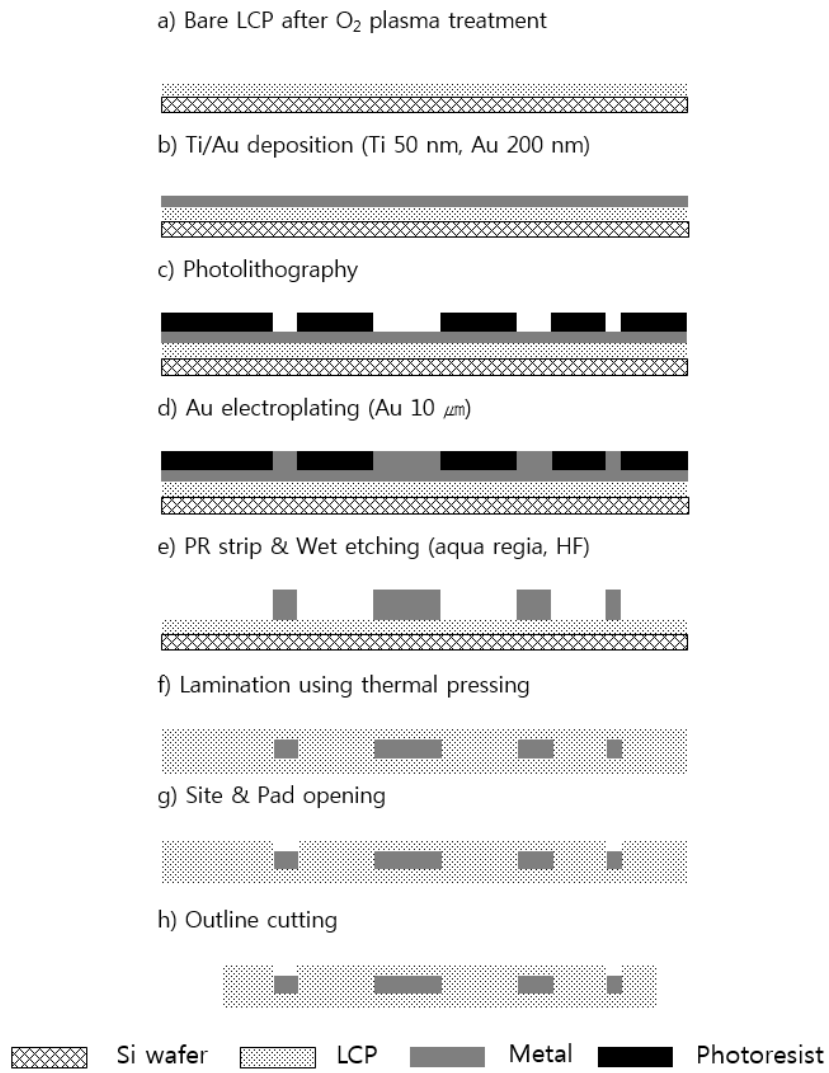

Figure 2-10. MEMS-based electrode fabrication process on LCP. a) Surface treatment using O2 plasma on bare LCP film; b) Metal seed layers of 50 nm Ti and 200 nm Au films deposition using E-gun evaporation; c) Photolithography using negative PR on metal seed layers; d) Electroplating of 10 μm thick Au film; e) Stripping PR and etching metal seed layers; f) Lamination using thermal pressing; g) Site and pad opening using laser ablation; h) Outline cutting using laser process.

The fabrication of the electrode is based on the MEMS process. Since the LCP is chemically inert and mechanically stable, it is suitable for the MEMS process. The MEMS process on the LCP substrate has been reported in previous studies [86]–[89]. The step-by-step fabrication process is briefly shown in Figure 2-10.

Before the MEMS process, a substrate LCP film is prepared by detaching from the source roll along a predesigned outline is defined by laser cutting. The outline contains align keys for stacking during lamination. After the cutting, film cleaning is conducted using methanol, acetone, and isopropyl alcohol. The substrate film is cleaned by soaking in these three solvents, from polar to non-polar order for one minute each.

a) As the first step of the MEMS process, the LCP film is fixed on a bare Si wafer. After the fixation, surface treatment process using plasma using reactive ion etcher (RIE 80 plus, Oxford Instrument, Abingdon, UK) under O_2 100 sccm, 0.1 mTorr, 150 W, 3 min. is conducted to activate the surface of the substrate film for improving the adhesion between the film and metal seed layer.

b) Metal seed layers of 50 nm thick Ti and 200 nm thick Au are deposited on the substrate by e-gun evaporator (ZZS550-2/D, Maestech, Seoul, Korea) in 5×

10^{-6} Torr chamber, at 3.0 Å/s deposition rate. The Ti film acts as an adhesion between the LCP film and Au.

c) After the metal seed layer deposition, a photolithography process is conducted. For the uniform application of photoresist (PR) for the photolithography process, uniform and firm adhesion between the handling wafer and the substrate film is needed. For this purpose, spin-coated silicone elastomer (MED-6233, NUSIL, Carpinteria, CA, USA) is used as an adhesive. The adhesion is based on van der Waals force between the substrate and the elastomer layer. The elastomer coating is using 3 mL of silicone elastomer to coat a 4-inch wafer. The coating is done at 2500 RPM for 100 seconds. After the coating, the elastomer is cured at 100 °C for at least 2 hours. A negative PR (AZ4620, Clariant, NJ, USA) is used for the photolithography. Spin coating of the PR is aided by hexamethyldisilazane (also known as HMDS) as an adhesive between the Au surface of the substrate and the PR. The PR coating is done for 40 seconds at 2000 RPM, and the coating is baked at 110 °C for 80 seconds. Patterns of the mask in Figure 2-7 are built on the metal seed layer with 10 μm using an aligner (MA6/BA6, SUSS MicroTec, Garching, Germany) for 70 seconds of exposing time.

d) After the photolithography, the patterns defined by photolithography are electroplated with gold up to 10 μm thickness. The electroplating process is done by outsourcing (Sung Won Forming, Ansan, Korea).

e) To isolate the conductors, the seed layer needs to be removed. First, the photoresist is stripped using PR stripper and wet etching is conducted to remove the metal seed layers. The Au layer is etched by aqua regia ($HCl : HNO_3 = 3 : 1$). Since the patterns are 10 μm thick and the Au seed layer is 200 nm thick, the seed layer dissolves in seconds while the patterns keep more than 9 μm of thickness. In the same way, the Ti seed layer is etched by a diluted HF solution. The wet etching completes the MEMS process part of the fabrication.

f) After the wet etching, the substrate film is detached from the wafer and every four layers of electrode described in Figure 2-8 and align holes are cut by UV laser (Samurai UV Laser marking system, DPSS Laser Inc., CA, USA) under 80% of laser power, 100 mm/s of marking speed, 20 kHz of frequency, and 20 μs of pulse width. Other layers are cut from bare LCP film by a UV laser process to prepare a cover layer, interlayers, and support layers at the same condition. The prepared layers are stacked on a lamination zig as shown in Figure 2-8 and thermal pressing

lamination is done. At the temperature of 286 ˚C, pressing force equivalent to the weight of 20 kgf is applied for 30 minutes.

g) After the lamination, electrode sites for facing target tissue and terminal pads for connecting the electrode with the pulse generator circuit are exposed by a laser ablation process. The laser ablation is performed in the same workbench with the laser cutting, but with 10 times mark speed of the cutting process. The increase of the marking speed results in the decrease of exposure time to the laser, therefore the power propagated to the LCP substrate from the laser source is decreased. Since the ablation targets are areas, not lines like the cutting process but the laser marks linear traces, paths of the laser ablation need to be elaborately designed as shown in Figure 2-11. Each ablation path has 4 directions consist of vertical, horizontal, diagonal_L, diagonal_R. And, each direction has 2 layers. For a layer, parallel lines with a spacing of 50 μm are located along the design, and the other layer in the same direction has 25 μm displacement in the parallel direction. Using this pathway and the marking speed of 1000 mm/s, 1 μm of the LCP ablated during a cycle of 8 layers.

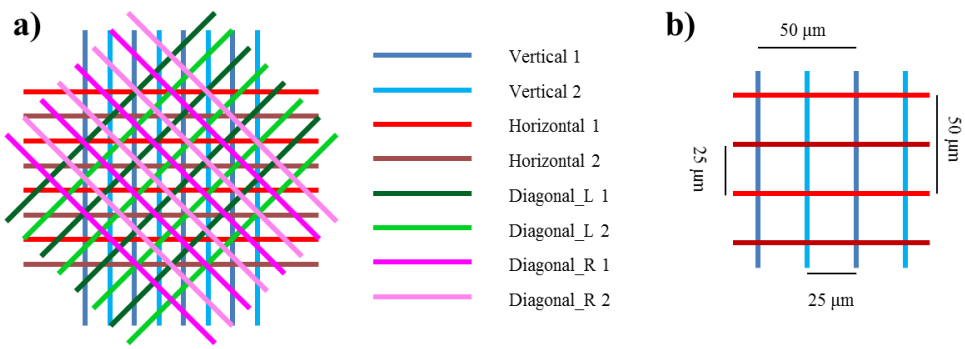

Figure 2-11. The laser path patterns for laser ablation. a) Each ablation path has 4 directions consist of vertical, horizontal, diagonal_L, and diagonal_R. And each direction has 2 layers. b) A layer has linear paths spacing 50 μm, and the other layer having the same direction is 25 μm displaced in parallel.

After the pad & site opening, the backside of the electrode region is thinned by UV laser in two steps using the same conditions with the ablation. The first step is applied to the entire electrode shank area. This step makes the thickness of the electrode between 200 ~ 250 μm by paring away the extra thickness. The range of the thickness is considered to be appropriate thickness for the LCP-DBS electrode because the range is the minimum thickness to minimize the tissue damage during the electrode implantation with enough rigidity for brain tissue penetration.

The second step is a thinning process for the electrode shank to bend. Since the electrode has to approach the deep brain from the outside, the electrode is aligned with the normal direction of the skull, but the package has to minimize the height, therefore, a thin flat package that sticks along the skull surface is considered as desirable design. Thus, the package and the electrode have to overcome the difference, by bending a certain part of the electrode. To achieve the bending, a certain region of the electrode has to be thinned into 170 μm thickness. The bending zone is 4 mm long, 2 mm wide. To enhance physical stability of the bending zone, wavy line is applied. The wavy line has been suggested in previous study of Jeong, *et al.*, in [90]. Figure 2-12 shows the design factors of the wavy line. In this study, the line width of the segments is 25 μm, and the angle of a unit segment is 240 °. Therefore the global width of the wavy line is determined to have 114.8 μm.

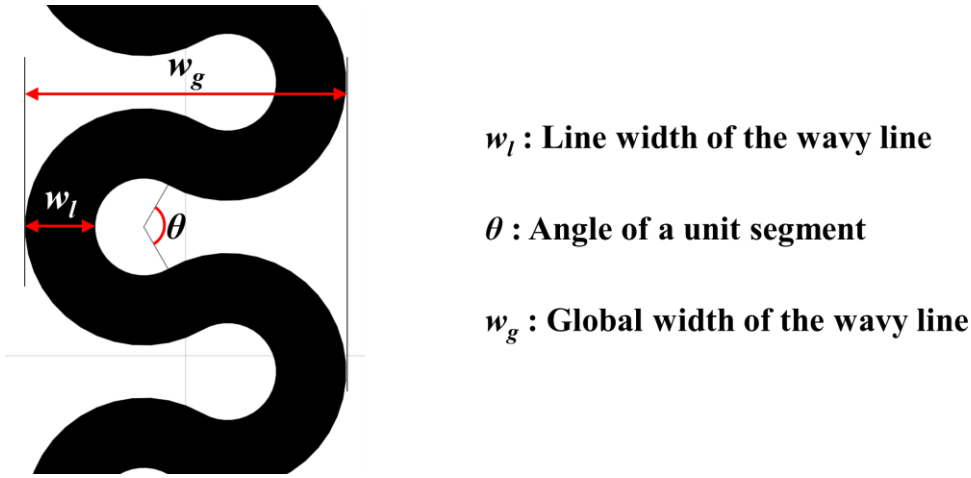

Figure 2-12. Design factors of the wavy line. In this study, the line width of the wavy line, w_l is 25 μm, the angle of a unit angle, θ is 240 °, and therefore the global width of the wavy line, w_g is 114.8 μm.

h) Finally, the electrode is cut out of the substrate by the UV laser cutting process. The most important factor of the outline cutting is aligning. Predefined align keys are crosses with linewidth of 1 μm patterned by MEMS process. Considering the possibility of misalignment, the outline is designed with a margin of 50 μm compared to the original design.

2.2.2.2. Circuitry

The circuit of the implantable device is fabricated in FR-4 based PCB. The circuit board is round with 11 mm diameter, 0.4 mm thick, patterned with copper. As shown in Figure 2-13, the ASIC chip should be placed in the center of the board since the chip has the biggest height due to its need for a protective epoxy coating. Surrounding the chip, 3.3 V regulator, Zener diodes, electrode terminals with DC block capacitors, and other discrete components are located. Since the circuit PCB must be connected with the coil at the bottom, every circuit element should be located on the top.

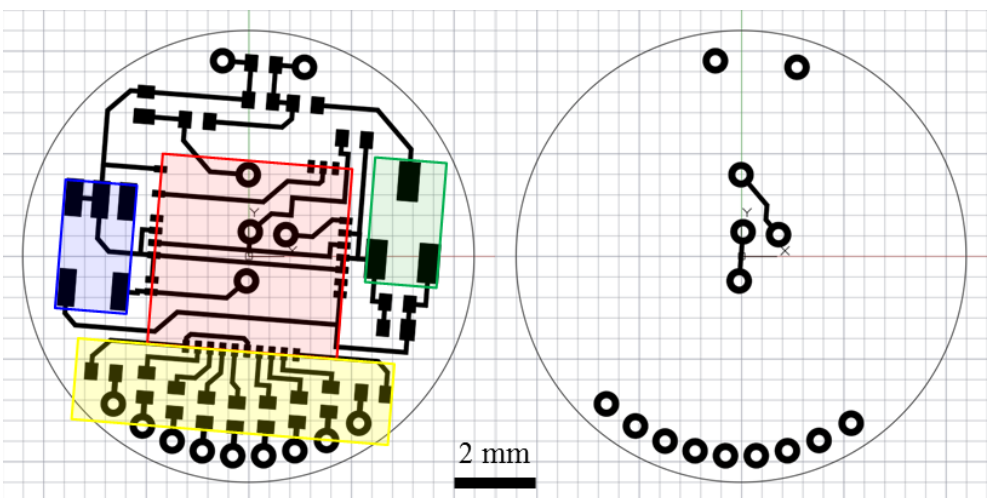

Figure 2-13. Layout designs of the implantable device circuit top(left) and bottom(right). The top layer has footprints for the stimulator ASIC chip (red box in the center), regulator (blue box in the left), Zener diodes (green box in the right), and electrode terminals DC block capacitors (yellow box in the below). The rest is containing tuning capacitors for the inductive link, resistors and capacitors for power and data circuit, and through hole vias for circuit-coil connection and circuit-electrode connection.

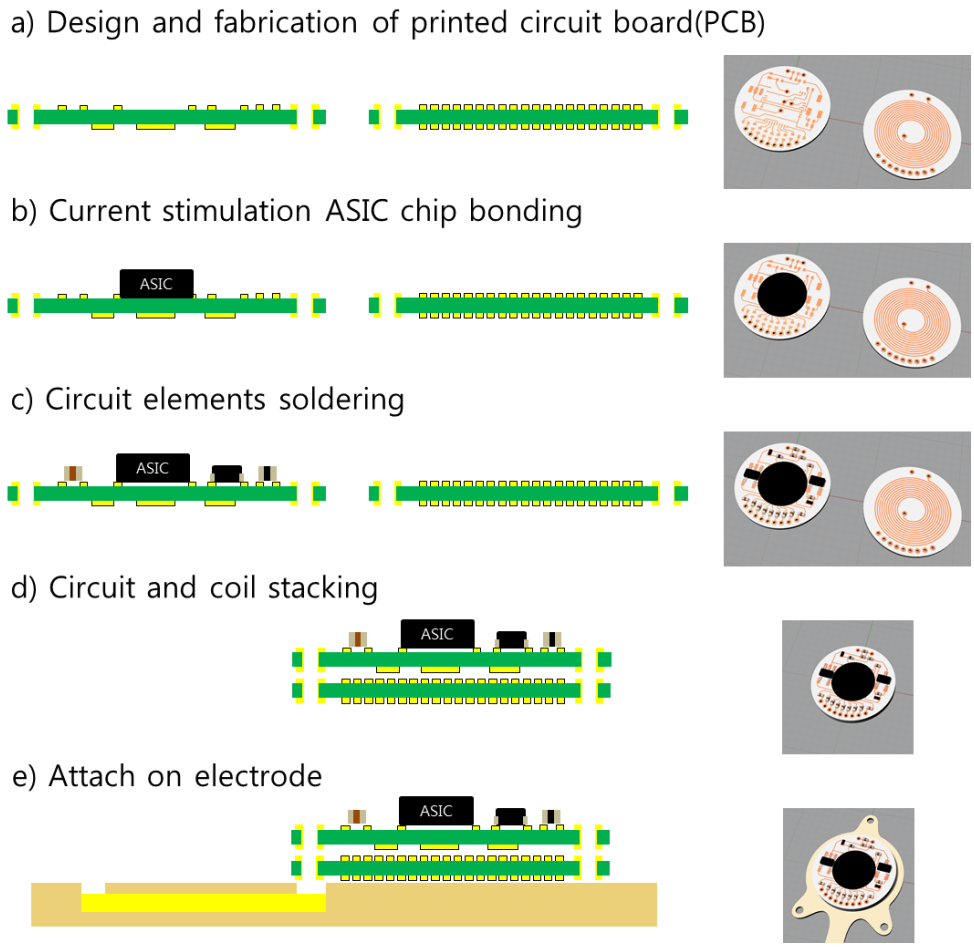

Figure 2-14. Circuit assembly process. a) Design and fabrication of circuit and coil PCB. The PCB is designed by OrCAD and fabricated by outsourcing. b) The current stimulation ASIC chip is bonded by wedge bonder and protective epoxy. c) Surface mountable discrete elements containing a regulator, diodes, resistors, and capacitors are soldered on the top layer of the circuit PCB. d) The circuit and coil boards are stacked by soldering. Through hole vias are used for two circuit-coil connections and nine circuit-electrode connections. The circuit-electrode terminals have convex forms to connect with the electrode pads. e) The circuit-coil complex is attached to the top of the electrode substrate with superglue and the electrode terminals are connected with the pad using silver-based conductive epoxy. The conductive epoxy is cured at 110 °C for 30 minutes.

Assembly of the circuitry is shown in Figure 2-14.

a) First, the designed PCB board of the circuit and coil are designed using OrCAD (Cadence Design Systems, San Jose, CA, USA) and fabricated by outsourcing (Hansaem Digitec, Incheon, Korea). Each of the PCBs is made of FR-4, have a thickness of 0.2 mm. The patterns are copper lines of 15 μm thick.

b) The stimulation ASIC chip is bonded on the circuit using wedge bonder and coated with protective epoxy. The bonding and epoxy coating process is done by outsourcing (Ilchang Electronics, Seoul, Korea).

c) The rest of the circuit containing a regulator, diodes, resistors, and capacitors are surface mountable discrete elements. These devices are soldered on the top layer of the circuit board.

d) The circuit board and the coil board are connected by soldering using through-hole via. There are two vias to connect circuit and coil, and nine vias to connect electrode terminals with electrode pads. For ensuring the firm connection of the via to the electrode, each via of channel terminals is soldered to have a convex form.

e) The most important part of this step is aligning the circuit complex with the electrode treated with conductive epoxy. Silver-based conductive epoxy (EPO-TEK® H20E, Epoxy Technology, MA, USA) is filled in the holes where the pad ablations have been performed. Then the prepared circuit complex is attached to the electrode with superglue and the epoxy is cured on the hot plate at 110 °C for more than 30 minutes.

2.2.2.3. Packaging

The packaging of the implantable device for the LCP-based miniaturized DBS system is defined as insulating the internal circuit from the outside. Since the LCP is thermoplastic polymer, basis of the packaging process is thermal bonding. In several previous studies, packaging is based on thermal pressing [88]. The thermal pressing is applying high temperature and high pressure by thermal press to the zig that is containing circuit and covers to be packaged. The pressing zig contains a LCP-based substrate with the circuit on it, a cover, and the LCP powder to fill the space inside the package. Although this is a very good method for fabricating robust and long-term reliable package, it has several disadvantages.

The package and the pressing jig shall be designed so that the pressure is evenly distributed throughout the package during the packaging process. Therefore, the LCP substrate used in this method shall have a circular shape in the XY plane and a concave form in the Z-axis direction so that the pressure applied in the negative direction of the Z-axis can be distributed evenly in three dimensions. In addition, substrates of the internal circuit and coil should be made from LCP-based FPCBs to withstand the high-temperature high-pressure packaging process, and silver epoxy should be used instead of solder to secure the element to this FPCB. This FPCB, in particular, if the pressure becomes uneven during the thermal pressing process, an open circuit on the FPCB or a short circuit between different layers. This is the biggest factor in lowering the yield of thermal pressing. The substrate made of these FPCBs should have a concave form that can contain the circuit and LCP powder, as mentioned above. This concave is formed by the thermal deformation. Thermal deformation is a process that transforms LCP substrates by applying relatively low pressure and temperature around the glass transition temperature. During this process, the yield is reduced due to short or snap of coil and circuit layers. This is the same in the thermal pressing process that takes place after the deformation. Even after this packaging method, it is not easy to find out what is the problem in the process

because it becomes a monolithic package full of LCP chunk integrated from the powder.

To overcome these problems, a method called ‘spot welding’ is used. To avoid the problems originating from the fact that the whole package is exposed to the high temperature and pressure, spot welding is using a method of bonding by applying high temperature in locally limited areas. The method is first proposed in the previous study by Yun *et al*.[91]

The first step of the packaging is fabricating package lids. The package lid has 5 mm of height and 13 mm of diameter on the outside. The lid is fabricated by thermal pressing. A pressing jig made of aluminum shown in Figure 2-15 a), and the cross-sectional profile of the structure is described in b). Since the lid should have 500 μm of thickness, and 100 μm of thickness is the thickest sheet we have, the lid needs to be deformed and laminated at once. Therefore, to fabricate lids, three CTZ films and two CTF films with a thickness of 100 μm are alternately stacked between the top and bottom of the jig.

The lamination and thermal deformation process are performed at a temperature of 285 ˚C, the pressure of more than 100 kgf for 30 minutes. After 30

minutes of process, the pressure is sustained until the temperature goes lower than 100 ˚C.

From a thermal deformation process, an LCP substrate with 5 package lid is fabricated. After the process, each lid is cut into a hat shape with a rim 2mm wide from the substrate for use in the packaging, and a cylindrical neodymium magnet with a diameter of 8 mm and a thickness of 1 mm is affixed at the center of it.

After that, the spot welding is used to seal the implantable device. The spot welding is a technique that is reported in a previous study [91], which uses a soldering iron to melt and bond LCP substrates by applying a high temperature of 350 to 400 ˚C locally.

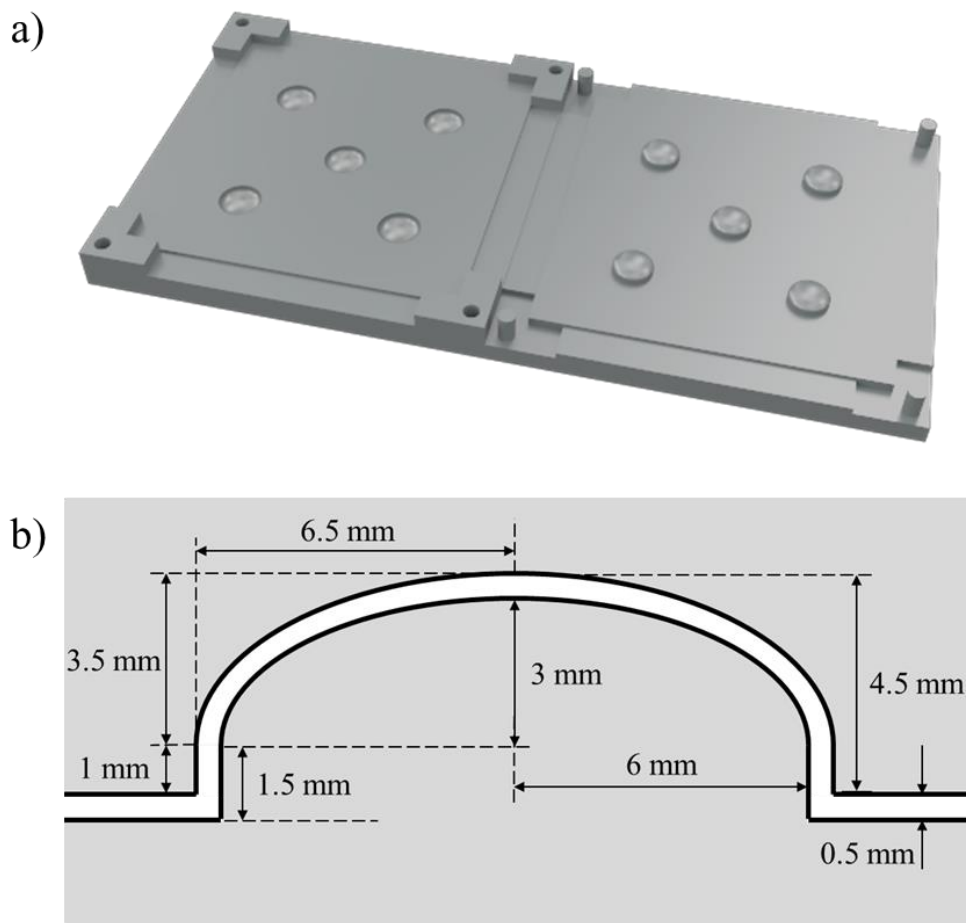

Figure 2-15. The pressing jig for fabricating package lid. a) A 3D model of the pressing jigs. The jigs have five convex and concave structures on the upper piece and the bottom piece. Therefore, a thermal deformation process generates five package lids. b) A cross-sectional profile of the deformation structure. The thickness of the lid is 500 μm, and the overall height of the lid is 5 mm.

2.3. External Device

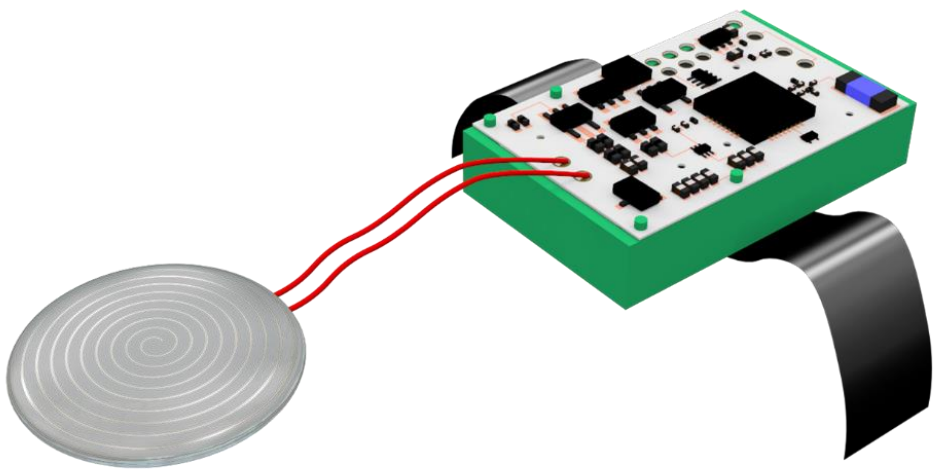

Figure 2-16. Conceptual 3D design of the external device.

The external device is designed to deliver power and data to the implantable device via the inductive link. If the stimulation parameter information is transferred by a handheld remote controller via ZigBee protocol. After receiving the information, the external device interprets the signal into PWM waveform which the implantable device can handle. To minimize the size of the implantable device, the power for generating the stimulation pulses is delivered from the external device. Therefore, it is a battery-powered device. Main factors to evaluate the effectiveness of the external device is two things. One is a recharge cycle, and the other is size and weight. If the device has short recharge cycle, it would be very inconvenience for the patient.

However, to have longer recharge cycle, the battery should get bigger. Concerning the inconvenience of the user, massive battery is not desirable for user, too.

2.3.1. Circuit Description

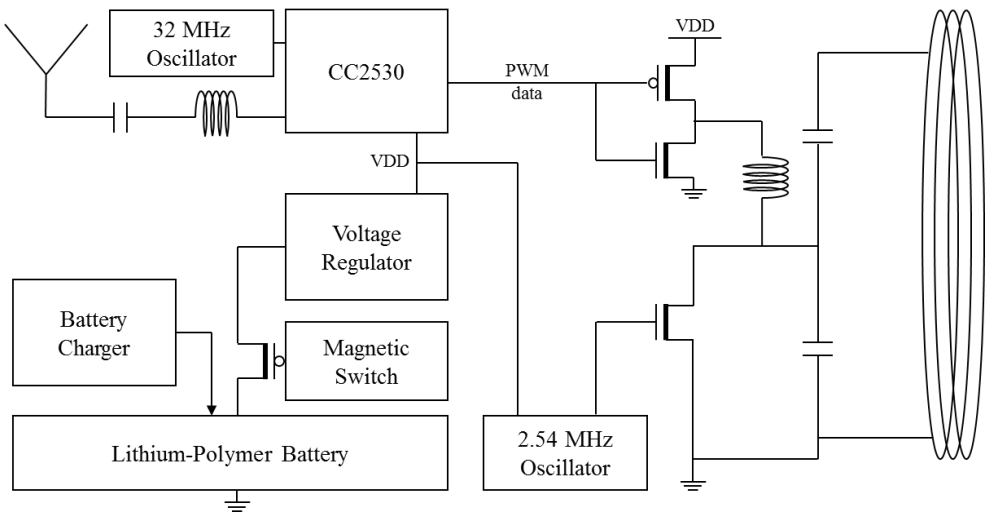

Figure 2-17. Block diagram for the external device. The device is powered by a Li-Po battery, which can be recharged via a battery charger. A magnetic switch gates the power flow of the battery, and the voltage regulator shifts the voltage level for the digital part of the circuit. The stimulation parameter is picked up by the ZigBee antenna and delivered to a ZigBee module included MCU, and the MCU translates the information into a PWM signal used to gate the class-E amplifier. The class-E amplifier uses 2.54 MHz RF as carrier frequency, and the PWM signal is encoded to the carrier frequency. The modulated signal is transferred to the implantable device via an inductive link from a TX coil to an RX coil. Since the inductive link transfers power and data to operate the implantable device, the implantable device can be miniaturized by removing the battery.

The block diagram of the external device is shown in Figure 2-17. The circuit consists of a power module, a ZigBee module, and the class-E amplifier. It is controlled by the parameters received through the ZigBee protocol from the handheld controller. The handheld controller used in this study is designed by Shim *et al.*, reported in [92].

The power module is a circuit that manages the 3.7 V Li-Po battery. A battery charger is a circuit for charging the battery from DC inputs. A magnetic switch and a D flip-flop are used to manage power supply of the whole system by gating the battery output. And a 3.3 V voltage regulator is placed to provide operation voltage to the ZigBee module and class-E amplifier.

The ZigBee signal received via an antenna (2450AT42A100E, Johanson Technology Inc., USA) is decoded into stimulation pulse parameters by a MCU (CC2530, Texas Instrument, USA). The MCU is programmed to generate one bit serial PWM signal based on the parameters according to the data protocol described in . As shown in the table, the parameters are including pulse rate, duration, amplitude, and sites. The PWM signal is one-bit serial data, which has a 127 kbps data rate. Each bit has a value of '0', '1', or 'F'. '0' and '1' are typical binary data, which are implemented as 25 % and 75 % of duration is high, where 'F' is an end-

of-frame implemented as 50 % of duration is high. A word is 18-bit long including ‘F’ bits at the first and the last of the word. Each word has a parity bit for even parity checking.

The class-E amplifier produces 2.54 MHz carrier frequency. The serial PWM signal is applied to the amplifier circuit as a switch, and then the 2.5 MHz carrier frequency is encoded with serial PWM signal. The PWM encoded carrier frequency is transferred to the implantable device via inductive link by transmitter coil.

Table 2. Data protocol of the stimulation ASIC chip.
(F = Frame, PR = pulse rate, P= Parity, PB = pulse puffer, DR = duration, CH = channel setting, S = site selection, A = amplitude).

Bits	17	16	15	14	13	12	11	10	9	8	7	6	5	4	3	2	1	0
PR set	F	0	0	0	X	X	PR0	PR1	PR2	PR3	PR4	PR5	X	X	X	X	P	F
DR set	F	0	0	1	PB0	PB1	DR0	DR1	DR2	DR3	DR4	DR5	X	X	X	X	P	F
AM set	F	0	1	0	CH0	CH1	AM0	AM1	AM2	AM3	AM4	AM5	AM6	AM7	AM8	AM9	P	F
S set	F	0	1	1	CH0	CH1	S0	S1	S2	S3	PB0	PB1	M/B	ON	X	X	P	F
Stim on	F	1	0	0	X	X	X	X	X	X	X	X	X	X	X	X	P	F
Stim off	F	1	0	1	X	X	X	X	X	X	X	X	X	X	X	X	P	F

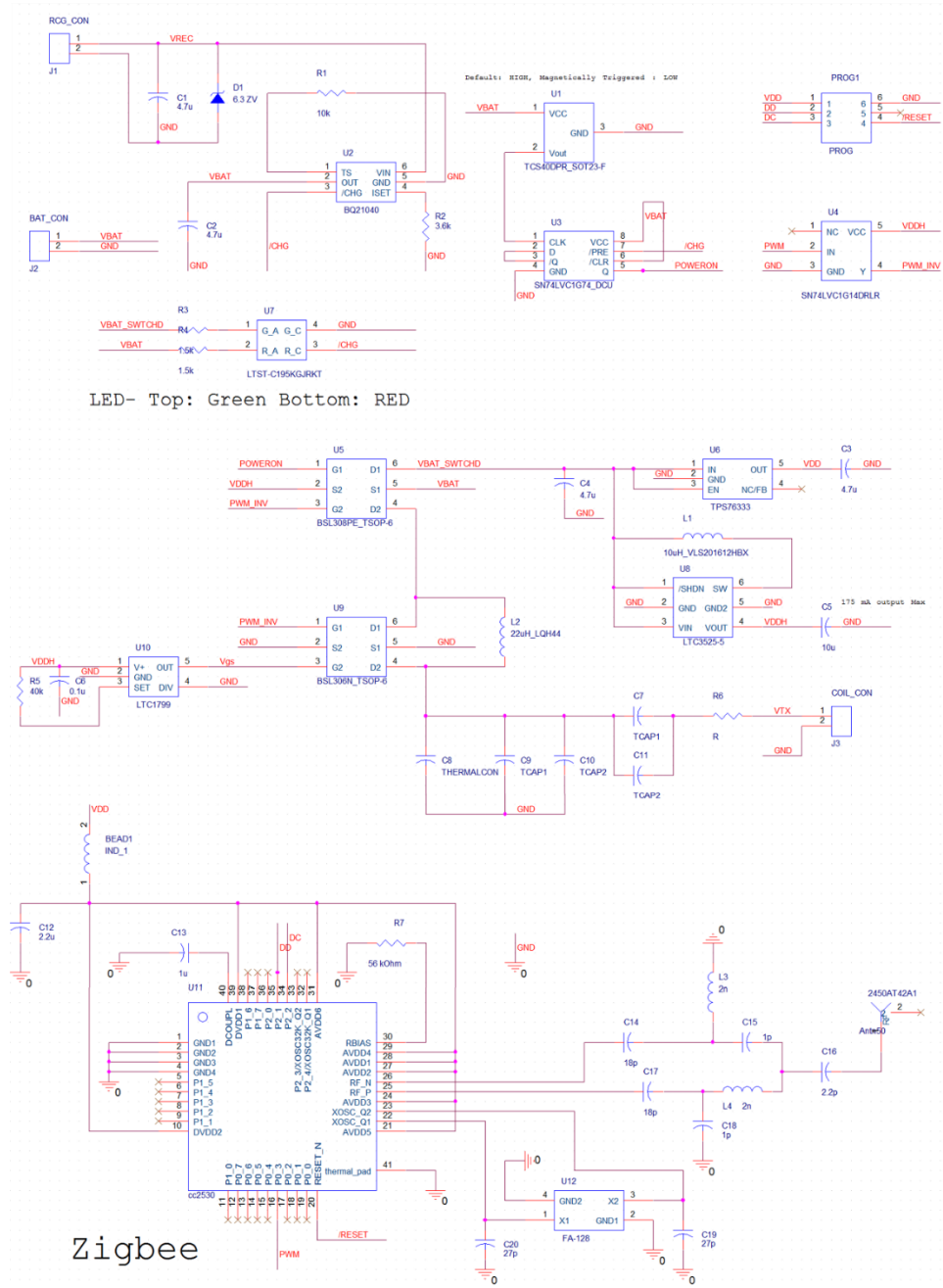

Figure 2-18. Schematic diagram of external device.

2.4. Evaluations

2.4.1. FEM simulation on RF radiation

Since the proposed system transfers power to the implantable device from the external via the inductive link using RF, it is necessary to check the RF radiation safety issue. To verify the RF radiation safety of the proposed system, a specific absorption rate (SAR) is calculated by FEM simulation using ANSYS HFSS (ANSYS Inc., PA, USA) over a model.

The SAR is a value that indicates how much energy the living tissue absorbs when exposed to RF or electromagnetic fields. It is defined as the absorbed power over tissue mass and has the unit of watts per kilogram (W/kg). The formula below is the formula of the SAR, which is calculated based on the electric field [93].

$$SAR = \frac{1}{\mathrm{V}} \int \frac{\sigma(\boldsymbol{r})|\mathbf{E}(\boldsymbol{r})|^2}{\rho(\boldsymbol{r})} d\boldsymbol{r} \ \ [\mathrm{W/kg}] \ \ (\text{ for } 100 \text{ kHz} \sim 10 \text{ GHz})$$

where σ is electric conductivity in Siemens per meter (S/m), **E** is a root-mean-square of the electric field in Volt per meter (V/m), and ρ is the density of the sample in kilogram per cubic meter (kg/m^3).

Since SAR is used as an indicator for official safety tests administered by public authorities, as we can see in 47 CFR 1.1310, there is a clear baseline.

Therefore, it is possible to demonstrate whether the model of the system presented in this study exceeds the corresponding threshold for the human model.

The simulation parameters are listed in Table 3. The simulation model is having 60 mm by 60 mm field in the x-y plane, and the thicknesses are selected as above. Since the proposed system assumes that the external device is above the parietal part of the head, the model of the skull and scalp is determined to have the thickness of the parietal part of the human head. Since the TX coil is going to be molded by silicone elastomer with 2 mm thickness, the coil in the model is 1 mm distant from the surface of the scalp. To verify the concentrating effect of the RX coil, two situations are supposed. One is called the TX coil only model, which represents the situation that only the TX coil is located on the scalp of a human. The other is the RX coil included model, which represents the situation that the RX coil is encapsulated in a package made of LCP.

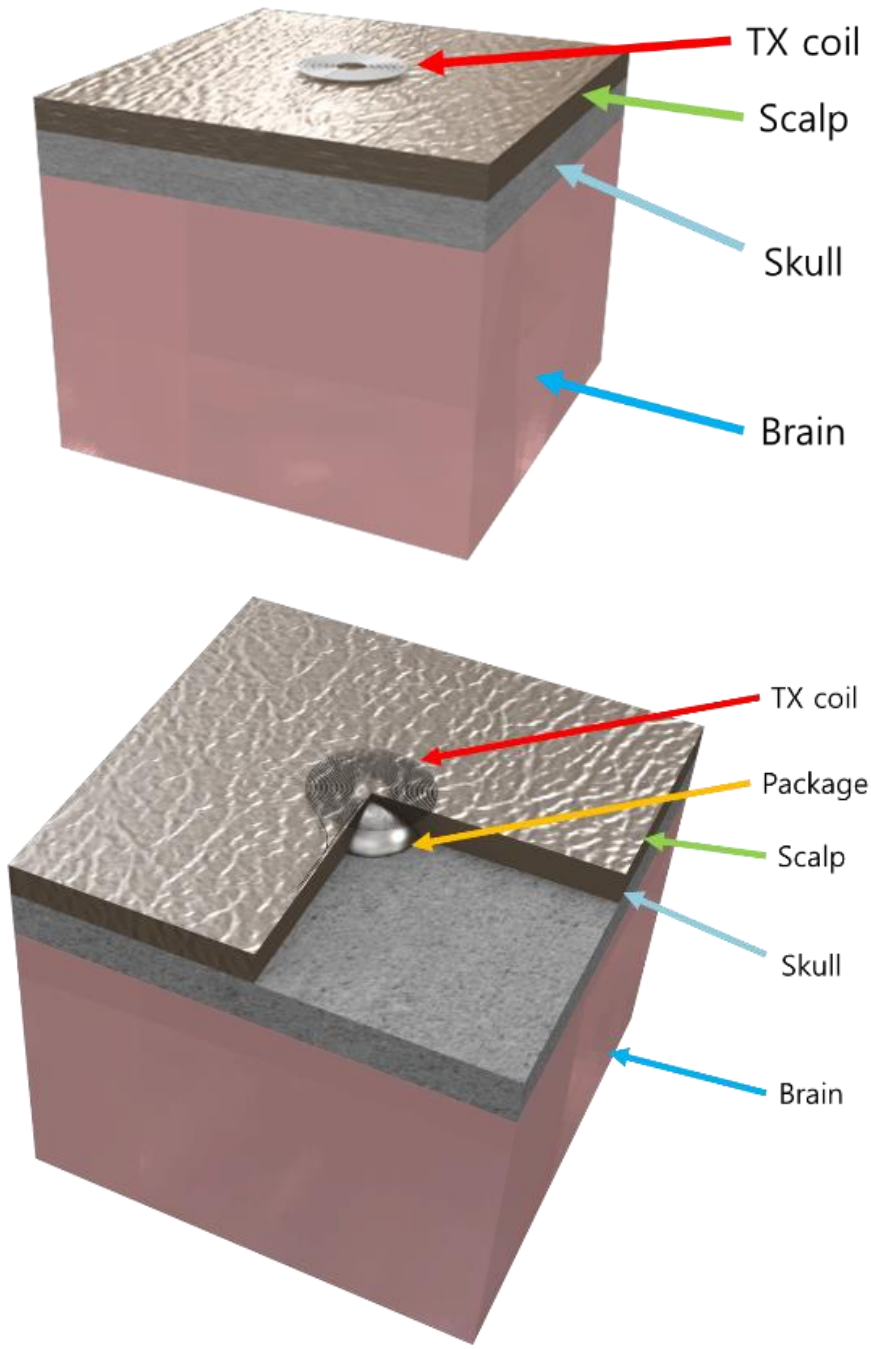

Figure 2-19. 3D model of the FEM simulation for SAR analysis. The TX coil only model (left) and RX coil included model(right)

Table 3. Parameters for FEM analysis for SAR model. The model supposes to be the parietal part of the human head, therefore the thicknesses of the scalp and skull are determined as below.

Tissue	Thickness [mm]	Conductivity [S/m]	Relative Permittivity	Relative Permeability
Scalp	4.284 [94]	0.0512 [95]	795 [95]	
Skull	5.915 [97]	0.0304 [95]	92.4 [95]	1 [96]
Brain	40	0.220 [95]	855 [95]	
LCP	0.5	10^{-17}	3.3	1

Four planes have been selected to be analyzed. 1) cross-sectional plane including the center point of the modeled TX coil, 2) air-scalp interface, 3) scalp-skull interface, and 4) skull-brain interface. 2-dimensional profiles of SAR on each plane are derived, and the peak value of the SAR is gathered.

2.4.2. In vitro test

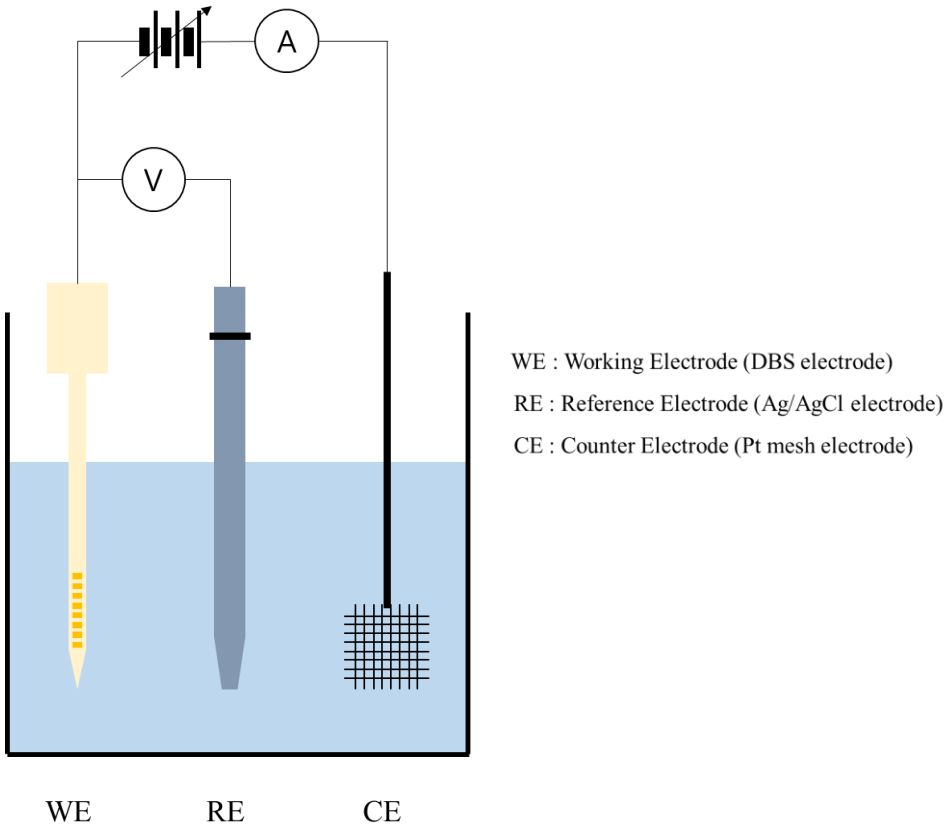

Figure 2-20. Overview of electrochemical impedance spectroscopy (EIS) setup. The system is as known as the three electrode system. The working electrode (WE) is an electrode under test, which is the DBS electrode here. The reference electrode (RE) is an Ag/AgCl electrode which sets the reference potential of the electrolyte. The counter electrode (CE) is an Pt mesh electrode, which is the counterpart of the working electrode. By measuring the voltage across WE-RE and the current across WE-CE, the electrochemical impedance and CSC_C can be calculated.

Since the *in vivo* environment is surrounded by physiological fluid, which is an electrolyte, the electrochemical properties of the electrodes must be analyzed to evaluate the performance of the neural electrode. To verify the electrochemical characteristics of the fabricated electrode, *in vitro* test using a 3-electrode system impedance analyzer (Solartron 1260/1287, AMETEK, UK). The topology of the 3-electrode system is shown in Figure 2-20. The device under test is connected as a working electrode, an Ag/AgCl electrode is connected as a reference electrode, a Pt mesh electrode is connected as a counter electrode, respectively, and all those electrodes are soaked in phosphate-buffered solution(PBS). Electrochemical impedance spectroscopy (EIS) and cyclic voltammetry are common techniques for electrochemical characterization of neural electrodes [98].

EIS is a method of measuring the electrical impedance by analyzing the current according to the frequency when a sinusoidal voltage is applied to the neural electrode immersed in the electrolyte solution. The typical test setting is a frequency range of 1 Hz to 105 Hz and voltage amplitude of 10 mV. The resistive conduction of the electrode and the charge transfer of the electrode-electrolyte interface are two main factors of the electrochemical impedance. Because the charge transfer can be modeled as a capacitive component, it converges to a very small value compared to

the resistive component at high frequency. Therefore, the resistive contribution of the electrode can be observed by measuring the high-frequency impedance [98].

The CV is a measuring technique which is conducted in a three-electrode system. The potential of the working electrode is swept between two-point cyclically. The typical sweep range is between -0.6 V and 0.8 V at between 1 to 100 mV/s scan rate [98]–[100]. The cathodic charge storage capacity(CSC_C) is calculated as the integral over time of the cathodic current [101].

2.4.3. *In vivo* Animal Experiment

To validate the proposed DBS system, an *in vivo* experiment is needed to be carried out. Rat is chosen as the animal subject for the *in vivo* experiment because it is widely used in various neuroscience researches including neuromodulation or DBS [102]–[108]. Thus, there are already several models have been reported that can be adopted to validate the efficacy of DBS stimulation [109]–[113]. Besides, in terms of validation of the miniaturized DBS system, since the rats are very small animals compared to humans, so head-mounting the device in rats means that the device is head-mountable in humans.

The main difference between the conventional DBS system and the suggested miniaturized DBS system is that the conventional system is modular, but our system is compact and monolithic. The monolithic system may be beneficial for package reliability or miniaturization, but implantation methods distinguished from the method for existing systems should be devised. Since the implantable device is monolithic, the implantation changes

Thus, the implant method for the *in vivo* experiments to verify this system is designed in the following ways, as shown in Figure 2-21.

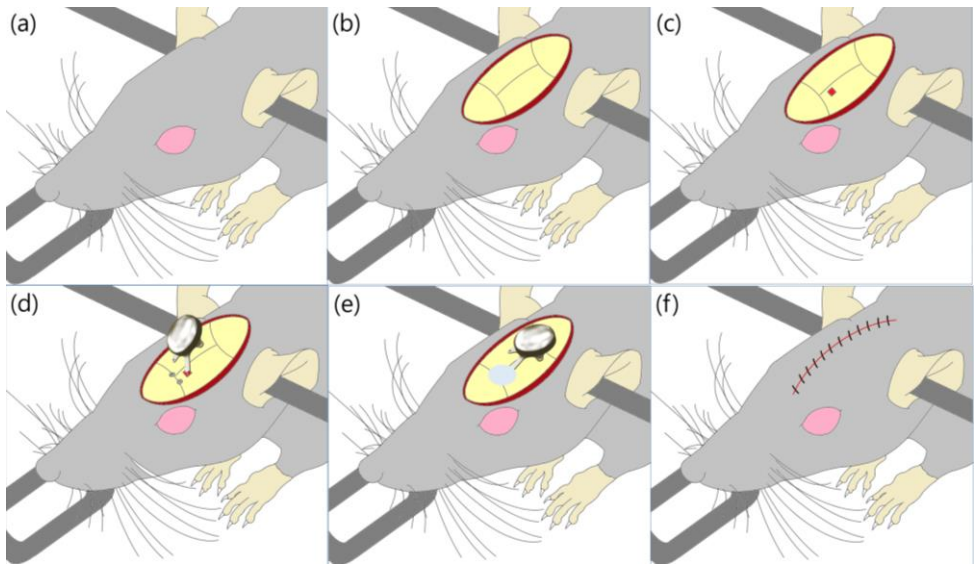

Figure 2-21. Implantation process of LCP-DBS on rat. a) The rat is anesthetized and fixed in a stereotaxic surgical instrument. b) An incision on the scalp of the rat is made, and the bleeding from the capillary around the skull is stopped by lesioning. c) A hole is drilled on the skull according to the coordination of the target tissue. d) The electrode is implanted. To assure the straight implantation of the electrode, a custom designed device holder is used to fix the device to the arm of the surgical instrument. e) After the electrode implantation, the bending zone of the electrode is folded to fix the package of the device with skull using surgical resin on the burr hole. After that, the package is placed parallel to the skull. Surgical screws and resin are applied to holes of the package to affix the package along with the skull. f) After fixing the package, the incision is sutured.

Figure 2-21 shows a step by step process for the implantation of the suggested DBS system. a) the rat is anesthetized and fixed in a stereotaxic surgical instrument, b) incision on the scalp is made, clean up bleeding around the skull. c) create a drill on the skull according to the coordination of the target tissue. d) the electrode is implanted. To assure the straight implantation of the electrode, a custom designed device holder is made to fix the device to the arm of the surgical instrument, e) After the package is implanted, the device is fixed with skull using a surgical resin on the burr hole, then the package part is folded and placed parallel to the skull. Surgical screws or resins are applied to holes of the package to affix the package along with the skull. f) After fixing the package, the scalp is sutured.

To demonstrate the efficacy of the system, an *in vivo* behavioral test using the suggested DBS system is conducted. The neuropathic pain model rat implemented by the spared nerve injury (SNI) method is selected as the target since pain reaction is responsive and easy to identify [114].

Figure 2-22 a) shows the method of SNI modeling. To induce the neuropathic pain, the subject is anesthetized, and the sciatic nerve of the rat is exposed. Then apply selective injury on two of three terminal branches of the sciatic

nerve (the tibial and common peroneal nerve). After the modeling, the pain threshold on the lateral side of the modeled limb sole is lowered.

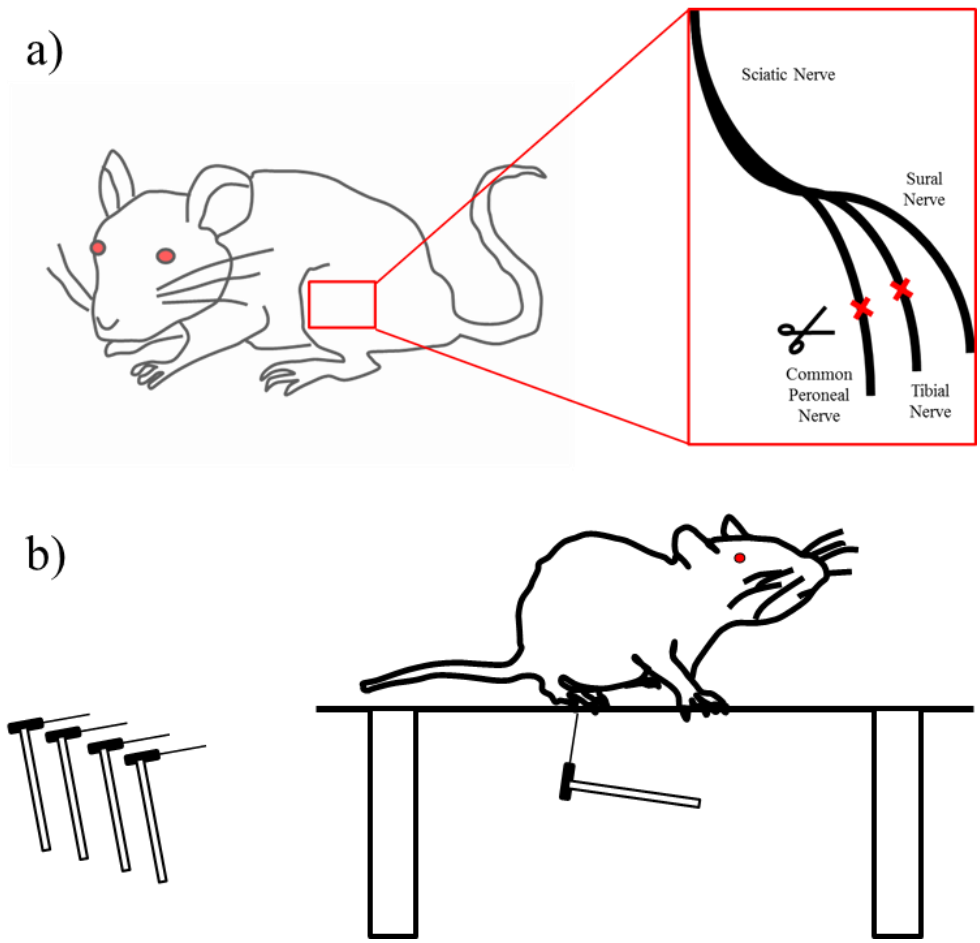

Figure 2-22. Methods for *in vivo* experiment on pain model rats. a) SNI pain modeling method, b) von Frey filament test.

To evaluate the pain level of the rat, the von Frey filament test is conducted. The pain model rat shows a painful response even under pressure from very thin filaments (between several g and 10 g) because the pain threshold has been lowered. There are several ways to evaluate these pain responses, but in this study, the ‘up & down method’ is used. This is a method of assessing pain response scores by poking the affected area of pain modeling. It starts with a von Frey filaments with multiple levels of pressure. This method is called ‘up & down’ because its scoring method is based on up and down. When a filament is applied on the subject and the subject shows a painful respond, go to lower pressure filament, and if the subject does not, go to higher pressure filament. The up & down von Frey test is conducted on the subject rats after modeling, during DBS stimulation, and

The up & down von Frey test is conducted to compare when there is or is no DBS stimulation in the pain model rats, and threshold of pain for each situation is derived to confirm how the threshold changes according to DBS stimulation.

The waveform and target tissue of the DBS stimulus was determined by referring to the previous study [115]. Rats measured thresholds by varying stimulation amplitudes at 130 Hz and 60 μs and observed the difference in the threshold for each amplitude.

Chapter 3

Results

3.1. System Fabrication

3.1.1. Implantable Device

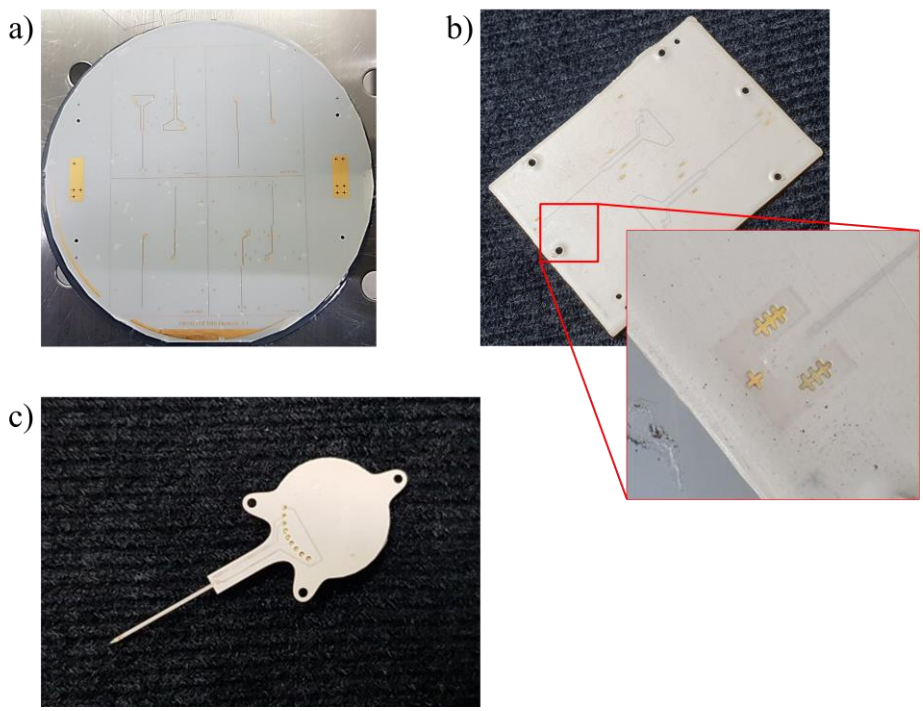

Figure 3-1. Electrode fabrication results. Electrode substrate a) after the MEMS patterning process, b) after multilayer lamination, c) after laser ablation and cutting.

The fabricated electrode of the LCP-DBS system is shown in Figure 3-1. Figure a) shows the LCP substrate of the electrode after the MEMS patterning process including four electrode layers. After the MEMS process, the laser cutting process for preparing interlayers, support layers, and the cover layer is done. The shape of the cover layer and interlayer is designed by CAD tool (AutoCAD,

Autodesk, CA, USA), and imported to the UV laser marking system for cutting. Table 4 shows the layers required for laminating an electrode substrate of the LCP DBS. Every layer except the cover layer and the electrode layers have the same shape as the interlayer and differ only in film type and thickness. Interlayer films were thinned from 25 μm thick film, which is the film of minimum thickness, through a laser process. This thinning process is related to the bend zone of the electrode. A cover layer, four electrode layers, and three interlayers are required to make an electrode with four layers of the conductor. When each layer has a thickness of 25 μm, it has a total thickness of 200 μm. where some sections need to be cut down to 170 μm to make a bend zone. In this case, not to cut off the electrode pattern of the electrode layer 4, the electrode layers must be located within 170 μm from the surface, and for this purpose, the thickness of the interlayer used as the adhesive layer is thinned by 10 μm.

The lamination was performed by a thermal press. To laminate the films, a zig made of steel used stainless for electrode substrate lamination was designed and manufactured. A set of the films for the lamination was piled up and loaded in the jig with two protection sheets of Teflon films at the top and bottom of the stack. Between the top of the Teflon film and the upper piece of the jig, a piece of the ceramic cushion was located to mediate the pressure. The jig was placed in the center

of the press, and jig remained without pressure until the temperature reached 286 ˚C. At 286 ˚C, 10 kgf of force is applied to the zig which has 12 cm^2 of the cross-sectional area for 30 minutes. Figure 3-1 b) shows the laminated substrate.

Table 4. A table for the films used in a lamination process of the LCP DBS electrode.

Layer	Film type	Thickness	Q'ty	Description
Coverlayer	CTF-25	25 μm	1	Has opening for align keys
Electrode layer	CTZ-25	25 μm	4	10 μm Metal layer on it
Interlayer	CTF-25	15 μm	3	Thinned by laser ablation
Supportlayer-50	CTZ-50	50 μm	3	Extra layer for substrate thickness
Supportlayer-25	CTF-25	25 μm	3	Adhesive layers for support layers

After the lamination, the electrode substrate is fabricated as Figure 3-1 b) shows. The substrate is first subjected to processes such as backside thinning, site and pad opening through laser ablation. Laser thinning was done by lowering the power to the target by lowering the scan rate of the cutting process in the UV laser marking system used for film cutting. During the cutting process, when the process is performed at a scan rate of about 100 mm / s, the cutting points are cut by 15 to 20 μm along the trace of the scanning point. Once diagonally, the average thickness was reduced by 2 μm for the area. This allowed precise thickness control. Sites and pad openings require a more complex process than thinning because they require

alignment. Through the holes in the cover layer mentioned above, the alignment keys located on electrode layer 1 are exposed. These align keys are embedded in the LCP to reveal the location of the conductors on the electrode layers 2 to 4 whose location is unknown.

After the laser ablation is completed, the electrode is subjected to the outline cutting process. Since the electrode substrate is a very thick LCP of 400 μm or more, it is cut through about 4000 repetitions at a scan rate of 100 mm / s. This is also an important step in aligning the cutting line because it can cut the conductors of the electrodes. However, in this manufacturing process, this problem was solved by designing with sufficient margin for the electrode thickness in consideration of the error and the margin of the electrode. Figure 3-1 c) shows the electrode detached from the substrate.

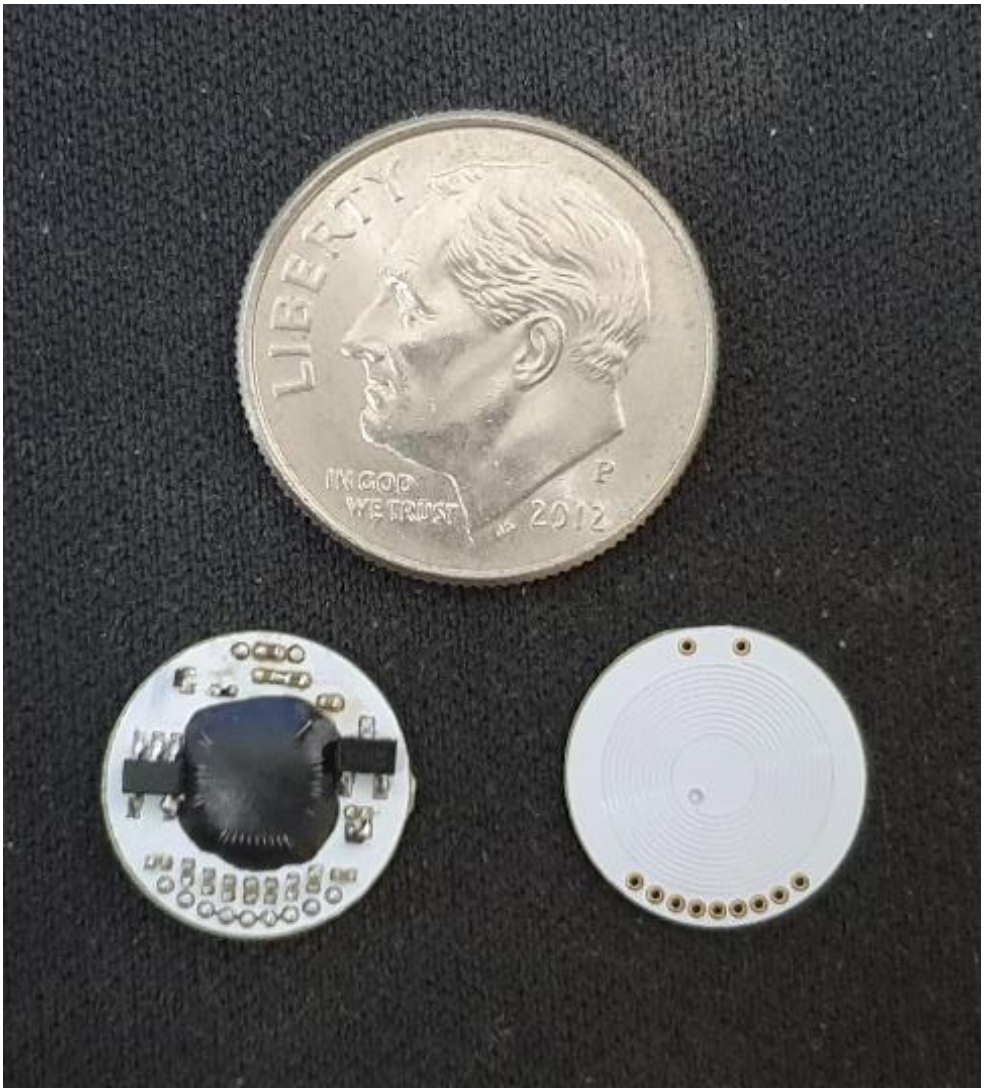

Figure 3-2. Fabricated coil and circuit for the implantable device. Top view(left) and bottom(right) after the integration.

During the electrode substrate was under the fabrication process, internal circuits are fabricated as shown in Figure 3-2. The internal circuit is processed by wedge bonding and soldering as described above. Especially, it has a unique structure that connects the individually manufactured coils to the circuit PCB. In this process, the circuit and the pad of the electrode must be connected to transfer the current stimulus waveform to the electrode. The pad on the circuit side is made of a through-hole via penetrating the circuit PCB and the coil PCB. Therefore, the connection between the via and the pad of the electrode is very important, and the pad of the electrode is a liquid crystal polymer. This part cannot be connected by soldering. The electrode pad is a 10 μm thick Au plated by LCP-based electrode process, so if you apply more than 300 degrees of heat to solder it, the LCP may be damaged due to heat or the pad may be detached due to weak adhesion of the metal seed layer. do. To solve this problem, make the via the side of the circuit so that the lead protrudes convexly, apply conductive epoxy on the electrode pad side, and then align the circuit. Fix on the electrode. The device with the circuit fixed on the electrode substrate undergoes curing of the conductive polymer at a temperature not exceeding 120 ˚C, the glass transition temperature of the LCP. Figure 3-3 b) shows the result of circuit-electrode integration.

The final production process is packaging. The packaging is a step to protect the circuit and the electrode from the hostile *in vivo* environment. It is performed by covering the lid made of LCP and partially heating. The package produced through this was produced as shown in Figure 3-3 c).

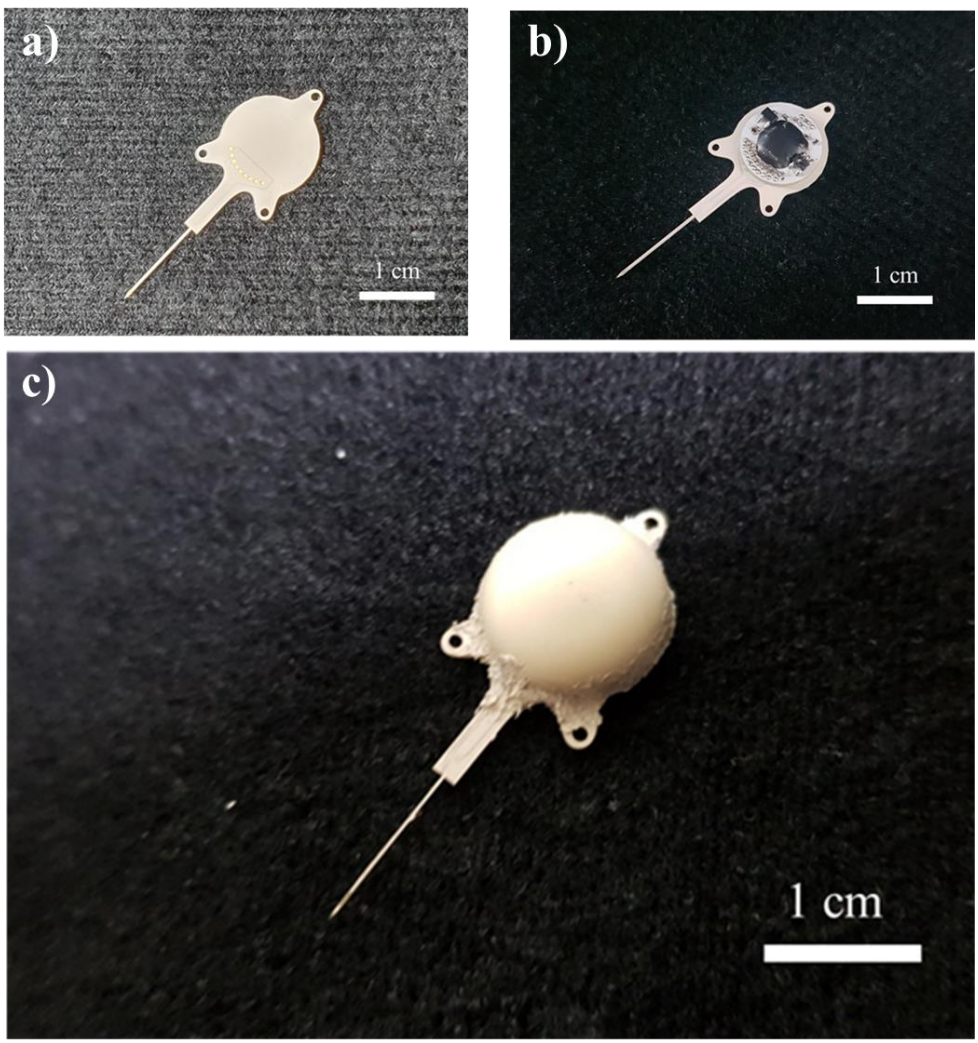

Figure 3-3. Package process of LCP DBS. a) bare electrode, b) electrode integrated with the circuits, c) packaged device.

3.1.2. External Device

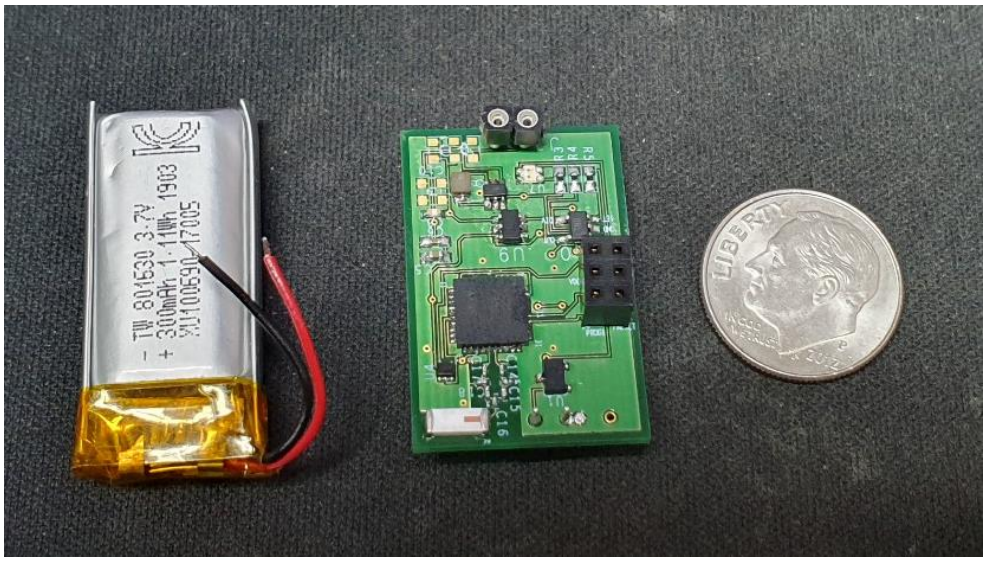

Figure 3-4. Fabricated external device for the suggested system.

The external unit is designed as a circuit using a battery as shown in Figure 3-4. The circuit measures 19.5 mm x 32 mm and has a height of about 12 mm when the batteries are combined. The circuit uses a 3.7 V supply, with a 300 mAh Li-Po battery.

In the active mode of the circuit, the current consumption of the entire circuit, including the ZigBee module and the class-E amplifier, was measured at about 280 mA, which was about 1.036 W, considering the input voltage of 3.7 V.

Using the fabricated circuit, a Benchtop test was conducted to test the interworking and operation of the internal circuit of the LCP DBS. Figure 3-5 shows

the results of the benchtop test. The PWM waveform generated by the MCU of the external device is generated with 3.3 V serial data and connected to a class-E amplifier having a 2.54 MHz carrier frequency to modulate the carrier frequency. This produces a waveform of 15 V or more in amplitude as shown in the TX coil.

The waveform generated from the TX coil of the external device is transmitted to the RX coil through an inductive link. The waveform measured by the RX coil is shown in the third graph of Figure 3-5 below. Here, the peak-to-peak voltage of RX reaches about 36 V. When the incoming waveform is half-wave rectified, the data signal for input to the data pin of the ASIC chip is completed. The ASIC chip that obtains power and data through this process emits a stimulus waveform like the output pulse shown in the figure.

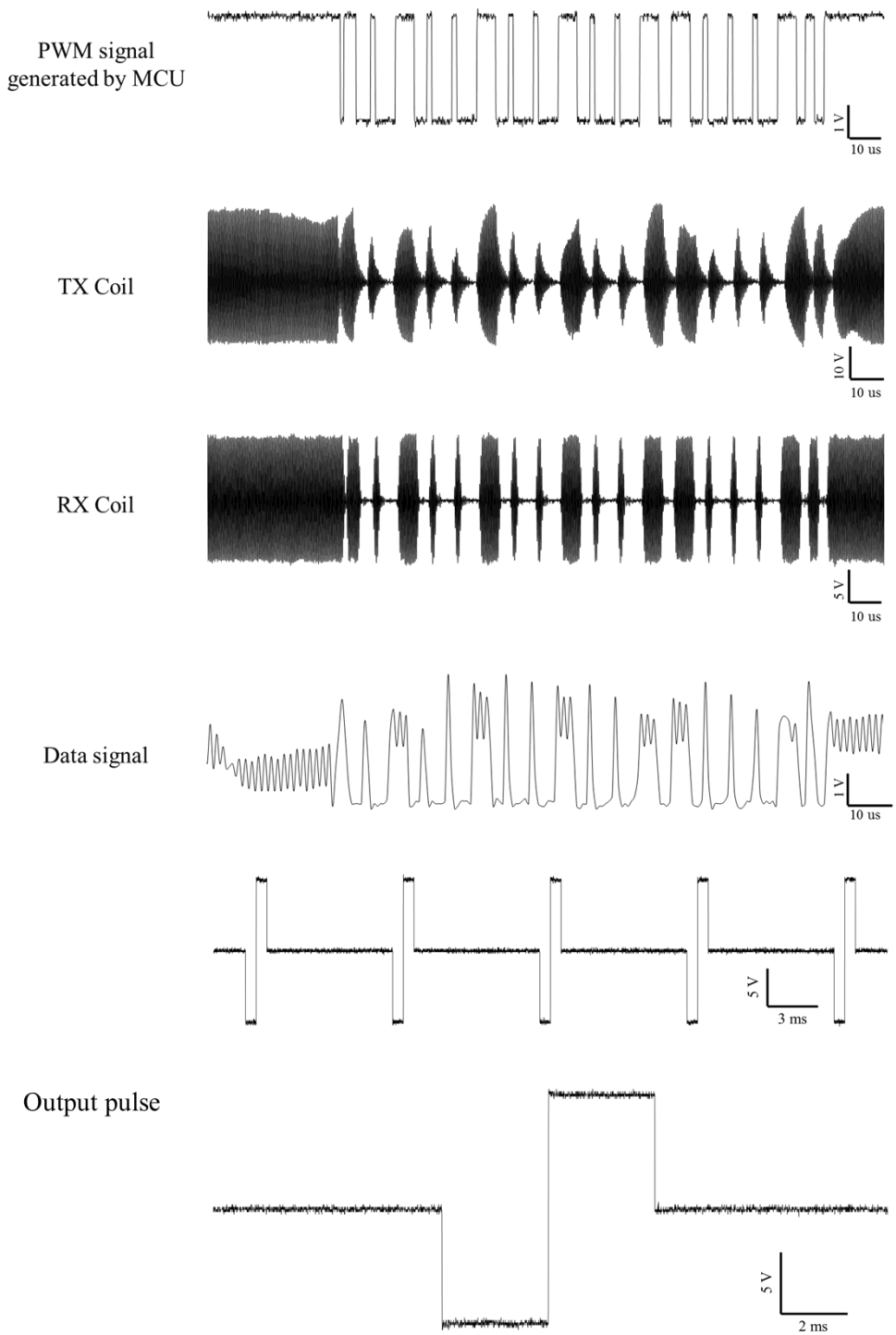

Figure 3-5. Results of the benchtop test using External device.

3.2. Evaluations

3.2.1. FEM simulation on RF radiation

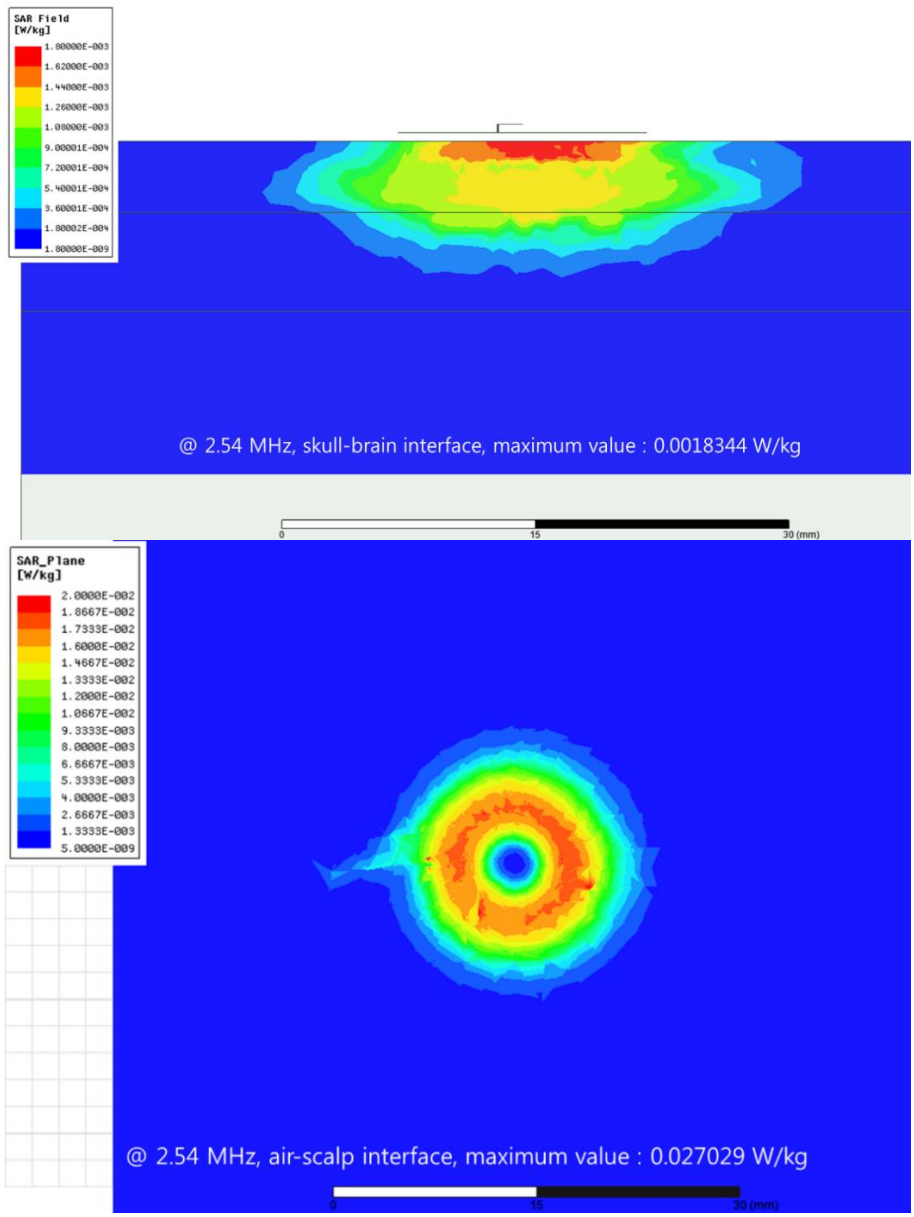

Figure 3-6. Simulation results of FEM SAR analysis on the 'TX coil only' model. SAR distribution on a sectional view (above) and on a planar view of the air-scalp interface (below).

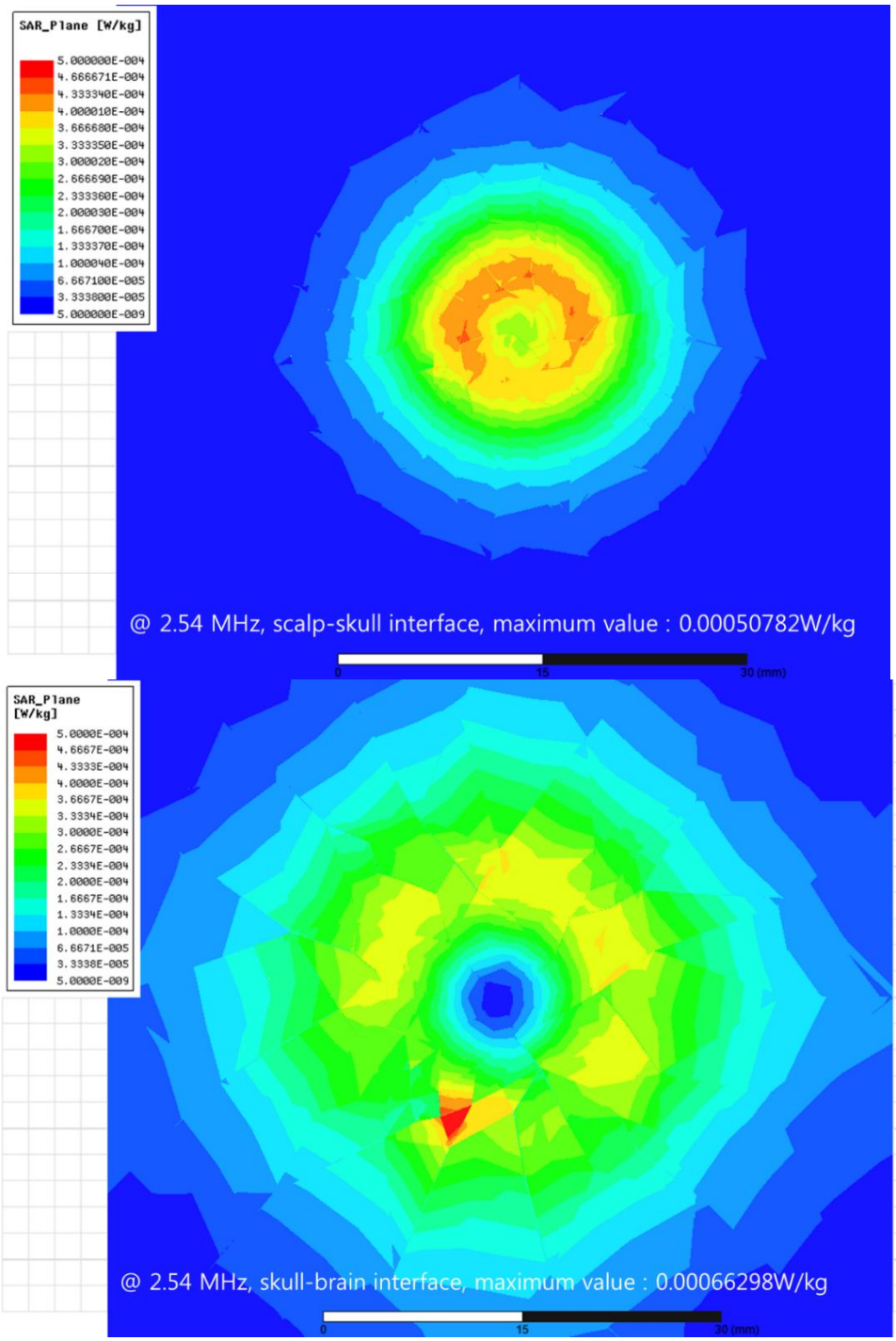

Figure 3-7. Simulation results of FEM SAR analysis on the 'TX coil only' model. SAR distribution on a planar view of the scalp-skull interface and skull-brain interface.

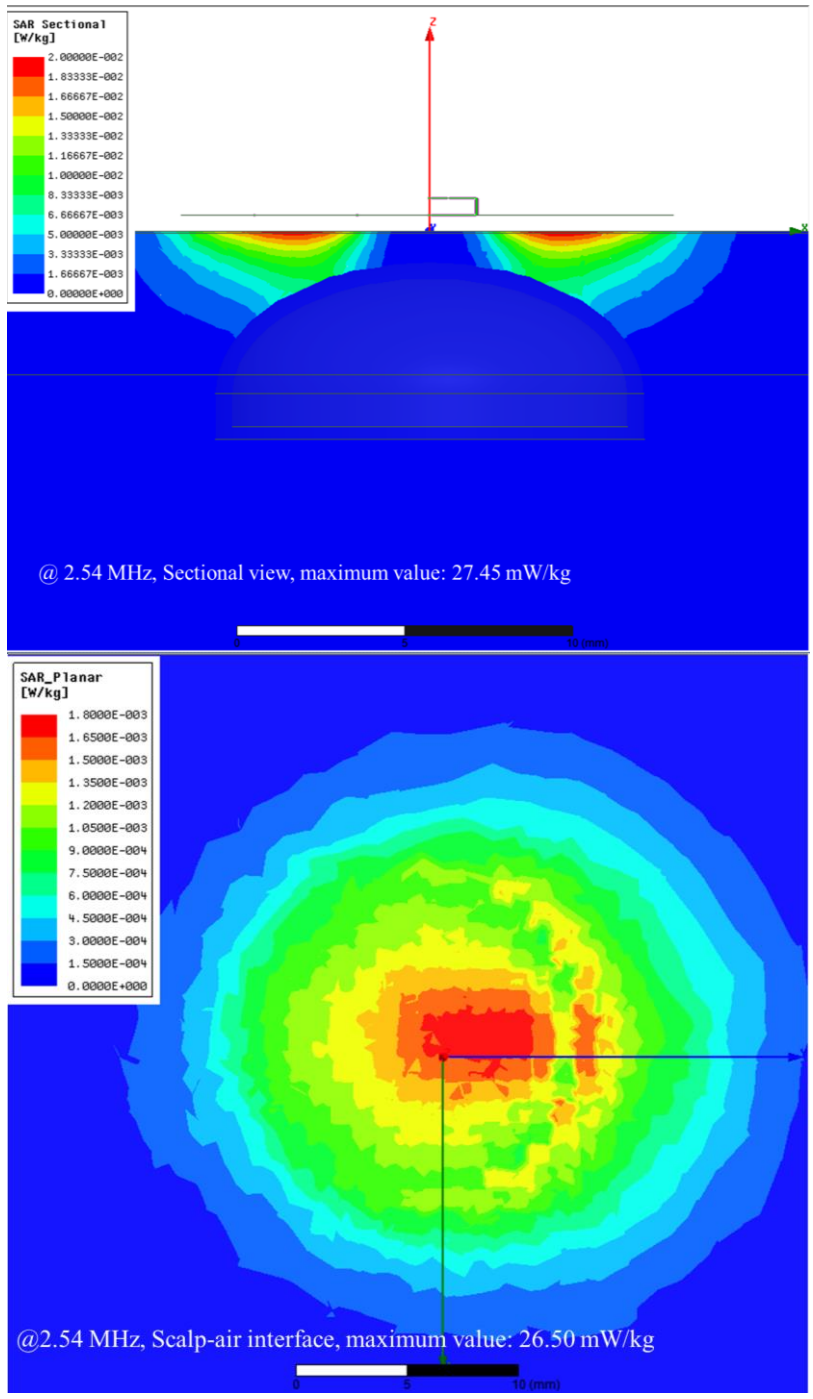

Figure 3-8. Simulation results of FEM SAR analysis on the 'RX coil included' model. SAR distribution on a sectional view (above) and on a planar view of the air-scalp interface (below).

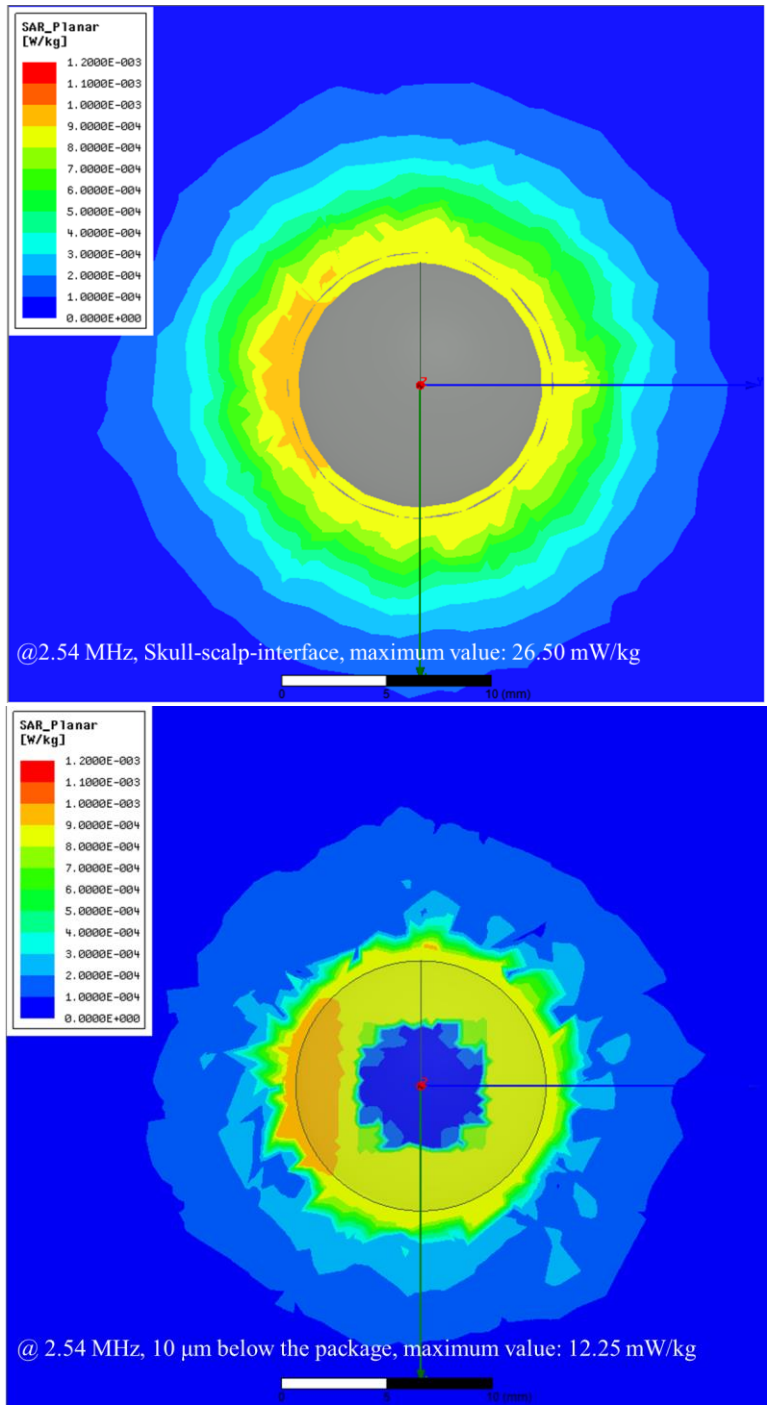

Figure 3-9. Simulation results of FEM SAR analysis on the 'RX coil included' model. SAR distribution on a planar view of the scalp-skull interface and 10 µm below the implanted package.

The FEM results for SAR verification were derived as shown in. Figure 3-6 ~ Figure 3-9 above. The graphs show the SAR distribution at the cross-sectional view, and three planar views at different y-coordinate, respectively, and the maximum SAR values in the corresponding fields. The largest SAR value in the TX coil only model was in the air-scalp interface, where is the closest to the coil, 27 mW/kg, which was much smaller than the 80 mW/kg permissible threshold of SAR. However, the largest SAR value in the RX coil included model was in the sectional view, but the point of the value was at the air-scalp interface. The value was 27.45 mW/kg, which has slightly bigger than the value of TX only model, but still much smaller than the regulatory threshold of SAR. However, in the sectional view,

By comparing the results of FEM simulation on two models, we could find that the existence of the RX coil may affect the electric field, but the 500 μm of the distance between the RX coil and tissue formed by the package was enough for decaying SAR power.

3.2.2. In vitro test

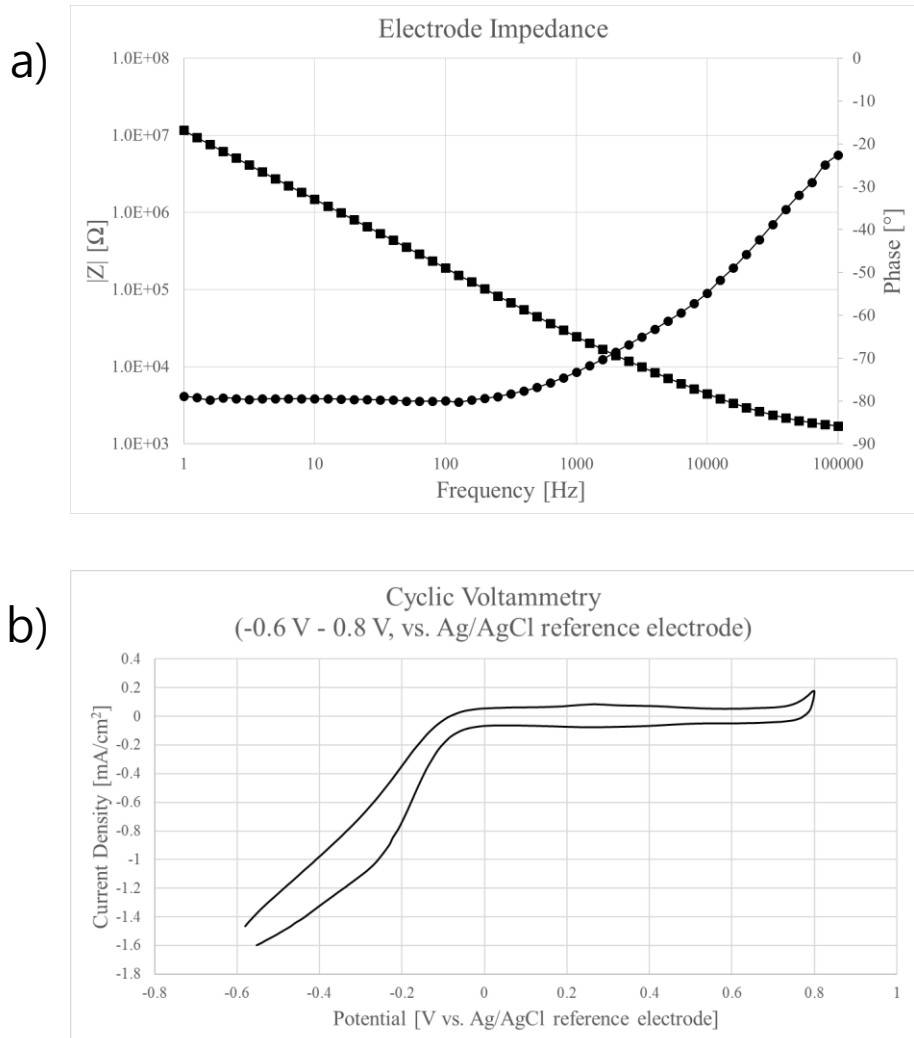

Figure 3-10. Results of the *in vitro* tests for the electrochemical characterization of the fabricated electrode. a) The impedance of the electrode over a frequency range of 1 Hz ~ 100 kHz. The magnitude of the electrochemical impedance of the electrode was measured as 24.55 kΩ at 1 kHz and the phase angle of the electrochemical impedance of the electrode was measured as -73.28 °. b) Results of the cyclic voltammetry using the suggested electrode over -0.6 V ~ 0.8 V at 100 mV/s scan rate. The CSC_C of the electrode was measured as 0.549 mC/cm^2.

The EIS results for the completed DBS electrode are shown in Figure 3-10 a). The impedance at 1 kHz of the corresponding electrode is -73.28 ° at about 24.55 kΩ. This seems to be a reasonable value considering the size of the electrode. However, assuming a compliance voltage of 20 V, it is highly likely that a saturated waveform will be generated for currents above about 0.8 mA.

Figure 3-10 b) shows the results of the CV of the DBS electrode. The graph shows that the CSC_C has a value of 0.549 mC / cm^2, considering the electrode size of 50 μm × 160 μm, which is similar to the CSC_C values measured with the same material electrode.

3.2.3. *In vivo* Animal Experiment

3.2.3.1. Electrode Implantation

Figure 3-11 shows the implantation process of the implantable device of the DBS system. As described on the left figure, a custom-designed electrode holder was used to fix LCP-DBS during stereotaxic surgery and it served the role of fixing the electrode straight. The holder consists of a frame and a cover. Both are made of steel used stainless, and a 3D model is described in Figure 3-12 a). There are four screw holes for fixing the frame and body tightly, and a rail is located in the middle of the

holder to prevent the misalignment. Since the electrode had the bending zone to ease the device to be loaded, it needs to be considered that the electrode would bend during the implantation. Therefore, an electrode holder is designed to fully cover the bending zone of the devices. Besides, this type of package has a problem in that the implant cannot be fixed and operated on the arm of the stereotaxic surgical instrument to be implanted using the stereotaxic surgical instrument. Among them, it has advantages such as simply detaching the device from the stereotaxic frame.

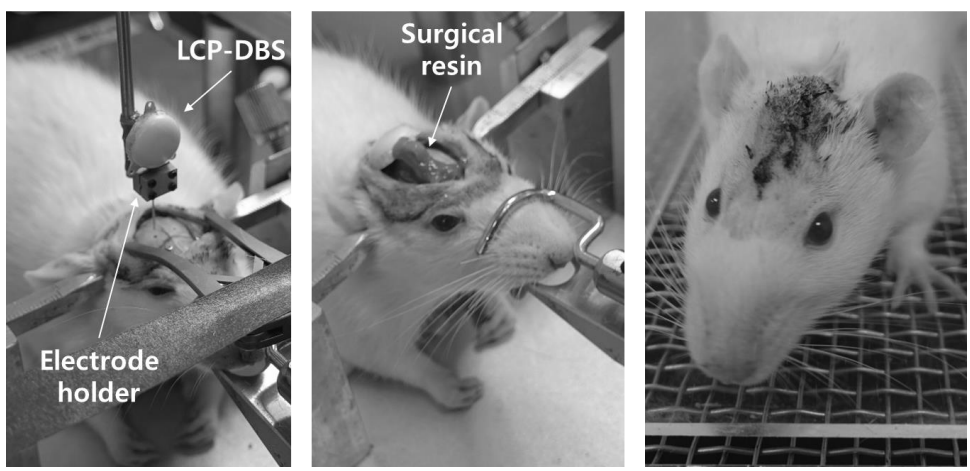

Figure 3-11. Results of LCP-DBS implantation on SD-rat. Left picture shows the implantation process of the implantable device of the suggested system using custom designed electrode holder. The electrode is located above the opening of the skull targeting the VPL. Picture in the middle shows the picture of the subject rat after the electrode implantation and the electrode is bended to keep the packaged implanted subcutaneously. The device was fixed with the skull of the rat by applying UV polymerized surgical resin. The other picture shows the scalp of the rat after a week of recovery period. The incision is sutured with surgical suture made of biodegradable silk. The picture was taken just before the von Frey behavioral test.

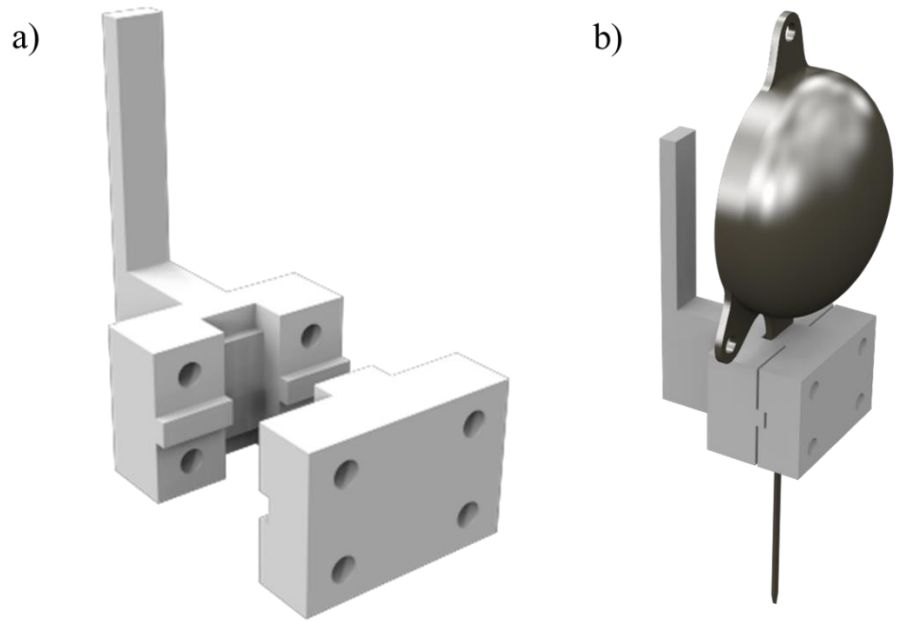

Figure 3-12. 3D-models of the custom designed electrode holder. a) A model of the electrode holder when the frame and cover are dissembled. The frame has an arm to be connected to the stereotaxic surgical frame, crevice for holding the device, and raised edges to be align keys with the cover. b) A model of the electrode holder when the implantable device of the LCP-DBS is mounted. After the device is assembled as shown in the picture, four titanium-based screws are used to interlock the frame and cover. After the implantation, UV polymerized surgical resin is applied to the contact point of the implantable device and the skull. The screws and the cover are removed after the device fixation and the frame is detached from the implantable device.

3.2.3.2. Von Frey tests

The figure on the right in Figure 3-11 shows a rat undergoing behavioral testing after the implantable device of DBS has been fully implanted and has undergone a period of acclimation. Rats were able to move freely after internal organ transplantation, and no sutures were torn apart or inflammatory reactions were observed until the rats were sacrificed.

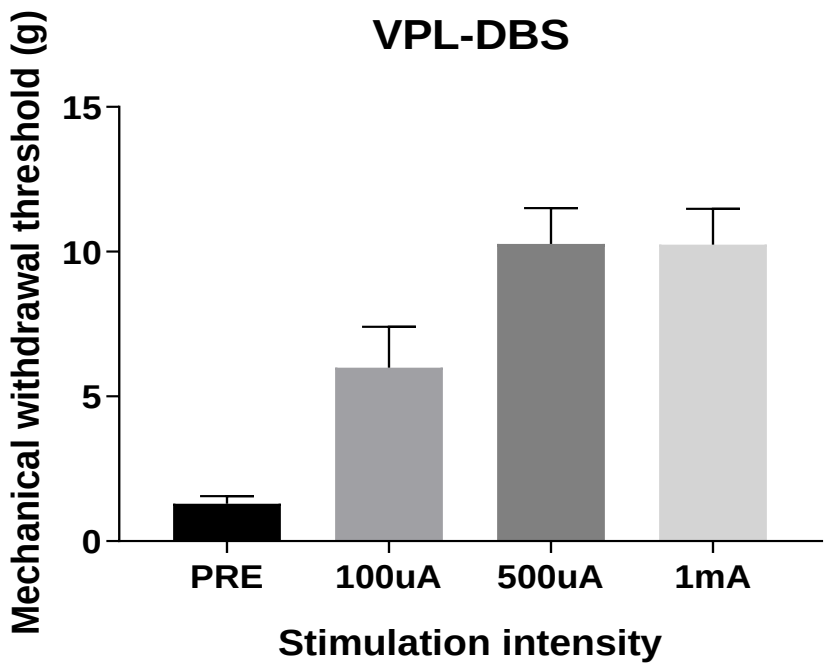

Figure 3-13. Results of *in vivo* behavioral test using neuropathic pain model rat. The mechanical withdrawal threshold of the pain modeled rat was measured to verify the effect of the DBS on pain relief.

The results of in vivo behavioral tests on the neuropathic pain model SD-rat are shown in Figure 3-13. The horizontal axis represents the intensity of the stimulation, and the vertical axis represents the threshold of strength with which the rat feels pain and lifts its feet. From the results, before applying the DBS stimulus signal (PRE in the graph), the withdrawal threshold was less than 2 g. However, when the current stimulation of 100 μA, was applied, the threshold for pain increased up to 7 g. When 500 μA of current stimulation was applied, the threshold soars up to 10 g. When it comes to 1 mA amplitude, the threshold is almost same with 500 μA stimulation. Considering that the stimulation method applied in the experiment is a bipolar stimulus, arithmetically, 16 V compliance voltage is applied. Although this circuit has a compliance voltage of up to 18 V, the inductive link is less efficient than the benchtop test when the implantable device is located in the body of the animal. Therefore, the saturated withdrawal threshold is induced by saturation of the current pulses from the implantable device due to the high electrochemical impedance of the electrode sites.

Chapter 4

Discussions

4.1. Implantable Device

4.1.1. Fabrication Process

Considering commercialization, the prototyping process described in this paper is not very economical. The economics mentioned here also include yield, cost and time spent on the manufacturing process, but also include the intuitive nature of the production process and suitability with the mass production process.

4.1.1.1. LCP as substrate

The LCP, which is the substrate material used in the suggested system, is a thermoplastic polymer. Using this property, the vendors provide LCP in the form of pellets, films, and fibers. Pellets are mainly used in injection molding methods. The injection molding using LCP has been used for decades for packaging IC chips or connectors [116], [117]. However, the films are produced in a thickness range of 25 μm to 100 μm, the main processing method is a thermal lamination. This process is used to fabricate multilayered FPCB by thermal lamination with a stack of patterned films. Finally, the fiber is mainly used as the material of the sheath of wires, Kevlar fiber, and outer skin of spacesuit to take advantage of physical, chemical inertness

and heat resistance. Recently, there are a few attempts to apply the LCP-fiber to the 3D printing with tens of μm scale microstructures [118], [119].

Considering the mass production process and ease of production, it seems to be appropriate to use three different types of LCP on purpose of each steps. First, electrode fabrication is suitable with film type LCP since it is compatible with the MEMS process. However, the pellet type LCP seems to be the best option for package process since injection molding is already used for hermetic sealing of IC components. Finally, fiber type LCP and 3D printing using it may provide LCP-based system a new vision such as microstructure electrodes.

4.1.1.2. MEMS Process

The LCP-based MEMS process used in this study is composed of metallization and patterning. In the current process, O_2 plasma is processed on the prepared LCP substrate to perform surface activation, and the seed layer is deposited through the e-gun evaporator to perform the metallization process. Afterward, the pattern is generated by an aligner using AZ-4620 which is a negative photoresist, the pattern is electroplated on the patterns, and the patterning process is carried out through seed layer etching after PR stripping

Physical vapor deposition (PVD), casting, cladding, and sputter-plating are considerable candidates of the metallization on the LCP substrate. PVD is a method of depositing metal thin film including sputtering and evaporation. Although sputtering has very good step coverage, the throughput of the sputtering process is relatively low, therefore unit price is higher than evaporation. The evaporation is based on heating the source material and coat the substrate with the vapor of the source metal. However, casting is a method of forming the LCP film on the target metal film. The molten LCP is coated onto the metal foil such as copper. Although the standard process is not set for gold films, but because the melting point of the gold is much higher than the LCP, casting can be a reasonable method for the metallization of the LCP. Cladding is a famous method of forming thin metal films on polymers. It uses high pressure to adhere metal films with the substrate. But the cladding mainly adopts copper as the metal foil, and cladding process of the LCP using gold foil is not yet been established. And also, because it is a roll-to-roll process, the initial investment cost is high and is suitable for mass production. The last, sputter-plating is a method for a roll-to-roll process. This process contains sputtering and cladding together. It has very good throughput but as the cladding, the fabrication environment is very expensive compared to other processes.

To form the patterns of the electrode for the suggested LCP DBS system, the MEMS process using AZ4620 negative photoresist, aligner and plating were used. Considering that the electrode used in this study has a relatively large line width of 30 μm and the area occupied by the pattern is very small compared to the entire wafer, we may consider an inexpensive and effective process to replace it. To apply this LCP electrode, the new method should have a resolution of smaller than 30 μm, and should guarantee capability of building gold structure with thickness of 10 μm or more.

Since the line width of the electrode is not so small, direct laser patterning (DLP) [120] can be considered. DLP is a method in which a gold structure is completed by simultaneous polymerization by applying a metamaterial mixed with a polymer and a metal salt, and applying a laser along the desired pattern. This method can be used to generate patterns over 150 nm, and the thickness of the pattern can be adjusted according to the type of solvent polymer and spin coating conditions.

Inkjet printing [121] may also be one of the options. Inkjet printing is a method of generating a pattern by spraying a metal ink in a desired pattern on a substrate, which is the most advantageous method in terms of efficient use of a material because the metal is sprayed only on a desired pattern.

The site and pad opening process using this alignment key and UV laser is the most deviating process in device development and also has a high failure rate. This is because of the nature of the UV laser setup that the user has to manually align the gears of the x-y plotter with a very weak light source through a low resolution camera. It seems to be a problem that can be solved if equipped with an automatic alignment system through a high resolution camera.

During the thermal lamination process, the applied pressure is very low (about 81.7 kPa) concerning the recommended process condition (MPa order) of the LCP film provided by the vendor of LCP films. This low pressure process is needed since the LCP at high temperature and high pressure becomes fluidic, and migration of metal patterns occurs. To minimize the migration of the patterns, low pressure process is used.

4.1.2. Package Size and Weight

The main feature of this internal circuit is that it is energized from the outside through an inductive link. As a result, the battery can be miniaturized compared to a commercial DBS including a battery in a package. This has the advantage of minimizing the size of the battery as well as limiting the risk of thermal reactions or

leakage due to breakage of the battery, which has a great risk in terms of the patient's health in case of leakage.

In the case of internal circuits, the largest area is the magnetic pole ASIC chip and the DC block capacitors of the electrode terminals. They are difficult to significantly reduce the area due to their role in internal circuits and their characteristics, but other discrete devices and regulators can be included in the ASIC chip to reduce the area. Considering the footprint and routing space of the circuit, the surgical range can be reduced by about 10%.

4.2. Improvement for Clinical Application

To advance the proposed system toward the clinically applicable DBS, there are some issues need to be solved. First, the fabrication process of the integrated internal device used in this study needs to be improved. A 4-inch wafer-based MEMS process is used since the size of 4-inch is appropriate for test sample MEMS process, while it is not suitable for the fabrication of electrodes for human deep brains with a depth of about 10 cm. To meet the size of the electrode, considering a single wafer includes all four layers and enough margin, the substrate wafer of the MEMS process requires larger than 8 inches. To be compatible with the MEMS process using

substrate wafers of more than 8 inches, it is required to establish process conditions that are suitable for new semiconductor process equipment that is compatible with the size.

Second, the configuration of the monolithic implantable device should be reconsidered. In the clinic, when the DBS is inserted, the patient's skull is opened by drilling and the electrode is implanted. After the electrode implantation, it shall be verified that the electrode is correctly located in the intended position. The location of the electrode is important because the electrode sites should meet the target tissue of the DBS. To determine the tissue around the electrode sites, a neural signal recorder is connected to the implanted electrode before the IPG implantation. Through this equipment, the target tissue is found through the recorded neural signal waveform and the micro position and stimulation channels among the electrode sites are selected to minimize side effects. However, a monolithic system such as the system proposed in this study, is not applicable for the process because electrodes cannot be connected to the recorder. To overcome this, to methods can be considered: to integrate a recording circuit in the circuit of the implantable device and to modularize the internal device to perform the recording in the same way as before.

Since the recording circuit is basically differential amplifier, the circuit can be integrated with current stimulation circuit [122], [123]. But, to deliver the neural signal waveform to the external recording device, the internal circuit should transmit signals, which consumes power. Therefore, the circuit should have a power source or a method of transmitting the signals made from external power supplied via inductive link. Both methods, however, requires additional elements to the internal circuit of the implantable device, which increases the size of the circuit, leading to an increase in the package.

Therefore, the development of modular devices is essential to solve this problem with current process methods. Modularity takes the form of connecting an electrode and a package through a connector. This implementation has several advantages: One is, the modular electrode can be manufactured to have specifications of compatible with the insertion process using a cannula, which is standard process for the DBS electrode implantation. Therefore, it eliminates the need of neurosurgical surgeons to learn new implantation methods. Another is that even if a malfunction or problem occurs outside of the electrode, the connector can be dismantled and replaced in the modular system and the electrodes can be connected to the new system without affecting the intracranial part. Considering these advantages, although not verified in this study, clinically applicable system

would be proposed in the way of using modular systems. Then, the biggest question is whether it is possible to develop a connector that can be used in vivo.

A few preliminary studies have been conducted about implantable connector using the LCP. The most important characteristics which the implantable connector requires are simplicity of the connection and reusability. The connectors will be tightened during the implantation surgery, so they must be combined in as simple a way as possible for the surgeon to be readily available. And, considering the surgery to replace part of the system, the reusability of the connector is also important. For this simplicity and reusability, we suggest a clip key type connector system.

Figure 4-1 a) shows a 3D model of the liquid crystal polymer-based implantable connector designed in this study. The connector has a form for fixing with a clip so that it can be easily removable, the reel is added to the clip can be wound around the length of the electrode or extension. The connector is manufactured through three-stage jig as shown in Figure 4-1 b), and the finished connector is as shown in Figure 4-1 c).

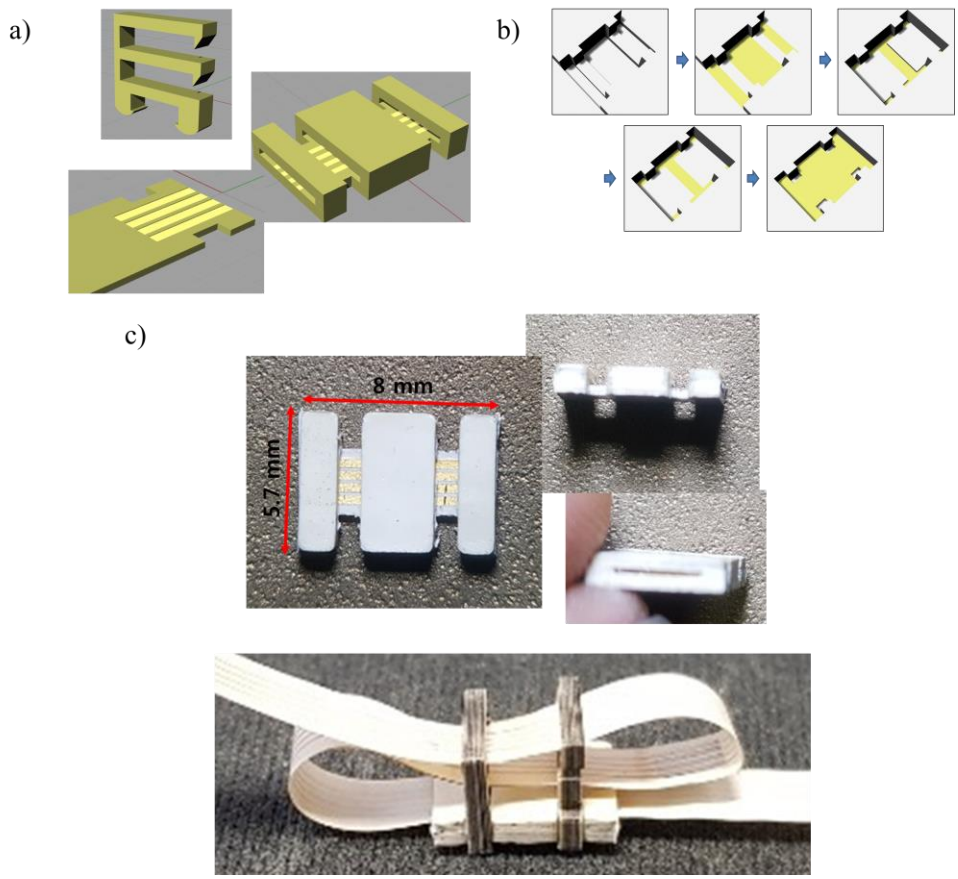

Figure 4-1. Designed LCP based implantable clip key type connector and fabrication results. a) The 3D-models of the clip key type connector. The connector has both terminal open to the upside (right), and clip keys (left above) are used to fix the terminal with the lead lines (left below). b) A part of the fabrication process for the clip key type connector. It shows the thermal lamination process of the connector body using 3-layer pressing zig. c) The fabrication results of the clip key type connector. The connector has 5.7 mm of width, 8 mm of length, and 1.3 mm of height. The last picture shows the suggested connector after the connection in both terminals. The structures of the key are used as reels that winds the extra length of the cable.

Although the connector has not yet been tested for long-term stability and hermeticity, the concept of the system expected when developing such a connector and modularizing the package and electrode is shown in Figure 4-2.

As shown in the figure, the system consists of an electrode, lead wire, package, and connectors. The Electrode is a 4-channel depth-type electrode. It has 10 mm of the stiff zone and 5 mm of the flexible zone. The stiff zone has 300 μm of thickness therefore the electrode has enough stiffness to be straight. The flexible zone has a thickness of 150 μm to has flexibility for 90 ° bending. The lead wire is 4-channel flexible flat cable with 4.5 mm of width and 100 μm of thickness. The lead wire connects the electrode and the package and covers the distance between the drill hole of the electrode and the package. To enhance the degree of freedom, the lead wire has enough length and flexibility. The package has a shape of half-ellipsoidal with a diameter of 13 mm and a height of 5 mm or less. The package also has 4-channel terminals to connect with the lead wire. Finally, the connector also has 4 channels and two clip keys to fix the lead wire. The clip key has a comb-like structure used as a reel for the extra length of the lead wire.

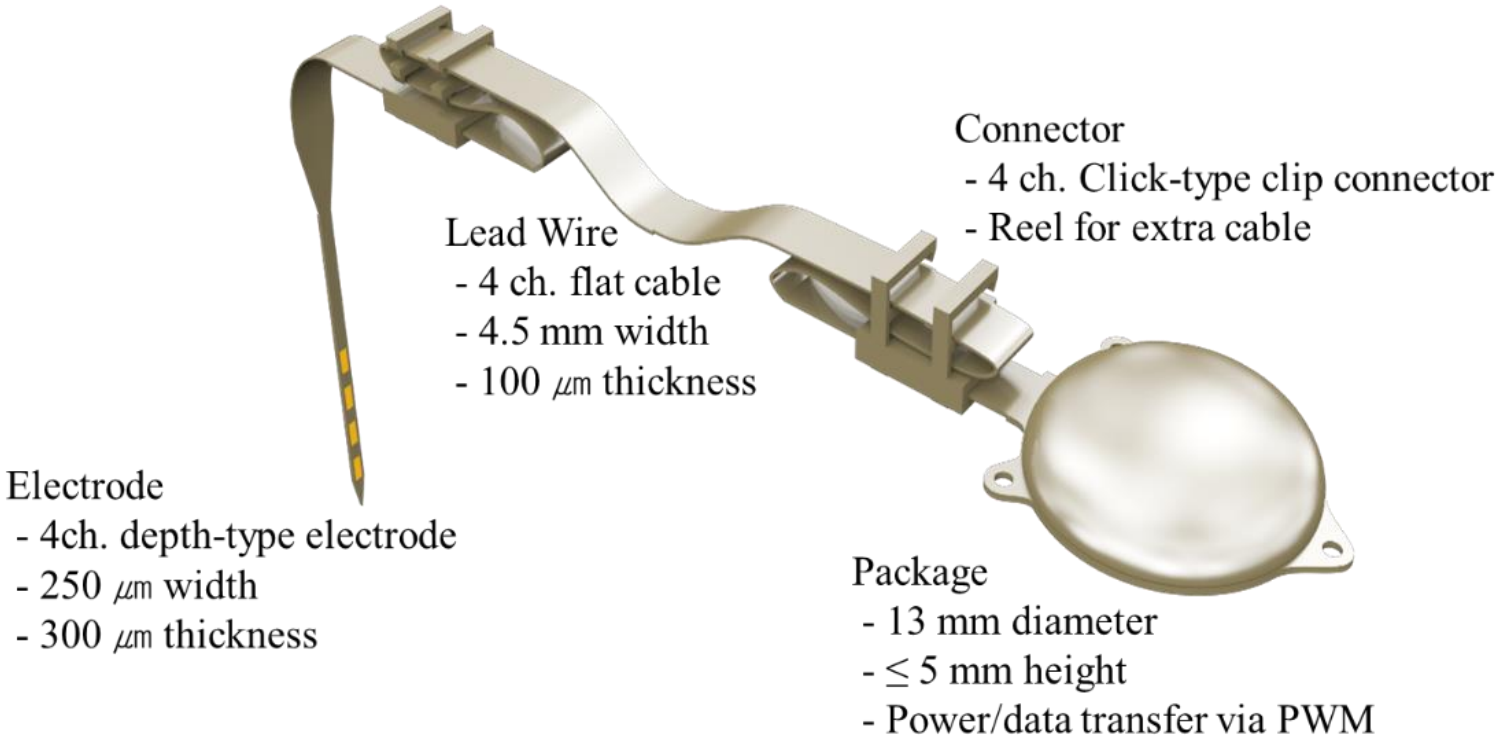

Figure 4-2. Concept art of LCP-based modular head-mountable DBS system

Chapter 5

Conclusion

In this thesis, a miniaturized deep brain stimulation system was developed. An implantable device of the system had a round half-ellipsoidal monolithic shape with a diameter of 13 mm and a height of 5 mm.

The stimulation electrode of the device was an 8-channel depth type electrode. The electrode was 18 mm long, while 11 mm from the tip has 300 μm width and 250 μm thickness, and the rest 7 mm has 4.5 mm width and 170 μm thickness for bending zone. It was fabricated by MEMS process using 4-inch wafer with the linewidth of 20 μm. The electrode has four layers, and each layer has 2 conductor channels. The stack of 4 electrode layers, 4 insulation layers, 3 supporting layers, and 3 adhesion layers was laminated by thermal pressing at 286 °, 20 kgf. After the lamination, electrode sites for the contact with the target tissue and pads for the connection with the internal circuit was exposed by UV laser ablation.

The internal circuit of the implantable device was established on FR-4 based PCB, which had a diameter of 11 mm and a thickness of 0.4 mm. The circuit was including a power circuit, a data circuit, and a current stimulator ASIC. A coil was used to receive power and data from the external device via an inductive link, which was built on a same size of PCB. Every circuit element except the current stimulator ASIC was soldered to the circuit PCB, and the ASIC chip was wedge bonded on the

PCB with aluminum wire and covered with protection epoxy. After the circuit assembly, the circuit was fixed on the electrode substrate, and the channels were connected to the pads on the electrode by soldering and conductive epoxy. An LCP based half-ellipsoidal lid was fabricated by thermal deformation of 5 films with 100 μm thick. The lid was spot-welded with the circuit integrated electrode substrate.

The external device for the system was also developed. The external device was controlled by the ZigBee telecommunication and powered by a Li-Po battery. Therefore the circuit of the external device included a ZigBee antenna, a MCU compatible with ZigBee telecommunication, the Li-Po battery, a charging circuit for the battery, a class-E amplifier, and a coil for RF signal transmission. First, the MCU converts the ZigBee input signal into a PWM signal as an input to the class-E amplifier. Then the class-E amplifier modulates a 2.54 MHz carrier frequency with the envelop of the PWM signal. Then the modulated carrier frequency is transmitted to the implantable device via the inductive link, containing the waveform parameter information in it.

By a benchtop test, the whole system has been demonstrated its operation. DC power supply for the external device, the PWM signal generated by the MCU, the transmitted RF signal generated by modulating the 2.54 MHz carrier frequency

with the PWM signal, the received RF signal, DC power supply for the implantable device, the PWM envelop acquired from the implantable device, and the output signal of the current pulse generator ASIC were observed. An *in vitro* electrochemical analysis of the electrode was done to find the characteristics of the electrode such as electrochemical impedance and CSC_C. Finally, to verify the efficacy of the whole system, *in vivo* behavioral experiments using von Frey filaments were conducted on neuropathic pain model rats. Implantation of the device confirmed that the implantable device was small enough to be implanted under the scalp of rats. And also, the system was proven to be effective on pain relief on the neuropathic pain modeled rat.

To improve the system toward clinical level, alternative fabrication processes were proposed and preliminary study of modularizing the LCP DBS system were conducted. A clip key type implantable connector was suggested, and the prototype sample was fabricated. The concept of the whole system using these connectors were suggested and described.

References

[1] P. Shirvalkar, M. Seth, N. D. Schiff, and D. G. Herrera, "Cognitive enhancement with cetral thalamic electrical stimulation," *Proc. Natl. Acad. Sci. U. S. A.*, vol. 103, no. 45, pp. 17007–17012, 2006.

[2] M. Okun, "Deep-Brain Stimulation - Entering the Era of Human Neural-Network Modulation," *N. Engl. J. Med.*, vol. 371, Sep. 2014.

[3] M. Hariz, "My 25 stimulating years with DBS in Parkinson's disease," *J. Parkinsons. Dis.*, vol. 7, pp. S33–S41, 2017.

[4] A. Amon and F. Alesch, "Systems for deep brain stimulation: review of technical features," *J. Neural Transm.*, vol. 124, no. 9, pp. 1083–1091, 2017.

[5] Medtronic, "ActivaTM RC catalog," 2019. [Online]. Available: https://www.medtronic.com/us-en/healthcare-professionals/products/neurological/deep-brain-stimulation-systems/activa-rc.html.

[6] Boston Scientific, "Vercise TM catalog," 2019. [Online]. Available: https://www.bostonscientific.com/en-US/medical-specialties/neurological-surgery/dbs/deep-brain-stimulation-products-vercise-overview.html.

[7] Abbott, "Infinity TM catalog," 2019. [Online]. Available: https://www.neuromodulation.abbott/us/en/hcp/products/dbs-movement-disorders/st-jude-medical-infinity-dbs-system.html.

[8] J. Kahan *et al.*, "The safety of using body-transmit MRI in patients with

implanted deep brain stimulation devices," *PLoS One*, vol. 10, no. 6, 2015.

[9] H. Lee, H. Park, and M. Ghovanloo, "A Power-Efficient Wireless System With Adaptive Supply Control for Deep Brain Stimulation," *IEEE J. Solid-State Circuits*, vol. 48, no. 9, pp. 2203–2216, 2013.

[10] E. Kocabicak, A. Jahanshahi, L. Schonfeld, S. A. Hescham, Y. Temel, and S. Tan, "Deep brain stimulation of the rat subthalamic nucleus induced inhibition of median raphe serotonergic and dopaminergic neurotransmission," *Turk. Neurosurg.*, vol. 25, no. 5, pp. 721–727, 2015.

[11] W. T. Doucette, J. Y. Khokhar, and A. I. Green, "Nucleus accumbens deep brain stimulation in a rat model of binge eating," *Transl. Psychiatry*, vol. 5, no. October, pp. 1–6, 2015.

[12] International Association for the Study of Pain, "Epidemiology of Neuropathic Pain : How Common is Neuropathic Pain , and What Is Its Impact ?," -, vol., no., pp. 1–2, 2015.

[13] International Association for the Study of Pain, "What is Neuropathic Pain," p. 2015, 2015.

[14] K. G. Brooks and T. L. Kessler, "Treatments for neuropathic pain," *Clin. Pharm.*, vol. 9, no. 12, pp. 1–12, 2017.

[15] E. Cavalli, S. Mammana, F. Nicoletti, P. Bramanti, and E. Mazzon, "The neuropathic pain: An overview of the current treatment and future therapeutic approaches," *Int. J. Immunopathol. Pharmacol.*, vol. 33, pp. 2058738419838383–2058738419838383, 2019.

[16] G. Kotzar *et al.*, "Evaluation of MEMS materials of construction for implantable medical devices," *Biomaterials*, vol. 23, no. 13, pp. 2737–2750, 2002.

[17] Y. Onuki, U. Bhardwaj, F. Papadimitrakopoulos, and D. J. Burgess, "A review of the biocompatibility of implantable devices: current challenges to overcome foreign body response.," *J. Diabetes Sci. Technol.*, vol. 2, no. 6, pp. 1003–15, 2008.

[18] C. Hassler, T. Boretius, and T. Stieglitz, "Polymers for neural implants," *J. Polym. Sci. Part B Polym. Phys.*, vol. 49, no. 1, pp. 18–33, 2011.

[19] B. J. Kim and E. Meng, "Review of polymer MEMS micromachining," *J. Micromechanics Microengineering*, vol. 26, no. 1, 2015.

[20] K. Scholten and E. Meng, "Materials for microfabricated implantable devices: A review," *Lab Chip*, vol. 15, no. 22, pp. 4256–4272, 2015.

[21] N. R. Patel and P. P. Gohil, "International Journal of Emerging Technology and Advanced Engineering A Review on Biomaterials: Scope, Applications & Human Anatomy Significance," *Int. J. Emerg. Technol. Adv. Eng.*, vol. 2, no. 4, pp. 91–101, 2012.

[22] P. Fattahi, G. Yang, G. Kim, and M. R. Abidian, "A review of organic and inorganic biomaterials for neural interfaces," *Adv. Mater.*, vol. 26, no. 12, pp. 1846–1885, 2014.

[23] D. W. L. Hukins, A. Mahomed, and S. N. Kukureka, "Accelerated aging for testing polymeric biomaterials and medical devices," *Med. Eng. Phys.*, vol. 30, no. 10, pp. 1270–1274, 2008.

[24] K. J. Hemmerich, "General aging theory and simplified protocol for accelerated aging of medical devices," *Med. Plast. Biomater.*, vol. 5, pp. 16–23, 1998.

[25] B. J. Lambert and F. W. Tang, "Rationale for practical medical device accelerated aging programs in AAMI TIR 17," *Radiat. Phys. Chem.*, vol. 57, no. 3–6, pp. 349–353, 2000.

[26] S. Minnikanti *et al.*, "Lifetime assessment of atomic-layer-deposited Al2O3-Parylene C bilayer coating for neural interfaces using accelerated age testing and electrochemical characterization.," *Acta Biomater.*, vol. 10, no. 2, pp. 960–7, 2014.

[27] W. Chun, N. Chou, S. Cho, S. Yang, and S. Kim, "Evaluation of sub-micrometer parylene C films as an insulation layer using electrochemical impedance spectroscopy," *Prog. Org. Coatings*, vol. 77, no. 2, pp. 537–547, 2014.

[28] J. Jeong, S. Hyun Bae, J. M. Seo, H. Chung, and S. June Kim, "Long-term evaluation of a liquid crystal polymer (LCP)-based retinal prosthesis," *J. Neural Eng.*, vol. 13, no. 2, p. 25004, 2016.

[29] R. Caldwell, H. Mandal, R. Sharma, F. Solzbacher, P. Tathireddy, and L. Rieth, "Analysis of Al_2O_3 —parylene C bilayer coatings and impact of microelectrode topography on long term stability of implantable neural arrays," *J. Neural Eng.*, vol. 14, no. 4, p. 046011, Aug. 2017.

[30] X. Xie *et al.*, "Long-term reliability of Al_2O_3 and Parylene C bilayer encapsulated Utah electrode array based neural interfaces for chronic

implantation," *J. Neural Eng.*, vol. 11, no. 2, p. 026016, 2014.

[31] X. Xie *et al.*, "Effect of bias voltage and temperature on lifetime of wireless neural interfaces with Al2O3 and parylene bilayer encapsulation," *Biomed. Microdevices*, vol. 17, no. 1, 2015.

[32] J. Jeong *et al.*, "Conformal Hermetic Sealing of Wireless Microelectronic Implantable Chiplets by Multilayered Atomic Layer Deposition (ALD)," *Adv. Funct. Mater.*, vol. 1806440, p. 1806440, 2018.

[33] X. Xie *et al.*, "Long-term bilayer encapsulation performance of atomic layer deposited Al2O3 and parylene c for biomedical implantable devices," *IEEE Trans. Biomed. Eng.*, vol. 60, no. 10, pp. 2943–2951, 2013.

[34] L. A. Escobar and W. Q. Meeker, "A Review of Accelerated Test Models," *Stat. Sci.*, vol. 21, no. 4, pp. 552–577, 2006.

[35] N. Lago, D. Ceballos, F. J Rodríguez, T. Stieglitz, and X. Navarro, "Long term assessment of axonal regeneration through polyimide regenerative electrodes to interface the peripheral nerve," *Biomaterials*, vol. 26, no. 14, pp. 2021–2031, 2005.

[36] R. R. Richardson, J. A. Miller, and W. M. Reichert, "Polyimides as biomaterials: preliminary biocompatibility testing," *Biomaterials*, vol. 14, no. 8, pp. 627–635, 1993.

[37] Y. Sun, S. P. Lacour, R. A. Brooks, N. Rushton, J. Fawcett, and R. E. Cameron, "Assessment of the biocompatibility of photosensitive polyimide for implantable medical device use.," *J. Biomed. Mater. Res. A*, vol. 90, no. 3, pp. 648–655, 2009.

[38] K. Lee, A. Singh, J. He, S. Massia, B. Kim, and G. Raupp, "Polyimide based neural implants with stiffness improvement," *Sensors Actuators, B Chem.*, vol. 102, no. 1, pp. 67–72, 2004.

[39] K. K. Lee *et al.*, "Polyimide-based intracortical neural implant with improved structural stiffness," *J. Micromechanics Microengineering*, vol. 14, no. 1, pp. 32–37, 2004.

[40] S. Schmidt, K. Horch, and R. Normann, "Biocompatibility of silicon-based electrode arrays implanted in feline cortical tissue," *J. Biomed. Mater. Res.*, vol. 27, no. 11, pp. 1393–1399, 1993.

[41] E. Tolstosheeva, V. Biefeld, and W. Lang, "Accelerated soak performance of BPDA-PPD polyimide for implantable MEAs," *Procedia Eng.*, vol. 120, pp. 36–40, 2015.

[42] J. M. Seo, S. J. Kim, H. Chung, E. T. Kim, H. G. Yu, and Y. S. Yu, "Biocompatibility of polyimide microelectrode array for retinal stimulation," *Mater. Sci. Eng. C*, vol. 24, no. 1–2, pp. 185–189, 2004.

[43] R. J. Vetter, J. C. Williams, D. R. Kipke, P. J. Rousche, D. S. Pellinen, and D. P. Pivin, "Flexible polyimide-based intracortical electrode arrays with bioactive capability," *IEEE Trans. Biomed. Eng.*, vol. 48, no. 3, pp. 361–371, 2001.

[44] K. Fukukawa and M. Ueda, "Recent Progress of Photosensitive Polyimides," *Polym. J.*, vol. 40, no. 4, pp. 281–296, 2008.

[45] W. C. Wilson and G. M. Atkinson, "Review of Polyimides Used in the Manufacturing of Micro Systems," *Nasa*, no. April, pp. 1–16, 2007.

[46] A. B. Frazier and M. G. Allen, "Metallic Microstructures Fabricated Using Photosensitive Polyimide Electroplating Molds," *J. Microelectromechanical Syst.*, vol. 2, no. 2, pp. 87–94, 1993.

[47] V. M. Lubecke, F. Pardo, and V. A. Lifton, "Polyimide spacers for flip-chip optical MEMS," *J. Microelectromechanical Syst.*, vol. 16, no. 4, pp. 959–968, 2007.

[48] R. Nayve *et al.*, "High-resolution long-array thermal ink jet printhead fabricated by anisotropic wet etching and deep Si RIE," *J. Microelectromechanical Syst.*, vol. 13, no. 5, pp. 814–821, 2004.

[49] T. Itabashi and M. P. Zussman, "High temperature resistant bonding solutions enabling thin wafer processing (characterization of polyimide base temporary bonding adhesive for thinned wafer handling)," *Proc. - Electron. Components Technol. Conf.*, pp. 1877–1880, 2010.

[50] Seung Woo Lee, Sung June Kim, Junghoon Kim, Kyou Sik Min, and Joonsoo Jeong, "Monolithic Encapsulation of Implantable Neuroprosthetic Devices Using Liquid Crystal Polymers," *IEEE Trans. Biomed. Eng.*, vol. 58, no. 8, pp. 2255–2263, 2011.

[51] B. Rubehn and T. Stieglitz, "In vitro evaluation of the long-term stability of polyimide as a material for neural implants," *Biomaterials*, vol. 31, no. 13, pp. 3449–3458, 2010.

[52] K. Palopoli-Trojani, V. Woods, C. H. Chiang, M. Trumpis, and J. Viventi, "In vitro assessment of long-term reliability of low-cost μηCoG arrays," *Proc. Annu. Int. Conf. IEEE Eng. Med. Biol. Soc. EMBS*, vol. 2016-Octob, pp.

4503–4506, 2016.

[53] V. Woods *et al.*, "Long-term recording reliability of liquid crystal polymer μ ECoG arrays," *J. Neural Eng.*, vol. 15, no. 6, 2018.

[54] B. J. Kim and E. Meng, "Micromachining of Parylene C for bioMEMS," *Polym. Adv. Technol.*, vol. 27, no. 5, pp. 564–576, 2016.

[55] S. Kuppusami and R. H. Oskouei, "Parylene Coatings in Medical Devices and Implants: A Review," *Univers. J. Biomed. Eng.*, vol. 3, no. 2, pp. 9–14, 2015.

[56] G. Samson and D. D. Cardenas, "Neurogenic Bladder in Spinal Cord Injury," *Phys. Med. Rehabil. Clin. N. Am.*, vol. 18, no. 2, pp. 255–274, 2007.

[57] S. Takeuchi, D. Ziegler, Y. Yoshida, K. Mabuchi, and T. Suzuki, "Parylene flexible neural probes integrated with microfluidic channels," *Lab Chip*, vol. 5, no. 5, pp. 519–523, 2005.

[58] B. D. Winslow, M. B. Christensen, W. K. Yang, F. Solzbacher, and P. A. Tresco, "A comparison of the tissue response to chronically implanted Parylene-C-coated and uncoated planar silicon microelectrode arrays in rat cortex," *Biomaterials*, vol. 31, no. 35, pp. 9163–9172, 2010.

[59] C. Metallo, R. D. White, and B. A. Trimmer, "Flexible parylene-based microelectrode arrays for high resolution EMG recordings in freely moving small animals," *J. Neurosci. Methods*, vol. 195, no. 2, pp. 176–184, 2011.

[60] B. G. X. Zhang, D. E. Myers, G. G. Wallace, M. Brandt, and P. F. M. Choong, "Bioactive coatings for orthopaedic implants-recent trends in

development of implant coatings," *Int. J. Mol. Sci.*, vol. 15, no. 7, pp. 11878–11921, 2014.

[61] M. Cieślik *et al.*, "Engineering of bone fixation metal implants biointerface - Application of parylene C as versatile protective coating," *Mater. Sci. Eng. C*, vol. 32, no. 8, pp. 2431–2435, 2012.

[62] L. Zhou *et al.*, "Parylene coating hinders Candida albicans adhesion to silicone elastomers and denture bases resin," *Arch. Oral Biol.*, vol. 55, no. 6, pp. 401–409, 2010.

[63] M. Santos, S. Soo, and H. Petridis, "The effect of Parylene coating on the surface roughness of PMMA after brushing," *J. Dent.*, vol. 41, no. 9, pp. 802–808, 2013.

[64] J. B. Fortin and T.-M. Lu, "Deposition kinetics for polymerization via the Gorham route," in *Chemical Vapor Deposition Polymerization*, Springer, 2004, pp. 41–55.

[65] C. Hassler, R. P. Von Metzen, P. Ruther, and T. Stieglitz, "Characterization of parylene C as an encapsulation material for implanted neural prostheses," *J. Biomed. Mater. Res. - Part B Appl. Biomater.*, vol. 93, no. 1, pp. 266–274, 2010.

[66] J. M. Hsu, L. Rieth, R. A. Normann, P. Tathireddy, and F. Solzbacher, "Encapsulation of an integrated neural interface device with parylene C," *IEEE Trans. Biomed. Eng.*, vol. 56, no. 1, pp. 23–29, 2009.

[67] J. Jeong, N. Chou, and S. Kim, "Long-term characterization of neural electrodes based on parylene-caulked polydimethylsiloxane substrate,"

Biomed. Microdevices, vol. 18, no. 3, 2016.

[68] J. H. C. Chang, Y. Liu, and Y. C. Tai, "Long term glass-encapsulated packaging for implant electronics," *Proc. IEEE Int. Conf. Micro Electro Mech. Syst.*, pp. 1127–1130, 2014.

[69] P. Wang *et al.*, "Long-term evaluation of a non-hermetic micropackage technology for MEMS-based, implantable pressure sensors," *2015 Transducers - 2015 18th Int. Conf. Solid-State Sensors, Actuators Microsystems, TRANSDUCERS 2015*, pp. 484–487, 2015.

[70] S. H. Kim, J. H. Moon, J. H. Kim, S. M. Jeong, and S. H. Lee, "Flexible, stretchable and implantable PDMS encapsulated cable for implantable medical device," *Biomed. Eng. Lett.*, vol. 1, no. 3, pp. 199–203, 2011.

[71] T. Adrega and S. P. Lacour, "Stretchable gold conductors embedded in PDMS and patterned by photolithography: Fabrication and electromechanical characterization," *J. Micromechanics Microengineering*, vol. 20, no. 5, 2010.

[72] Y. Lei, Y. Liu, W. Wang, W. Wu, and Z. Li, "Studies on Parylene C-caulked PDMS (pcPDMS) for low permeability required microfluidics applications," *Lab Chip*, vol. 11, no. 7, pp. 1385–1388, 2011.

[73] J. Jeong, S. Woo Lee, K. Sik Min, S. Shin, S. Beom Jun, and S. June Kim, "Liquid Crystal Polymer (LCP), an Attractive Substrate for Retinal Implant," *Sensors Mater.*, vol. 24, no. 4, pp. 189–203, 2012.

[74] J. Jeong, S. H. Bae, K. S. Min, J. M. Seo, H. Chung, and S. J. Kim, "A miniaturized, eye-conformable, and long-term reliable retinal prosthesis

using monolithic fabrication of liquid crystal polymer (LCP)," *IEEE Trans. Biomed. Eng.*, vol. 62, no. 3, pp. 982–989, 2015.

[75] C. J. Lee, S. J. Oh, J. K. Song, and S. J. Kim, "Neural signal recording using microelectrode arrays fabricated on liquid crystal polymer material," *Mater. Sci. Eng. C*, vol. 24, no. 1–2, pp. 265–268, 2004.

[76] K. S. Min *et al.*, "A Liquid Crystal Polymer-Based Neuromodulation System: An Application on Animal Model of Neuropathic Pain," *Neuromodulation Technol. Neural Interface*, vol. 17, no. 2, pp. 160–169, 2014.

[77] K. S. Min, S. H. Oh, M.-H. Park, J. Jeong, and S. J. Kim, "A Polymer-Based Multichannel Cochlear Electrode Array," *Otol. Neurotol.*, p. 1, 2014.

[78] T. M. Gwon *et al.*, "Fabrication and evaluation of an improved polymer-based cochlear electrode array for atraumatic insertion," *Biomed. Microdevices*, vol. 17, no. 2, p. 32, 2015.

[79] J. Jeong, S. Shin, G. J. Lee, T. M. Gwon, J. H. Park, and S. J. Kim, "Advancements in fabrication process of microelectrode array for a retinal prosthesis using Liquid Crystal Polymer (LCP)," *Proc. Annu. Int. Conf. IEEE Eng. Med. Biol. Soc. EMBS*, pp. 5295–5298, 2013.

[80] D. Ha, W. N. De Vries, S. W. M. John, P. P. Irazoqui, and W. J. Chappell, "Polymer-based miniature flexible capacitive pressure sensor for intraocular pressure (IOP) monitoring inside a mouse eye," *Biomed. Microdevices*, vol. 14, no. 1, pp. 207–215, 2012.

[81] S. H. Bae, J. Jeong, S. J. Kim, H. Chung, and J.-M. Seo, "Investigation of

Surgical Techniques for Optimization of Long-Term Outcomes of LCP-Based Retinal Prosthesis Implantation," *Transl. Vis. Sci. Technol.*, vol. 7, no. 4, p. 17, 2018.

[82] A. E. Hess, J. Dunning, D. Tyler, and C. A. Zorman, "Development of a microfabricated flat interface nerve electrode based on liquid crystal polymer and polynorbornene multilayered structures," *Proc. 3rd Int. IEEE EMBS Conf. Neural Eng.*, pp. 32–35, 2007.

[83] S. Mohtashami, M. R. Howlader, and T. Doyle, "Comparative electrochemical investigation of Pt, Au and Ti electrodes on liquid crystal polymer for the application of neuromuscular prostheses," *ECS Trans.*, vol. 35, no. 16, pp. 23–33, 2011.

[84] S. J. Kim, J.-W. Kim, J. H. Wee, P. Park, J. Seo, and J. H. Park, "Nerve cuff electrode using embedded magnets and its application to hypoglossal nerve stimulation," *J. Neural Eng.*, vol. 13, no. 6, p. 066014, 2016.

[85] T. M. Gwon, J. H. Kim, G. J. Choi, and S. J. Kim, "Mechanical interlocking to improve metal–polymer adhesion in polymer-based neural electrodes and its impact on device reliability," *J. Mater. Sci.*, vol. 51, no. 14, pp. 6897–6912, 2016.

[86] S. W. Lee, K. S. Min, J. Jeong, J. Kim, and S. J. Kim, "Monolithic encapsulation of implantable neuroprosthetic devices using liquid crystal polymers," *IEEE Trans. Biomed. Eng.*, vol. 58, no. 8, pp. 2255–2263, 2011.

[87] K. S. Min *et al.*, "A liquid crystal polymer-based neuromodulation system: An application on animal model of neuropathic pain," *Neuromodulation*,

vol. 17, no. 2, pp. 160–169, 2014.

[88] J. Jeong, S. H. Bae, K. S. Min, J.-M. Seo, H. Chung, and S. J. Kim, "A miniaturized, eye-conformable, and long-term reliable retinal prosthesis using monolithic fabrication of liquid crystal polymer (LCP)," *IEEE Trans. Biomed. Eng.*, vol. 62, no. 3, pp. 982–989, 2014.

[89] S. Shin, J.-H. Kim, J. Jeong, T. M. Gwon, S.-H. Lee, and S. J. Kim, "Novel four-sided neural probe fabricated by a thermal lamination process of polymer films," *J. Neurosci. Methods*, vol. 278, pp. 25–35, 2017.

[90] J. Jeong, S. H. Bae, K. S. Min, J.-M. Seo, H. Chung, and S. J. Kim, "A miniaturized, eye-conformable, and long-term reliable retinal prosthesis using monolithic fabrication of liquid crystal polymer (LCP)," *IEEE Trans. Biomed. Eng.*, vol. 62, no. 3, pp. 982–989, 2015.

[91] S. Yun *et al.*, "Remote-Controlled Fully Implantable Neural Stimulator for Freely Moving Small Animal," *Electronics*, vol. 8, no. 6, p. 706, 2019.

[92] S. Shim *et al.*, "A handheld neural stimulation controller for avian navigation guided by remote control," *Biomed. Mater. Eng.*, no. Preprint, pp. 1–11, 2019.

[93] K. Gosalia, J. Weiland, M. Humayun, and G. Lazzi, "Thermal elevation in the human eye and head due to the operation of a retinal prosthesis," *IEEE Trans. Biomed. Eng.*, vol. 51, no. 8, pp. 1469–1477, 2004.

[94] H. Hori, G. Moretti, A. Rebora, and F. Crovato, "The thickness of human scalp: normal and bald.," *J. Invest. Dermatol.*, vol. 58, no. 6, pp. 396–399, 1972.

[95] P. A. Hasgall *et al.*, "IT'IS Database for thermal and electromagnetic parameters of biological tissues. Version 4.0, May 15, 2018. doi: 10.13099," VIP21000-04-0. Onl: www. itis. ethz. ch/database, 2018.

[96] Z. Xu, Q. Li, and W. He, "Analytical Solution for the Forward Problem of Magnetic Induction Tomography with Multi-layer Sphere Model," in *Proceedings of the 2010 International Conference on Life System Modeling and Simulation and Intelligent Computing, and 2010 International Conference on Intelligent Computing for Sustainable Energy and Environment: Part III*, 2010, pp. 42–50.

[97] H. A. M. Mahinda and O. P. Murty, "Variability in thickness of human skull bones and sternum - An autopsy experience," *J. Forensic Med. Toxicol.*, vol. 26, no. 2, pp. 26–31, 2009.

[98] S. F. Cogan, "Neural Stimulation and Recording Electrodes," *Annu. Rev. Biomed. Eng.*, vol. 10, no. 1, pp. 275–309, 2008.

[99] S. Shin *et al.*, "High charge storage capacity electrodeposited iridium oxide film on liquid crystal polymer-based neural electrodes," *Sensors Mater.*, vol. 28, no. 3, pp. 243–260, 2016.

[100] J. Seo, J. H. Wee, J. H. Park, P. Park, J. W. Kim, and S. J. Kim, "Nerve cuff electrode using embedded magnets and its application to hypoglossal nerve stimulation," *J. Neural Eng.*, vol. 13, no. 6, 2016.

[101] A. Cisnal, J. C. Fraile, J. Pérez-Turiel, V. Muñoz-Martinez, C. Müller, and F. R. Ihmig, "A measurement setup and automated calculation method to determine the charge injection capacity of implantable microelectrodes,"

Sensors (Switzerland), vol. 18, no. 12, 2018.

[102] A. Post, M. B. Müller, M. Engelmann, and M. E. Keck, "Repetitive transcranial magnetic stimulation in rats: Evidence for a neuroprotective effect in vitro and in vivo," *Eur. J. Neurosci.*, vol. 11, no. 9, pp. 3247–3254, 1999.

[103] B. Linderoth, C.-O. Stiller, L. Gunasekera, W. T. O'Connor, U. Ungerstedt, and E. Brodin, "Gamma-aminobutyric Acid Is Released in the Dorsal Horn by Electrical Spinal Cord Stimulation: An In Vivo Microdialysis Study in the Rat," *Neurosurgery*, vol. 34, no. 3, pp. 484–489, Mar. 1994.

[104] C. B. McCracken and A. A. Grace, "High-frequency deep brain stimulation of the nucleus accumbens region suppresses neuronal activity and selectively modulates afferent drive in rat orbitofrontal cortex in vivo," *J. Neurosci.*, vol. 27, no. 46, pp. 12601–12610, 2007.

[105] J. A. Hosp, K. Molina-Luna, B. Hertler, C. O. Atiemo, and A. R. Luft, "Dopaminergic Modulation of Motor Maps in Rat Motor Cortex: An In Vivo Study," *Neuroscience*, vol. 159, no. 2, pp. 692–700, 2009.

[106] K. H. Lee *et al.*, "High-frequency stimulation of the subthalamic nucleus increases glutamate in the subthalamic nucleus of rats as demonstrated by in vivo enzyme-linked glutamate sensor," *Brain Res.*, vol. 1162, no. 1, pp. 121–129, 2007.

[107] W. Meissner *et al.*, "Deep brain stimulation of subthalamic neurons increases striatal dopamine metabolism and induces contralateral circling in freely moving 6-hydroxydopamine-lesioned rats," *Neurosci. Lett.*, vol.

328, no. 2, pp. 105–108, 2002.

[108] J. Wang *et al.*, "Integrated device for combined optical neuromodulation and electrical recording for chronic in vivo applications," *J. Neural Eng.*, vol. 9, no. 1, p. 16001, 2011.

[109] A. Z. Kouzani, O. A. Abulseoud, S. J. Tye, M. K. Hosain, and M. Berk, "A Low Power Micro Deep Brain Stimulation Device for Murine Preclinical Research," *IEEE J. Transl. Eng. Heal. Med.*, vol. 1, no. May, pp. 1500109–1500109, 2013.

[110] C. Forni, O. Mainard, C. Melon, D. Goguenheim, L. Kerkerian-Le Goff, and P. Salin, "Portable microstimulator for chronic deep brain stimulation in freely moving rats," *J. Neurosci. Methods*, vol. 209, no. 1, pp. 50–57, 2012.

[111] H. Y. Liu *et al.*, "Chronic deep brain stimulation in the rat nucleus accumbens and its effect on morphine reinforcement," *Addict. Biol.*, vol. 13, no. 1, pp. 40–46, 2008.

[112] K. Badstuebner, U. Gimsa, I. Weber, A. Tuchscherer, and J. Gimsa, "Deep Brain Stimulation of Hemiparkinsonian Rats with Unipolar and Bipolar Electrodes for up to 6 Weeks: Behavioral Testing of Freely Moving Animals," *Parkinsons. Dis.*, vol. 2017, 2017.

[113] R. de Haas *et al.*, "Wireless implantable micro-stimulation device for high frequency bilateral deep brain stimulation in freely moving mice," *J. Neurosci. Methods*, vol. 209, no. 1, pp. 113–119, 2012.

[114] I. Decosterd and C. J. Woolf, "Spared nerve injury: an animal model of

persistent peripheral neuropathic pain," *Pain*, vol. 87, no. 2, pp. 149–158, 2000.

[115] J. Kim, S. E. Lee, J. Shin, H. H. Jung, S. J. Kim, and J. W. Chang, "The neuromodulation of neuropathic pain by measuring pain response rate and pain response duration in animal," *J. Korean Neurosurg. Soc.*, vol. 57, no. 1, pp. 6–11, 2015.

[116] W. J. Jackson and H. F. Kuhfuss, "Liquid crystal polymers, I. Preparation and properties of p-hydroxybenzoic acid copolyesters," *J. Polym. Sci. Part A Polym. Chem.*, vol. 34, no. 15, pp. 3031–3046, 1996.

[117] Z. Ophir and Y. Ide, "Injection molding of thermotropic liquid crystal polymers," *Polym. Eng. Sci.*, vol. 23, no. 14, pp. 792–796, 1983.

[118] L. T. De Haan *et al.*, "Accordion-like actuators of multiple 3D patterned liquid crystal polymer films," *Adv. Funct. Mater.*, vol. 24, no. 9, pp. 1251–1258, 2014.

[119] S. Gantenbein, K. Masania, W. Woigk, J. P. W. Sesseg, T. A. Tervoort, and A. R. Studart, "Three-dimensional printing of hierarchical liquid-crystal-polymer structures," *Nature*, vol. 561, no. 7722, pp. 226–230, 2018.

[120] S. Shukla *et al.*, "Subwavelength direct laser patterning of conductive gold nanostructures by simultaneous photopolymerization and photoreduction," *ACS Nano*, vol. 5, no. 3, pp. 1947–1957, 2011.

[121] P. T. Bishop *et al.*, "Printed gold for electronic applications," *Gold Bull.*, vol. 43, no. 3, pp. 181–188, 2010.

[122] H. T. Lancashire, D. Jiang, A. Demosthenous, and N. Donaldson, "An ASIC

for Recording and Stimulation in Stacked Microchannel Neural Interfaces," *IEEE Trans. Biomed. Circuits Syst.*, vol. 13, no. 2, pp. 259–270, 2019.

[123] R. Ramezani *et al.*, "On-Probe Neural Interface ASIC for Combined Electrical Recording and Optogenetic Stimulation," *IEEE Trans. Biomed. Circuits Syst.*, vol. 12, no. 3, pp. 576–588, 2018.

국문초록

심뇌자극술은 파킨슨씨병, 본태성 진전, 긴장이상, 신경병증성 통증 등의 신경성 병증의 증상 완화를 위한 신경외과적 기술이다. 1997년 미 식품의약국에서 파킨슨씨병 환자 용 DBS에 대해 허가가 난 이후로 전 세계적으로 약 15만 명 이상의 환자가 DBS 이식수술을 받았다. 하지만 상용 DBS 장치는 그 크기와 구조로 인해 감염이나 수술 난이도를 비롯한 여러 문제점을 가지고 있다. 이런 문제점의 가장 주요한 점은 바로 이식형 파형생성기 (IPG) 이다. 이 IPG는 티타늄 합금 기반으로 제작된 상대적으로 크기가 큰 장치이기 때문에 흉부에 이식되어야 한다. 따라서 정수리 근처에 위치하는 전극과의 연결을 위해서는 연장선을 필요로 하게 되는데, 이 연장선이 흉부부터 정수리까지 피하에 터널을 뚫으며 연결되어야 하는 매우 침습적인 수술이기에 수술 시간도 오래 걸리고, 염증의 가능성도 크다. 이를 해결하기 위해 DBS의 소형화에 대한 여러 연구가 이루어지고 있다.

신경병증성 통증은 체성신경계의 병변 또는 질병으로 인해 발생하는 통증이다. 2014년 기준 세계적으로 약 7~8%의 유병률을 가지고 있었다. 신경병증성 통증의 환자들은 우울증, 관상 동맥 질환, 심근 경색증 환자 등에 비견될

정도로 낮은 등급의 삶의 질을 갖는 것으로 확인된다. 약물 내성을 가진 중증 신경병증성 통증 환자들에게는 신경자극술이 상당히 고려해 볼만 한 시술이다.

본 연구에서는 피하에 헤드마운터블한 소형화된 DBS 시스템을 개발했다. 시스템은 이식형 내부기와 외부기로 구성된다. 내부기는 20 mm의 전극을 가지고 있으며 13mm 직경에 5 mm 높이의 소형화된 패키지를 가지고 있기 때문에 환자의 두피와 두개골 사이에 이식될 수 있다. 이를 통해 수술시 절개 범위를 최소화하고 장치 이식 수술의 어려움을 줄일 수 있다. 이식형 장치는 생체적합성 폴리머인 액정폴리머를 기반으로 일체형으로 제작되었으며, 이전 연구에서 체내 수분 환경에서 매우 우수한 장기 신뢰성을 보여주었다. 이 장치는 다채널 탐침형 전극, 전류 자극 파형 생성용 ASIC 및 수신 코일로 구성된다.

외부기 역시 소형화 되어있기 때문에, 내부기가 이식된 환자의 두피 위에 부착될 수 있다. 이 외부기는 폭 20 mm, 길이 35 mm, 두께 12 mm를 가지며, 리튬폴리머 배터리, ZigBee 수신회로, 클래스 E 증폭기를 포함하고 있다. 송신 코일은 내부기에 유도 결합을 통해 전력과 파형을 전송하기 위해 환자의 몸에 붙어있게 된다.

이처럼 배터리가 외부기에 위치하고 있기 때문에 이 시스템은 상용 DBS 장치들에 비해 몇가지 장점을 가지는데, 이는 MRI 호환성과 체내에 위치하는 배터리로 인한 문제로부터의 해방을 들 수 있다. 해당 외부기의 동작을 확

인하기 위해 벤치탑 테스트를 진행하였고, 전극을 평가하기 위해 in vitro 실험을 진행하였으며, DBS 시스템 자체의 성능을 확인하기 위해 SNI 모델로 통증을 유발한 rat에 대해 von Frey 행동반응 실험을 진행하였다. 실험대상 동물들에게는 VPL을 타겟으로 DBS가 이식되었으며, DBS 자극의 동반여부에 따라 동물에게 물리적 자극을 주면서 발을 들어올리는 자극의 최소크기를 구하였다. 마지막으로 개발된 시스템에 대한 몇가지 논의를 진행하였다.

주요어: 심뇌자극술, 생체 이식형 전자 장치, 액정 폴리머, 신경병증성 통증, 자기 유도 결합
학번: 2014-21699

감사의 글

박사과정 졸업을 앞두고 보니, 대학원 진학을 처음 꿈꾸게 되었던 고등학교 2학년 시절이 생각납니다. 교실에 놓여있던 잡지에서 BMI에 관한 기사를 처음 읽고, 이 분야의 연구를 하고싶다는 막연한 마음으로 전기공학부에 입학하게 되었습니다. 군대를 다녀오고, 대학원에 입학하고, 이 자리에 서고 보니 어느덧 14년이란 세월이 흘러 저는 서른 두 살이 되었습니다. 애초에 마음먹었던 진로와는 다른 길로 가고 있지만, 이렇게 생각이 바뀌고 모르던 것을 배워가며 나아가는 것이야말로 삶의 모습이 아닐까 생각합니다. 제가 이렇게 변화하고 배워가며 이 자리에 오기까지, 이기적이고 편협한 제 기억보다 훨씬 많은 분들의 감사한 도움이 있었을 거라고 생각합니다. 이 글이 그런 분들께 바치는 제 존경과 감사를 충분히 표현하지 못하더라도, 부디 부족한 저를 너그러운 마음으로 보아주시기 바라겠습니다.

가장 먼저 제가 어떤 말로 감사를 드려도 부족할 저희 가족들에게 감사드립니다. 초등학교, 중학교, 고등학교, 대학교도 모자라 대학원까지 총 22년이라는 긴 시간동안 저를 공부시키기 위해 고생하신 부모님께 송구스럽고 감사합니다. 못난 아들을 두 분의 아들이라는 이유만으로 어떠한 조건도 없이 아끼고 사랑해 주셔서 감사합니다. 세상 모두가 그렇듯 저는 두 분으로 말미암아 세상에 태어났으며, 두 분의 희생 없이는 이 자리까지 겪었던 모든 행복을 가지지 못했을 것입니다. 부족하지만 두 분께 어디 내놓아도 자랑스런 아들이 될 수 있도록 더 노력하여 지금까지 받은 과분한 사랑과 지원은 평생 갚아 나가도록 하겠습니다.

또 제 동생 건희에게 고맙다는 말을 전하고 싶습니다. 군 복무 후에 학교가 멀다는 핑계로 부모님 곁을 떠난 저 대신, 두 분께 때로는 믿음직한 아들로, 때로는 살가운 아들로 제 몫까지 대신하기 위해 많은 노력을 했다는 것을 알고 있습니다. 가족일수록 이런 이야기를 하는게 쉽지 않아 동생에게 다정한 말을 많이 하지는 못했지만, 이 글을 빌어 항상 동생이 있어서 고맙고 든든하다는 말을 해주고 싶습니다.

다음으로 지도교수님이신 김성준 교수님께 감사를 드리고 싶습니다. 학부 4학년 시절 의용생체공학 개론을 수강하면서 처음 만나 뵙게 된 교수님은 전공분야에 대해 크나큰 열정과 식견이, 그리고 무엇보다도 확고한 신념을 가지신 것이 느껴지는 분이었습니다. 이러한 교수님의 모습에 매료되어 막연한 생각으로 연구실에 들어온 저에게, 연구라는 것은 사실 많이 낯설고, 어렵고, 복잡한 것이었습니다. 그럼에도 제가 무사히 박사학위를 마칠 수 있었던 것은 온전히 교수님의 관심과 지도가 있었기 때문이라고 생각합니다. 제가 방향을 잃을 때마다 그 원인에 대해 고민해 보도록 독려해 주시고, 제 시야에서는 보이지 않는 것을 깨우칠 수 있도록 새로운 관점들을 제시해 주셨습니다. 제가 비록 전공과는 거리가 있는 방향으로 진로를 잡게 되었지만, 교수님께 받은 연구를 대하는 자세에 대한 가르침은 평생 잊지 않도록 하겠습니다. 정말 감사합니다 교수님.

제 박사학위 심사에서 위원장을 맡아주신 박병국 교수님께도 감사드립니다. 대학원 과정에서 교수님의 수업에서 얻은 반도체 공정에 대한 지식은 학위과정 내내 큰 도움이 되었습니다. 또한 바쁘신 와중에도 보여 드리기 부끄러울 만큼 부족한 제 논문에 여러 좋은 조언을 해 주셔서 정말로 감사합니다.

더불어 제 학위 심사에 참여해주신 연세대학교 의과대학 장진우 교수님께도 감사드립니다. 교수님께서 품으신 신경보철에 대한 비전과 공학적인 식견은 저에게 큰 귀감이 되었습니다. 가끔은 저에게 따끔한 충고도 아끼시지 않는 모습에서 저를 아끼고 걱정하시는 마음이 느껴져 오히려 감사했습니다. 게다가 진료를 비롯한 여러 업무로 바쁘신 와중에도 제 심사에 참석해 주시기 위해 시간을 내 주셔서 송구스럽고 감사했습니다.

더불어, 서종모 교수님께도 감사드립니다. 대학원 과정에서 수강했던 교수님 수업에서 배운 의학의 기초적인 지식이 의용생체공학을 전공하는 데 매우 큰 도움이 되었습니다. 더불어 학위 심사 때 짚어 주신 논문에 대한 개선 사항도 조금 더 내실 있는 학위 논문이 되는 데 큰 도움이 되었습니다.

마지막 심사위원이셨던 부산대학교 의과대학 정준수 교수님께도 감사드립니다. 제가 학부생이던 2013년 여름에 박사과정에 재학중인 선배로 처음 뵙고 제 학부 졸업논문 연구도 도움을 받았었는데, 이제는 교수님이 되어 제 박사학위 졸업에도 도움을 받게 되었습니다. 항상 침착하고 성실한, 그리고 특히 연구

를 잘하시는 본받고 싶은 선배였는데, 저는 그렇게 되지는 못해 아쉽습니다. 정준수 교수님은 많은 학생들에게 훌륭한 가르침을 주시리라 믿어 의심치 않습니다. 항상 응원하겠습니다.

제 학위 심사에 심사위원으로 모시지는 못했지만 학위과정 내내 물심양면으로 도움을 주셨던 이화여자대학교 전상범 교수님께도 감사 인사를 전하고 싶습니다. 6년간 한결같이 학생들을 챙기시고, 지도하시는 모습을 지켜보면서 교수님들의 고충과 학위과정이 갖는 의미에 대해 많이 이해하게 되는 기회가 되었습니다. 감사합니다.

그 다음으로 연구실 선배들께 감사드리고 싶습니다. 수 년 동안 서로 함께 고생하고 노력하시는 모습들을 지켜본 선배들이 보여주신 모범이 부족한 저를 이 자리까지 있게 하지 않았나 합니다. 한 분 한 분 적으려니 뭔가 오글거리지만, 이 때 아니면 언제 하겠나 싶은 이야기들을 적어 보겠습니다.

민규식 선배는 제가 알고 있는 선배들 중 웃음소리가 가장 호탕한 분입니다. 연구실에 오던 첫날 “안녕! 내가 왕고야! 하하하하” 하시며 매점으로 향하던 형의 모습이 아직도 잊혀지지 않네요. 그 후로 얼마 함께 지내지 못하고 졸업하시게 되어서 아쉬웠는데, 후에 토닥의 대표님으로 다시 자주 뵙게 되어 매우 반가웠습니다. 주변 지인들을 보면 사업이 매우 힘들고, 유지하기조차 쉽지 않다고 하는데, 힘들다고 말씀하시면서도 몇 년째 훌륭하게 토닥을 이끌어 가시는 걸 보면 참 대단하시다는 생각이 듭니다. 연구실 행사나 결혼식에서 뵈었던 형수님과 너무너무 귀여운 대찬이, 혜원이, 요셉이 모두 건강하고 행복하시기를 기원하겠습니다.

김진호 선배는 제가 연구실에서 가장 믿고 따르던 선배입니다. 연구실 최고의 도량과 주량을 가진 진호 형은 제가 인간적으로 가장 닮고 싶던 형입니다. 정환이 형, 진호 형과 함께 봉천동과 충무로를 누비던 날들은 20대의 저에게 많은 위안이 되고 힘이 되었습니다. 이제는 예전처럼 자주 뵙지 못하지만, 다시 형들과 함께할 날을 기대하고 있겠습니다. 열심히 돈도 모아둘게요. :) 이제는 어엿한 가장이시니 아름다운 형수님과 귀여운 다온이와 함께 오래오래 행복하시길 기원하겠습니다.

이성은 선배는 DBS 연구에 있어서 제 사수였고, 인턴 시절부터 연구실에 대해 하나부터 열까지 많은 것들을 알려주신 선배입니다. 신입생 시절에는 이런 고마움을 모르고 형에게 많이 까불었던 것 같은데, 그래도 항상 친동생 대하듯 너그러이 대해 주셔서 감사했습니다. 형은 알고 계실지 모르겠지만 형에게 까불던 대가는 후배를 통해 섭섭치 않으실 만큼 치렀으니 억울하실 필요는 없을 것 같습니다. 회사에 가면 좀 더 자주 뵙길 기대하겠습니다.

엄경식 선배는 제가 가장 처음 봤던 연구실 분입니다. 학부 4학년때 수강했던 의용생체공학개론의 담당 조교였는데, 어느 날 갑자기 조교님께서 쓰러지셨다는 소식을 듣고 놀랐던 기억이 있습니다. 다행히 무사히 복귀하셔서 연구실에서 만나 뵙게 되었지만 연구실에 입학한 후에도 언젠가 같이 술 한 잔 하자는 약속을 계속 지키지 못하다가 얼마 전에야 이루게 되었네요. 항상 침착하지만 장난기 많고 재미있는 형이 계셔서 연구실 생활이 즐거웠습니다. LG보다는 나중이겠지만 한화도 어서 강팀이 되기를 기원할게요. 이제는 부산대학교 교수님이 되어 연구와 후학 양성을 위해 힘쓰고 계신데, 형수님과 아들을 위해서 바쁘시더라도 항상 건강 잘 챙기시기 바라겠습니다.

박정환 선배는 특유의 입담과 귀여움(!)을 모두 갖춘 분입니다. 양손을 흔들며 하는 인사는 정환이 형의 트레이드 마크였습니다. 친절하고 인자한 형에게 자주 까불고 막말을 했던 것 같아 죄송한 마음이 크네요. 그래도 항상 저를 챙겨 주시고, 걱정해주신 마음은 잘 알고 있었습니다. 항상 감사하게 생각합니다. 박사후 과정으로 한국을 떠나시기 전까지 매달 마지막 금요일에는 월급날인 진호 형을 찾아가 육해공을 완성하던 시절이 그립기도 합니다. 그래도 이제 곧 싱가폴에서 고생을 끝내시고 귀국하신다는 소식을 들어 다시 뵙게 될 날이 기대됩니다.

신수원 선배는 참 배려가 넘치는 분이었습니다. LCP 공정을 가르쳐 주신 분도 수원 누나였습니다. 제 인턴 시절에 태목이 형과 연애 중이란 걸 눈치채고 두 분이 함께 계시는 걸 지켜보는 재미도 쏠쏠했습니다. 제가 태목이 형을 따라 전기공학부 야구부 EBC에 들어가고 6년동안 동아리 활동을 하면서, 태목이 형이 뛰는 거의 모든 경기를 응원하러 오셨던 것으로 기억합니다. 게다가 지고 있던 경기도 누나가 오시면 모두 역전했던 것을 보면, 태목이 형 외의 나머지 팀

원들에게도 큰 힘이 되었습니다. 지금은 토닥의 코어인력이 되셨다고 들었는데, 연구하던 길을 걸으며 보람과 성취를 느끼실 것이 부럽기도 하고 대단해 보이기도 합니다. 토닥의 승승장구와 함께 태목이 형과도 행복하시길 빌겠습니다.

권태목 선배는 제가 연구실에 있으면서 가장 자주 함께 술을 마셨던 선배입니다. 2년 선배였지만 때로는 친형처럼 따듯한 격려도 해주시고, 때로는 맞선임(?!)처럼 따끔한 지적도 아끼시지 않는 형입니다. 형과 함께 자주 가던 김치찌개 집 앞을 지날 때마다 형이 해 주셨던 조언과 격려들이 생각나곤 합니다. 저에게 대학원 생활 동안 저에게 가장 큰 활력이 되었던 EBC를 소개해주신 형이고, 더불어 저에겐 함께 키스톤 콤비로 가장 많은 경기를 출장한 유격수이며, 또 연구실 학생들끼리 하는 농구에서도 패배를 모르는 최고의 슈터였습니다. 요즘 회사에서 일이 많이 바쁘신 것 같던데, 형이라면 다 잘 해내실 거라 믿습니다. 내년에는 제가 회사로 가서 더 자주 뵙고 예전처럼 술 한잔 기울이게 될 수 있지 않을까 합니다. 그동안 감사했고, 앞으로도 잘 부탁드립니다.

그 다음으로는 저와 연구실 생활을 오래 함께한 동기, 후배들에게 감사하고 싶습니다. 부족한 제가 의지하고, 다독이며 고생을 함께한 이들이기에 어떤 때에는 친동생보다 더 형제처럼 느껴 지기도 합니다. 이제는 각자의 길을 걸으며 함께했던 지난 시절을 추억하게 되겠지만, 어디서든 자신의 몫을 다 할 수 있는 이들이기에 아쉬움 보다는 다시 만날 때의 기대가 더 큽니다.

김채빈 군은 저와 학부 졸업프로젝트, 인턴 시절부터 함께해 온 친구입니다. 나이도 같아 자주 대화하며 속 깊은 이야기도 나누곤 했는데, 제가 성격이 못나 채빈이에게 더 잘해주지 못했던 것이 못내 아쉽기는 합니다. 지금은 플로리다에서 따듯한 겨울을 연구원으로서 지내고 있을 텐데, 앞으로도 좋은 연구를 하며, 좋은 사람들과 행복하길 기원하겠습니다.

서정민 군은 저와 가는 길이 참 많이 겹치는 친구입니다. 초등학생 시절 어린이 명예경찰 포돌이, 고등학생 시절 서울시 과학전시관 산하 영재교육원, 전기공학부 C반, 연구실, 그리고 삼성전자 메모리 사업부까지. 나이는 저보다 어리지만 생각이 깊고 열정적이던 동기입니다. 그리고 하스스톤이라는 신문물을 연구실에 도입한 정민이는 저희들 사이에서 카기꾼이라고도 불립니다. 항상 유쾌하고, 재미있고, 일도 잘하는 정민이를 보면서 동생이지만 많이 배웠습니다.

이제 회사에 들어가면 6개월 선배님으로 모셔야 할텐데, 그동안 당한 걸 갚겠다고 벼르고 있지는 않나 갑자기 걱정이 됩니다. 정민이야 말로 회사에서 자주 보게 될 테지만, 회사에서도 제수씨와도 행복한 일들만 펼쳐지길 기원하겠습니다.

심신용 군은 연구실에서 가장 신뢰할 수 있는 후배입니다. 항상 신중하고, 말을 가려 할 줄 아는 현명한 동생입니다. 가끔은 그 완벽함을 깨 보고 싶어 일부러 짓궂은 장난을 쳐도 화 한번 내는 적 없이 허허 웃는 진중한 친구입니다. 또한 연구실에 입학한 뒤 나간 미팅에서 만난 여자친구와 5년이 넘는 연애를 하는 순정남이기도 합니다. 그리고 이번 졸업생 중 유일하게 연구를 계속하며 박사후 과정으로 진학하는 친구인 만큼, 연구에 대한 능력과 열정이 발군인 훌륭한 연구자입니다. 우여곡절 끝에 가게 된 새로운 터전에서도 지금처럼 중심을 잘 잡고 연구에 정진한다면 저희 연구실 출신 마지막 교수님도 될 수 있지 않을까 합니다. 다만 여기저기 잔병치레가 많은 친구라 건강을 잘 챙기면서 생활했으면 하는 바람이 있습니다.

최광진 군은 연구실 후배들 중 가장 저를 잘 따르던 고마운 후배였습니다. 의정부 맛집인 삼겹살 집 아들인 광진이는 두부와 콩은 좋아하지 않지만 마블을 좋아하고, 트와이스를 좋아하며 항상 밝고 유머 넘치는 선량한 친구입니다. 건장한 체격에 비해 운동신경은 살짝 아쉽지만, 무엇을 하든 열심히 하는 광진이는 연구실에서 가장 이해심이 넓은 동생입니다. 제가 재미없는 농담을 해도 가장 잘 받아주고, 국방부 과제에서도 전극, 커넥터, 케이블 같은 소모품의 제작을 주로 맡아서 고생하면서도 열심히 자기 본분을 다하는 학생이었습니다. 졸업 후에는 토닥으로 가게 되어 지금처럼 자주 보기는 힘들겠지만, 언제 어디에 있든 묵묵히 제 몫을 다할 친구이니 걱정은 하지 않겠습니다. 모쪼록 좋은 분들이 가득한 곳에서 보람과 성취가 가득한 길을 걷길 기원합니다.

윤승현 군은 저와 가장 많은 시간을 함께 보낸 후배입니다. 유쾌하고 장난기도 많지만 제가 바빠서 식사를 거르는 날이면 조용히 매점에서 먹거리를 사다 주는 사려 깊은 후배입니다. 연구실에서 항상 열심히 일하는 승현이는 국방부 과제에서도 중추적인 역할을 해낸 훌륭한 연구자이기도 합니다. 하지만 박사과정 동안 여러 번 마음의 상처를 입고 오실로스코프 양과의 10층 데이트로 시간을 보내던 모습이 주변 이들을 안타깝게 만들기도 했습니다. 졸업 후에는

승현이도 좋은 짝을 만나서 행복을 이루길 바라겠습니다. 연구실 생활 동안 저와 가장 많이 티격태격 했던 후배였는데, 정말 어떨 땐 친동생보다 더 동생같이 느껴지는 후배입니다. 함께 회사로 가게 되는 만큼 앞으로도 힘든 일이 있을 때 의지할 수 있는 사이로 자주 볼 수 있으면 좋겠습니다.

성재훈 군은 제가 조금 더 가까이 두고 보고싶은 욕심이 나는 동생입니다. 어린 나이에 저라면 견디기 힘들 것 같은 여러 풍파를 겪었지만, 그래도 긍정적인 마인드로 극복해내는 어른스러운 친구입니다. 연구실에 인턴으로 들어와서도 쉽지 않은 과업을 맡아 훌륭히 해내는 것을 보고 감탄하게 되기도 했습니다. 곧 미국으로 돌아가 듀크에서 공부를 마칠 계획인 것으로 알고 있는데, 부디 앞으로는 고생보다는 즐거운 일들만 가득하길 바랍니다. 특히 미국으로 떠나타지에서 힘들더라도, 함께했던 모두가 응원하고 있음을 기억했으면 좋겠습니다.

박종화 군은 굉장히 관찰력이 뛰어나고 섬세한 후배입니다. 키스트 위탁석사과정으로 연구실에 들어와 자주 보진 못했지만, 만날 때마다 승현이와의 즐거운 대담으로 연구실 사람들에게 '인과응보'가 무엇인지 알려준 재미있는 친구입니다. 특히 음대 작곡과를 졸업하고, 신경과학 분야 석사에 도전하고, 또 졸업 후에는 벤처 사업가로 변신하는 용기를 가진 멋진 친구입니다. 앞으로는 (승현이와 함께) 더 자주 만나 재미있는 이야기 많이 들을 수 있기를 바라겠습니다.

저희 연구실 선후배가 아니더라도, 학위과정에서 도움을 주신 분들은 너무나도 많습니다. 그 중에서도 이현유 선생님께 감사하지 않는 졸업생은 아마 없을 거라 생각합니다. 저희 연구실에서 집행되는 연구비 행정 중 이현유 선생님의 손을 거치지 않는 일은 없었다고 해도 과언이 아닙니다. 유능한 선생님께서 행정업무를 도맡아 처리해 주셔서 학생들은 마음 편히 연구에 집중할 수 있었습니다. 항상 감사하게 생각하고 있습니다. 저희가 졸업한 이후에도 항상 건강하시고, 종종 다시 뵐 수 있기를 바라겠습니다.

DBS라는 제 연구 주제의 특성상, 신경과학 및 동물 실험 등에서 저에게 가장 큰 도움을 주신 연세대학교 장진우 교수님 연구실 소속 연구진 분들을 빼놓을 수 없겠습니다. 함께 한 많은 실험들은 부족한 제가 박사 학위를 따는 데 없어서는 안될 중요한 경험이 되고, 데이터가 되었습니다.

정현호 교수님은 제가 너무나도 존경하는 분입니다. 학생들과 격의없이 소통하시고, 함께 연구하는 저희를 배려해 주시고, 항상 친절하게 대해주시는 훌륭한 인품을 가진 분이십니다. 제자 여러 번 실망스런 결과를 보여드려도 보내주신 격려와 위로는 저에게 큰 힘이 되었습니다. 감사합니다.

또한 연구원 분들께도 감사드립니다. 세상 만사 무얼 여쭤봐도 모르시는 게 없는, 지금은 멋진 기장님이 되신 진형이형, 힘들다는 말씀 한마디 없이 저와 승현이의 졸업을 위해 많이 힘써 주신 고진수 박사님(다음에 뵐 땐 꼭 진수형이라고 부르겠습니다 ^^), 제가 연대에 처음 방문했을 때부터 친형처럼 챙겨주신 재우형, 동갑내기 친구라 더 쉽게 친해질 수 있었던, 뭐든지 열심히 하는 찬호, 지금은 졸업해서 연대를 떠났지만, 언제 봐도 반가운 민식이, 밝은 성격에 특유의 친화력으로 반말을 들어도 기분 나쁘지 않은 박민경 선생님. 모두 그동안 너무너무 감사했고, 원하시는 일들이 다 잘 이뤄지길 바란다는 말씀을 전하고 싶습니다.

연세대학교 이외에도 연구에 도움을 주신 많은 분들께 감사드립니다. 연구실 선배님으로서 제 고민을 자기 일처럼 걱정해 주시던 토닥 이호승 이사님, 제가 부족한 분야에 대해 조언해 주신 토닥 우진이형, 실험을 하러 이대에 갈 때면 환경 세팅, 주차권 제공 등 없어선 안될 역할을 해준 이대 윤경이 모두 본인들이 생각하시는 것보다 저에게 훨씬 큰 도움을 주셨습니다. 감사합니다.

6년동안 스스로의 욕심에 미치지 못하는 제가 원망스럽기도 했고, 저에 비해 훨씬 잘 해내고 있는 주위 대학원생들을 보면서 자괴감이 들기도 했습니다. 하지만 그런 제가 끝까지 포기하지 않도록 주위에서 위로하고 응원해주던 분들에게도 감사 인사를 전하고 싶습니다.

항상 그 자리에 있어 준 오래된 친구들이 있습니다. 19년째 단짝친구인 무엇이든 잘 하는 만능괴물 유석이, 대를 걸쳐서 우정을 쌓아가고 있는, 섬세하고 배려심 넘치는 태준이, 잠에 약해서 항상 가장 먼저 쓰러지지만 노는 자리에 없으면 너무너무 아쉬운 재영이, 초등학교 예비 소집일에 처음 만난, 올바른 스승을 꿈꾸는 문학인 병준이, 숫기는 없지만 못하는 것도 없는, 근데 요즘 체형이 조금 우리 쪽으로 넘어와 걱정인 필성이, 미식축구를 하던 덩치만큼 아는 것도(!) 많은 승민이, 요즘은 자주 못보지만 일할 때도 놀 때도 집중력이 뛰어난

한상. 모두 10대에 처음 만난 이래로 서로에게 평생 기억될, 눈물 나게 신나고 배꼽 빠지게 찌질한 추억들을 함께한 친구들입니다. 그동안 모나고 성급한 저에게 보여준 인내와 우정에 고맙다는 말을 전하고 싶습니다.

제 대학생활에서 가장 많은 추억들을 함께한, 남산골 사람들에게도 감사하고 싶습니다. 12-12 사태를 극복하고 이제는 훌륭한 의사가 되는 일만 남은, 저에게 누적기록으로 경차 한 대 값을 투자하신 치형이형, 제 과오로 소원해진 시기도 있었지만 제가 마음 깊이 좋아하는 진지한 진석이형, 학부 동기에 남산골 동기라는 이유로 저에게 가장 많은 괴롭힘을 당해야 했던 착하고 여린 종선이, 저의 최초의 동거인(?!)이자 이제는 (아마도) 가정적인 남편으로 진화한 통통이 원일이, 어디서 무얼 하든 잘 해 낼 거라 걱정은 안되지만 너무 다 가져서 부러운 준호, 조금은 엉뚱하지만 그만큼 사람 좋고 듬직한 성현이, 생긴 거랑 다르게 동기들 사이에서 여자 안승희(…)라 불릴 만큼 화끈하고 의리 넘치는 은경이, 동기들 중에 가장 저를 많이 혼내지만 힘들 때 이야기를 가장 잘 들어주는 혜린이, 그 밖에 제가 미처 다 적지 못한 남산골 여러분 모두 힘든 저에게 위로가 되고, 지친 저에게 격려가 되어 주셔서 감사합니다.

남산골 못지 않게 좋은 인연이 되어준 국인 여러분에게도 감사드립니다. 국인의 기둥이자 빛과 소금, 알면 알수록 대단한 남자 승환이형, 스무살 풋내기 시절에 만나 저의 흑역사와 찌질함을 모두 알고 있는 배울 점 많은 예비신랑 선일이, 특유의 침착함과 진중함이 매력적인, 이제는 가장으로써 제수씨와 이든이와 행복한 삶을 살고 있는 상준이, 의사님이 되셔서 자주 보진 못했지만 언제 만나도 즐겁고 반가운 세훈이, 분명 저보다 후배인데 취업도 결혼도 출산도 먼저 해서 누나같은 서현이, 힘든 일도 유머로 넘길 줄 아는 항상 씩씩한 유진이, 친동생인 건희보다도 더 저를 잘 따르던 고마운 동건이, 어른스럽고 진중한데 위트까지 갖춘 세훈이, 오빠보다는 형이라는 호칭이 더 익숙한 똘똘한 현정이, 항상 밝고 귀여운 개구쟁이 막냇동생 같은 강욱이, 불꽃 같은 20대를 다시없이 재밌게 보내는 동규, 대위로 열심히 국가를 지키는 미래의 법조인 성하, 저를 국인에서 고립시키려는 음모를 가진 삼성전자 슨배님 다정이, 해준 것도 없는 형을 잘 따라주는 창균이, 그리고 여기 적지 못한 많은 국인 여러분들 모두 학위과정동안 저와 기쁨도 슬픔도 모두 함께해 주셔서 감사합니다.

대학원 생활동안 저에게 가장 큰 낙이 되어주었던 것은 EBC에 소속되어 알게 된 야구입니다. 2014년에 연구실 입학 후 야구에 대해 아무것도 모르던 제가 6년동안 빠져 있게 된 것은 야구 자체보다도 좋은 사람들과 함께했기 때문입니다. 겉으로는 무뚝뚝하시지만 항상 많이 가르쳐 주려고 애쓰시는 성규 형, 저에게 야구가 가장 즐거웠던 해로 기억되는 한해를 만들어 주신 세윤이 형, 바쁘신 와중에도 후배들을 위해 희생하시는 EBC의 전설 한규 형, 아이들 키우느라 바쁘신 와중에도 참석하셔서 후배들 멘탈까지 잘 챙겨 주시는 원섭이 형, 지난해 주장을 하셔서 친해지게 되어 너무 다행이다 싶은, 속도 생각도 깊은 세준이 형, 처음엔 무서웠지만 이제는 반가운 김교수님 현이 형, 주장들이 가장 고마워하는, 야구 열정으로 불타오르는 이제는 예비신랑 준일이 형, 과묵하지만 듬직한, 후배들을 편하게 해주시던 규섭이 형, 제가 만나본 사람 중 가장 성격이 좋은 승현이 형, 애증의 류감독님, 저의 포지션 경쟁자 철이 형, 이제는 만년 유망주 탈출, 포텐폭발 파워블로거 호성이, 연습을 가장 열심히 나오던 미래의 주장 상현이, 항상 괴롭히고 짖궂은 말을 해도 이겨내는 멘탈갑 정훈이, 친구 아니랄까봐 역시 멘탈 좋은 건희, 같은 LG 팬으로써 희로애락을 함께했던 연군이, 결혼 준비한다고 경기 안 나오는, 버릇없이 형보다 먼저 장가가는 성준이, 저희 팀은 아니지만 항상 저에게 애정이 담긴 조언을 해 주시던 기정이 형, 주장을 하던 시절 고민이 많던 저에게 술친구가 되어준 기훈이, 모두들 저에게 있어 가장 즐거웠던 시간들을 함께 해 주셨던 것에 감사합니다.

대학원 입학 시절에 대해 이야기하다 보니, 반도체 공동연구소 공정장비 연구생 동기 친구들에 대해서도 생각이 납니다. 함께 Metal 연구생으로 김건주 기사님과 많은 시간을 보냈던 유쾌한 친구 학준이, 동네 친구가 없는 저에게 가장 가까운 동네친구가 되어준 목소리가 매력적인 진중한 규현이, 규현이와 함께 저의 우울한 주말을 함께 보내주던, 130 km/h의 강속구를 연습중인 유쾌한 석원이, 일본에서 대학을 나와서 그런지 사상이 독특한, 이제는 결혼을 앞둔 쪼꼬바 원하, 형들 사이에 어울리면서 전혀 기죽지 않는 개구쟁이 대곤이. 이 친구들과 함께한 시간들이 있어 연구에 대해 진지하게 고민하고, 발전하기 위해 노력할 수 있었습니다. 감사합니다.

고등학생 시절 저에게 평생 갈 가르침을 주셨던 선생님들께도 감사드립니다. 1학년 때부터 '이렇게 해서 내 후배 될 수 있겠어?'라는 말씀으로 저를 채찍질해 주셨던 박민역 선생님, 항상 '사람은 그릇을 키워야 한다'라는 말씀으로 공부보다도 인격적으로 완성된 사람이 되라고 가르쳐 주신 김준기 선생님. 졸업 후에 자주 찾아 뵙지 못해서 죄송한 마음이지만, 항상 선생님들께 감사하고 있습니다.

마지막으로, 몇몇 선배들께서는 신중하게 결정하길 권고하셨지만, 대학원 6년간 한결같이 저에게 믿음과 지지를 보내주고, 제 곁에서 제가 가치있는 사람이라 믿게 해준 여자친구였던 임유선 양에게 감사하다는 이야기를 하고 싶습니다. 그녀 덕분에 박사 학위라는 목표에 집중할 수 있었습니다. 고맙습니다.

다시한번, 제가 부족하여 미처 다 적지 못한 모든 분들을 포함하여, 여러분께 감사합니다. 세상에 저 혼자 이룬 것은 아무것도 없고, 모든 것은 주위 사람들의 도움이 있었기 때문이라는 어느 분의 말씀처럼, 여러분께서 저를 이 자리에 있게 하셨다 생각하고 저도 남에게 도움이 될 수 있는 사람이 되기 위해 노력하겠습니다.

감사합니다.

2020년 1월

안승희 올림